



University of
Nottingham
UK | CHINA | MALAYSIA

Characterisation of the cilia-associated Kinesin-16, *KIF12*

Hanan Alghamdi

MSc (merit)

Thesis submitted to the University of Nottingham towards the degree
of Doctor of Philosophy

31st October 2022

Abstract

Kinesin-16 is a family of kinesins that are only found in organisms that possess cilia or flagella. The human Kinesin-16, *KIF12*, is implicated as a polycystic kidney disease (PKD) modifier. Dysfunction of *KIF12* may also be involved in the progression of certain types of diabetes and mutations to *KIF12* have been shown to be strongly correlated with paediatric cholestatic liver disease.

KIF12 localises to the primary cilia and may affect the function of cilia by playing a role in either transport within the cilia or controlling microtubule dynamics and the assembly and length of cilia. The activity of *KIF12* in relation to microtubules and the coupled ATP turnover have not yet been defined. Therefore, my research interest is to characterise *KIF12* microtubule interaction and ATPase cycle. This information will aid in elucidating a molecular understanding of the cellular role of *KIF12*.

Using a truncated version of *KIF12* which comprised the first 434 amino acids and included the motor domain and a stretch of coiled-coil, I studied *KIF12* in a microtubule "gliding assay" and a single molecule "stepping assay" to characterise microtubule motility. The results of these assays show that *KIF12* does not exhibit any ability to translocate in a directional manner along microtubules. A microtubule

depolymerisation assay showed that *KIF12* has no depolymerisation activity but may stabilise microtubules. Observing the impact of *KIF12* in a dynamic microtubule assay, shows that it causes a small but significant increase in microtubule growth length but no significant increase in growth rate. I did not observe *KIF12* interacting with

microtubules in a dynamic microtubule assay as in the presence of unpolymerized tubulin KIF12 is sequestered away from the microtubules by binding to unpolymerized tubulin. An attempt to quantify the affinity of KIF12 for unpolymerized tubulin and microtubules suggest that KIF12 has higher affinity for unpolymerized tubulin than microtubules. ATP turnover by KIF12 is not accelerated by the presence of unpolymerized tubulin resulting in KIF12 remaining in a tightly bound ATP containing state when interacting with unpolymerized tubulin. Microtubules accelerate the ATPase of KIF12 ~20-fold, suggesting that KIF12 is driven into a nucleotide state that binds less tightly to microtubules by interaction with microtubules.

Due to solubility issues for the full-length protein, I worked with a truncated version of KIF12. Expression and purification of the remaining tail region of KIF12 was carried out but it proved difficult to obtain a soluble protein of sufficient purity. Nevertheless, studying partially purified KIF12 tail suggests that this region does not interact with microtubules and lack of this region likely does not impact the affinity of KIF12 for microtubules.

A mutant form of KIF12, KIF12 Δ PPGGG, results in a less severe disease phenotype in a PKD mouse model. This deletion was found to decrease the affinity of KIF12 for microtubules. Neither wild type KIF12-434 nor KIF12-434 Δ PPGGG could distinguish GTP-lattice (GMPCPP microtubules) from GDP lattice (Taxol microtubules). However, both recognise and concentrate at the ends of Taxol- stabilised microtubules indicating that

KIF12 can distinguish a conformational difference between the end and the lattice of Taxol-stabilised microtubules.

Finally, as an attempt to obtain and study full-length KIF12, I expressed full length GFP tagged KIF12 in a HEK293 cell line. It did not prove possible to purify the protein from these cells. However, observation of the localisation of KIF12 in cells shows that KIF12 decorates the microtubule network. No evidence for translocating activity was observed for KIF12 expressed in HEK293 cells.

The data collected on KIF12-434 and full length KIF12, show that KIF12 interacts with microtubules both *in vitro* and in cells in a diffusive fashion and does not display translocating activity on microtubules. This suggests that KIF12 does not play a transport role in cilia. KIF12 has a small but significant stabilising effect on both GMPCPP-stabilised microtubules and dynamic microtubules and likely acts in cilia as a microtubule regulating kinesin. It is possible that KIF12 is involved in regulation of cilia assembly or disassembly. Further investigations are required for a complete characterisation of this KIF12 and its function in cilia and involvement in disease progression.

Declaration

This thesis is the result of my own work, except where included data is explicitly mentioned, which has been undertaken during my period of registration for this degree at The University of Nottingham.

Contents

Abstract	2
Declaration	5
Contents	6
Table of figures.....	13
Tables	16
Acknowledgments	17
Publications.....	18
Abbreviations	19
Chapter 1 Introduction	21
1.1 The cytoskeleton.....	21
1.2 Microtubules.....	21
1.2.1 Microtubule accessory proteins	25
1.3 Kinesins.....	26
1.3.1 Translocating kinesins	28
1.3.2 Kinesins that regulate microtubule dynamics.....	33
1.4 The Kinesin-16 family	36
1.5 Cilia/Flagella.....	41
1.5.1 Basal body	43
1.5.2 Transition zone.....	43
1.5.3 Ciliary gate	44

1.5.4	Axoneme	44
1.6	Ciliogenesis	46
1.7	Intraflagellar transport (IFT)	47
1.7.1	Intraflagellar trains	47
1.7.2	Intraflagellar motors.....	48
1.7.3	Intraflagellar complex proteins.....	48
1.8	Ciliary Kinesins	50
Aims		52
Chapter 2 Methods		53
2.1	Cloning using USER™ (uracil-specific excision reagent).....	53
2.2	Cell culture and protein expression in insect Sf9 and HEK293a cells	55
2.2.1	Sf9 Cell culture.....	55
2.2.2	Transformation of DH10Bac.....	55
2.2.3	Baculovirus production.....	57
2.2.4	Protein expression.....	58
2.2.5	Protein solubility	58
2.2.6	HEK293a cell culture	59
2.2.7	HEK293a cell transfection and protein expression	59
2.2.8	Cell fixation.....	61
2.3	Protein purification	62

2.3.1	One step purification of KIF12-His6 proteins	62
2.3.2	Two step purification of KIF12-His6 and StrepII/SBP proteins.....	63
2.4	Expression of Kinesin-1	64
2.5	Purification of Kinesin-1	65
2.6	Sodium dodecyl sulphate polyacrylamide gel electrophoresis (SDS-PAGE)	66
2.7	Preparing tubulin.....	66
2.7.1	Cycling tubulin.....	66
2.7.2	Labelling tubulin	67
2.8	Assembling microtubules.....	67
2.8.1	Microtubules for microscopy	67
2.8.2	Double-cycled freezable microtubules	68
2.9	Silanisation of coverslips	68
2.10	Microtubule gliding assay	69
2.11	TIRF microscopy for stepping assay	72
2.12	Microtubule depolymerisation using microscopy	74
2.13	Microtubule dynamic assay	74
2.14	Competition assay	75
2.15	Microtubule affinity assay	76
2.16	ATPase assays	76

2.16.1 Discontinuous assay with ADP production monitored by HPLC.....	76
2.17 ADP dissociation.....	77
2.18 Statistical tests	79
Chapter 3 In vitro characterisation of the activity of KIF12	80
3.1 Expression and purification of KIF12	80
3.2 KIF12-434 does not act as a translocating kinesin.....	83
3.2.1 Expression and purification of Kinesin-1	84
3.2.2 Kinesin-1 microtubule gliding assay	85
3.2.3 KIF12-434 does not act as a translocating kinesin	86
3.3 Stepping assay confirms that KIF12-434 dose not translocate on microtubules.....	87
3.3.1 Kinesin-1 stepping assay.....	87
3.3.2 KIF12-434 does not translocate on microtubules	88
3.4 KIF12-434 does not depolymerise microtubules but may stabilise them.....	90
3.5 KIF12-434 increases microtubules growth rate but cannot be detected on microtubule plus ends.....	92
3.6 KIF12-434 can be sequestered from microtubules by unpolymerised tubulin.....	96
3.7 KIF12-434 is able to distinguish the ends of Taxol-stabilised .	102
3.8 KIF12 tail does not seem to interact with microtubules	105

3.9	KIF12-434 has a low microtubule-stimulated ATPase.....	111
3.10	KIF12-434 microtubule-dependent ADP dissociation is not the rate limiting step.....	113
Chapter 4 In vitro characterisation of the activity of KIF12-434ΔPPGGG		120
4.1	KIF12 -434ΔPPGGG is less soluble than the wild type	123
4.2	KIF12 -434ΔPPGGG purification using Nickle affinity chromatography.....	124
4.3	KIF12 -434ΔPPGGG seems to have a lower affinity for microtubule than the wild type	126
4.4	KIF12 -434ΔPPGGG is able to distinguish the ends of Taxol-stabilised microtubules.....	127
Chapter 5 In vivo characterisation of the activity of KIF12.....		133
5.1	Expression and purification of full length KIF12 using Nickle affinity chromatography	133
5.2	Full length KIF12 localises to microtubules in cell.....	136
5.3	Full length KIF12 exhibits only diffusive motility in cell	138
5.4	The impact of the full length KIF12 on microtubule dynamics was not possible to determine	140
Chapter 6 Discussion.....		142
6.1	KIF12 does not act as a translocating kinesin	142

6.2	KIF12-434 does not depolymerise microtubules but may have a stabilising effect on microtubules	143
6.3	KIF12-434 increases microtubules growth rate but cannot be detected on microtubule plus ends.....	144
6.4	KIF12-434 can be sequestered from microtubules by unpolymerised tubulin.....	145
6.5	KIF12-434 is able to distinguish the ends of Taxol-stabilised microtubules but not those of GMPCPP- stabilised microtubules.	147
6.6	KIF12 tail does not seem to interact with microtubules	149
6.7	KIF12-434 has a low microtubule-stimulated ATPase.....	149
6.8	KIF12-434 Δ PPGGG is less soluble than the wild type	150
6.9	KIF12-434 Δ PPGGG seems to have a lower affinity for microtubule than the wild type	151
6.10	KIF12-434 Δ PPGGG can distinguish the ends of Taxol-stabilised microtubules but not those of GMPCPP- stabilised microtubules	152
6.11	Full length KIF12 characterisation.....	153
6.11.1	<i>In vitro</i> characterisation	153
6.11.2	<i>In vivo</i> characterisation	154
6.12	Further areas for exploration	154
	Appendices	184
	Appendix 1	184
	A1.1 Alignment of human KIF12 and mouse KIF12.	184

Appendix 2	185
A2.1 USER cloning - PCR primers	185
Appendix 3	187
A3.1 Oligomeric state assessment of purified wild type KIF12-434.....	187
Appendix 4	188
A4.1 Difference in solubility between the wild type KIF12-434 and KIF12-434 Δ PPGGG expressed in Sf9 cells.....	188
Appendix 5	189
A5.1 KIF12-434 effect on microtubule dynamics.....	189

Table of figures

Figure 1.1. Microtubule structure	22
Figure 1.2. Microtubule GTP cap	24
Figure 1.3. Kinesin-2 structure	31
Figure 1.4. Distributions of kinesin families among eukaryotic organisms	37
Figure 1.5. KIF12 localises to the primary cilium	40
Figure 1.6. The structure of a cilium	46
Figure 1.7. Intraflagellar transport (IFT) machinery	50
Figure 2.1. Construction of Channels for microtubules gliding assay	69
Figure 2.2. Gliding assay setup	71
Figure 2.3. TIRF assay experimental setup	73
Figure 3.1. Domain layout for the wild type mammalian KIF12 .	82
Figure 3.2. Purification of KIF12-434	82
Figure 3.3. Purification of Kinesin-1	84
Figure 3.4. Kinesin-1 moves microtubules in a directional fashion	85
Figure 3.5. KIF12-434 dose not move microtubules in a directional manner	86
Figure 3.6. Kinesin-1 stepping assay	87
Figure 3.7. KIF12-434-GFP does not show a translocating motility along microtubules	89
Figure 3.8. Microtubule depolymerisation by MCAK	91

Figure 3.9. KIF12-434 slows down microtubule depolymerisation rate.	92
Figure 3.10. Microtubule dynamics assay setup.	93
Figure 3.11. KIF12-434 affects microtubule dynamics	94
Figure 3.12. KIF12-434 interacts with microtubule seeds in the absence of unpolymerised tubulin.	97
Figure 3.13. KIF12-434 is sequestered away by unpolymerised tubulin from microtubules	98
Figure 3.14. KIF12-434 binds two tubulin dimers rather than one dimer.	99
Figure 3.15. KIF12-434 binding to tubulin dimers model.	100
Figure 3.16. KIF12-434 affinity for microtubule	102
Figure 3.17. KIF12-434 cannot distinguish GMPCPP from Taxol stabilized microtubules.	104
Figure 3.18. KIF12 tail constructs	106
Figure 3.19. Purification of KIF12 tail [434-651]-GFP-7xhis	107
Figure 3.20. Purification of KIF12 tail [434-651]-GFP-SBP-6xHis	109
Figure 3.21. Purification of KIF12 tail [478-651]-GFP-SBP-6xHis	109
Figure 3.22. KIF12 tail does not interact with microtubules	111
Figure 3.23. ADP and ATP were separated by HPLC and produced peaks with concentration dependent integrals.	111
Figure 3.24. KIF12-434 has a low microtubule-stimulated ATP turnover	113

Figure 3.25. Structural formula of Mant-ADP.....	114
Figure 3.26. The ATP turnover cycle.....	115
Figure 3.27. ADP dissociation from KIF12-434 is weakly stimulated by microtubules.....	117
Figure 4.1. Sequence and structural alignment of wild type KIF12 and KIF12ΔPPGGG.....	120
Figure 4.2. Structural alignment of KIF12 and Kinesin-1	122
Figure 4.3. Domain structure of KIF12ΔPPGGG.	122
Figure 4.4. Wild type KIF12-434-GFP and KIF12 -434ΔPPGGG- GFP estimated level of expression and solubility.....	124
Figure 4.5. Purification of KIF12 -434ΔPPGGG -GFP-7His.....	125
Figure 4.6. KIF12 -434ΔPPGGG -GFP affinity for microtubule ..	127
Figure 4.7. KIF12ΔPPGGG cannot distinguish between the tip of primary cilium and the main body of the cilium.....	128
Figure 4.8. KIF12-434ΔPPGGG cannot distinguish GMPCPP from Taxol stabilized microtubules.....	131
Figure 4.9. Affinity of wild type KIF12-434 and KIF12ΔPPGGG- 434 for GMPCPP- and Taxol- stabilised microtubules.	132
Figure 5.1. HEK293a cells were successfully transfected with 6his-full length KIF12-GFP.....	135
Figure 5.2. Purification of 6xHis-Full-length KIF12-GFP	136
Figure 5.3. KIF12 localizes to microtubules.....	137
Figure 5.4. Full length KIF12-GFP localization on microtubules	138

Figure 5.5. Full-length KIF12-GFP shows a diffusive movement in cell	139
Figure 5.6. Impact of KIF12 on microtubule dynamics in cell could not be measured	140
Figure A1.1. Alignment of human KIF12 and mouse KIF12	184
Figure A3.1. Around one-third of purified KIF12-434 is dimeric	187
Figure A5.1. KIF12-434 affects microtubule dynamics.	190

Tables

Table 1. Summary table of the translocating kinesins and kinesins that regulate microtubule dynamics.	35
Table 2. Summary table of the impact of different proteins on microtubule dynamics.	95
Table 3. Summary table of KIF12-434 ATPase and mADP dissociation data.....	117
Table 4. Band quantification on SDS-PAGE of wild type KIF12-434...	188
Table 5. Band quantification on SDS-PAGE of KIF12-434 Δ PPGGG	188

Acknowledgments

I would like to thank the following people, without whom I would not have been able to complete this research project, and without whom I would not have made it through my PhD degree!

Special thank you to my supervisor Claire Friel whose insight and knowledge into the subject matter, support and encouragement have been invaluable throughout this project. To Bill Wickstead for his valuable comments and suggestions. I would also like to extend my thanks to my lab colleague Hannah Belsham who helped a lot with the lab work and data analysis. Thank you also to the School of Life Sciences Imaging Facility and Chris Gell and Robert Markus in particular for technical assistance and advice. Thank you to Princess Nourah bint Abdulrahman University for the funding opportunity to undertake this project. Thank you to my family for all the support you have shown me through this journey, especially to my mum and dad, thanks for all your unconditional support without which this would have not been possible. To my twin sister Asmahan, I simply couldn't have done this without you, special thanks. To all friends for their encouragement, support, and the lovely moments we shared during this journey.

Publications

Alghamdi, H. M. & Friel, C. T. 2020. 'The Kinesin-16 Family'. In: FRIEL, C. T. (ed.). *The Kinesin Superfamily Handbook*. 1st Edition: CRC Press.

Belsham H. R., Alghamdi H. M., Dave N., Rathbone A. J., Wickstead B., Friel C. T. *A synthetic ancestral kinesin-13 depolymerizes microtubules faster than any natural depolymerizing kinesin*. *Open Biol.* 2022. 12(8):220133.

Abbreviations

AcMNPV – *Autographa californica* multiple nuclear polyhedrosis virus

ADP – Adenosine-5'-diphosphate

ATP – Adenosine-5'-triphosphate

BBS - Bardet-Biedl syndrome

BIIC – Baculovirus Infected Insect Cell

BME – β -mercaptoethanol

BSA – Bovine Serum Albumin

C- – carboxy-

CNG - Cyclic nucleotide-gated ion channels

DMSO – Dimethyl Sulfoxide

DNA – 2-Deoxyribose Nucleic Acid

dNTP – 2-deoxynucleoside-5'-triphosphate

DTT – Dithiothreitol

EDTA – Ethylene Diamine Tetraacetic Acid

EGTA – Ethylene Glycol Tetraacetic Acid

FBS – Foetal bovine Serum

GDP – Guanosine-5'-diphosphate

GFP – Green Fluorescent Protein

GMPCPP – Guanylyl α , β -methylene diphosphate

GTP – Guanosine-5'-triphosphate

His6 – Hexahistidine tag

HEPES – 4-(2-hydroxyethyl)-1-piperazineethanesulfonic acid

Hh - Hedgehog

HPLC – High Performance Liquid Chromatography

IMCD3 - inner medullary collecting duct

kDa - Kilodaltons

HC – Heavy chain

KIF – Kinesin family member

LB – Luria Broth

Mant-ADP - 2'/3'-O-(N-Methyl-anthraniloyl)-adenosine-5'-diphosphate

MAP – Microtubule Associated Protein

MCAK – Mitotic Centromere Associated Kinesin/ KIF2C

MDCK - Madin-Darby canine kidney

N- – amino-

OD – Optical density

PCR – Polymerase Chain Reaction

Pi – Inorganic Phosphate

PIPES – 1, 4-Piperazinediethanesulphonic acid

PKD – Polycystic kidney disease

PMSF – Phenylmethanesulphonyl Fluoride

RNA – Ribonucleic acid

SDS – Sodium Dodecyl Sulphate

SDS-PAGE – Sodium dodecyl sulphate polyacrylamide gel electrophoresis

Sf9 cells – Spodoptera frugiperda cells

TAMRA – 5-carboxytetramethylrhodamine

TIRF – Total Internal Reflection Fluorescence

WT – wild type

Chapter 1 Introduction

1.1 The cytoskeleton

The cytoskeleton helps cells retain their shape and internal organization. It also provides mechanical support that enables cells to carry out fundamental functions, such as division and movement. There are three main types of cytoskeletal components that vary in size and protein composition. Actin filaments are the smallest class, with a diameter of approximately 9 nm. They are made of two protofilaments of the protein subunit actin, which wrap round each other in a helical structure. Intermediate filaments are rope-like fibres with a diameter of about 10 nm and composed of a variety of protein subunits. Microtubules are hollow cylinders of around 25 nm in diameter constructed from the protein tubulin. Heterodimers of α - and β -tubulin attach in a head-to-tail fashion to form protofilaments, and these protofilaments join together to form the closed tube (Alberts et al., 2014, Fletcher and Mullins, 2010).

1.2 Microtubules

Microtubules are cytoskeletal filaments that are involved in a wide variety of cell activities. This includes serving as tracks for intracellular transportation, forming the mitotic spindle, forming axonemes of cilia and flagella, and regulating cell morphogenesis in all eukaryotes. Structurally, microtubules are built up by the assembly of α -/ β -tubulin heterodimers. These heterodimers are attached in a head to tail manner to form long protofilaments. Typically 13 protofilaments assemble

laterally to form the hollow cylindrical structure of a microtubule (Figure 1.1) (although microtubules grown *in vitro* have been observed to have from 12 to 17 protofilaments (Chrétien and Wade, 1991)). In microtubule with 13 or 14 protofilaments the tubulin dimers are arranged so that lateral contacts are homotypic; meaning that they are α - α and β - β , except down a single seam (Figure 1.1) (Song and Mandelkow, 1993). At the seam the lateral interactions are heterologous; meaning that they are α - β or β - α . Microtubules have a distinct polarity which is crucial for their biological role. The two ends have different molecular configurations. One end is called the plus end which is capped with β -tubulins and is the faster-growing end, while the other is a slower-growing end called the minus end where α -tubulins are exposed.

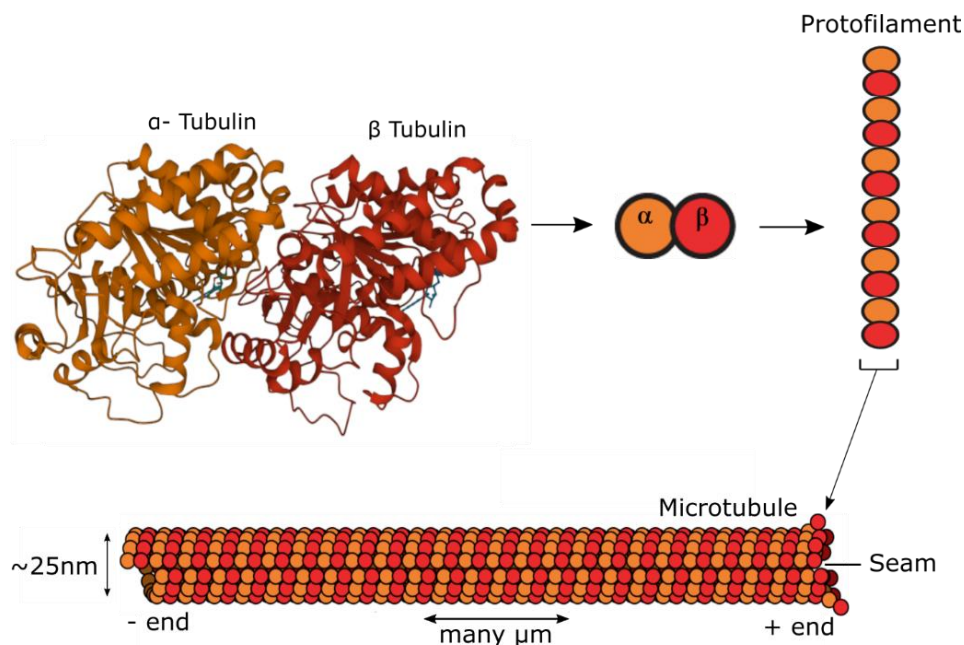


Figure 1.1. Microtubule structure. α - β -tubulin heterodimer; α tubulin binds to GTP and β tubulin binds to GDP or GTP (PDB ID: 1JFF (Löwe et al., 2001)). The dimers can polymerize end-to-end to form protofilaments. Protofilaments assemble laterally to construct microtubules. A microtubule is hollow cylinder with a plus-and a minus-end, consisting of, on average, 13 parallel protofilaments.

Microtubules are dynamically unstable, meaning that they can assemble and disassemble very rapidly by the addition or removal of tubulin subunits. This behaviour, which is termed dynamic instability, has been confirmed to be fundamentally driven by hydrolysis of GTP to GDP in the tubulin subunits (Mitchison and Kirschner, 1984). The α - β tubulin subunit has two nucleotide-binding sites. The non-exchangeable N-site in α -tubulin can only be filled with GTP. The exchangeable E-site in β -tubulin can exchange bound nucleotide (Nogales et al., 1998). When the E-site is occupied by GTP polymerisation is favoured. Polymerisation occurs by the addition of tubulin subunits mainly at the plus end, where the β -tubulin is exposed. Upon polymerisation the E-site GTP can be hydrolysed to GDP that becomes trapped in the microtubule lattice. GTP bound tubulin has a relatively straight conformation, whereas GDP tubulin and is characterised by an increased longitudinal curvature. Therefore, upon hydrolysis tubulin subunits undergo a structural conversion that weakens lateral bonds, destabilising the subunit in the microtubule lattice. (Wang and Nogales, 2005, Alushin et al., 2014). Although a bulk of tubulin in microtubule lattice has hydrolysed GTP to GDP in the E-site, there exists a region of subunits at the end of growing microtubules that have not hydrolysed their GTP and therefore stabilize the microtubule against depolymerisation. This region is called a GTP cap (**Figure 1.2 A**) and is formed when new GTP-bound tubulin subunits are added more rapidly than GTP hydrolysis occurs. It was thought that the loss of GTP cap occurs when the hydrolysis rate is faster than the polymerisation rate leading to expose an unstable GDP

lattice and trigger depolymerisation (Mitchison and Kirschner, 1984). The switch from growth to rapid depolymerisation (shrinkage) is called catastrophe (Chrétien et al., 1995) (**Figure 1.2 B**). It was believed that catastrophe is a single-step event that involves a sudden loss of a protective cap structure (Mitchison and Kirschner, 1984).

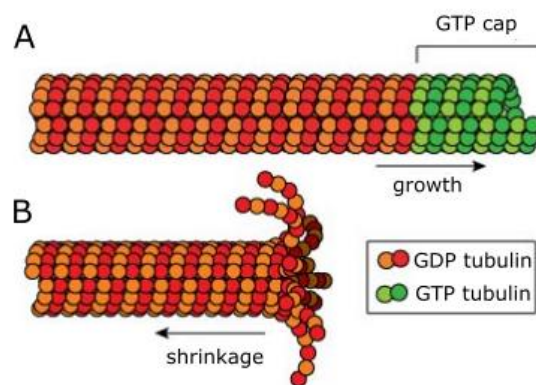


Figure 1.2. Microtubule GTP cap. A) GTP cap forms when the addition of new tubulin subunits is faster than GTP hydrolysis. B) The loss of GTP cap leads to switch between microtubule growths to shrinkage (catastrophe).

However, lately it was shown that catastrophe is a multi-step process and microtubule-age dependent, as it has been shown that short-life microtubules are less likely to go through catastrophe, which means that microtubules undergo aging and the frequency of catastrophe is not consistent, but increases with time (Gardner et al., 2011). The multi-step catastrophe is believed to be as a result of stochastic fluctuations in the size, shape, and extent of lateral bonding of the cap (Margolin et al., 2011). It is also suggested to be due to an accumulation of several

random destabilizing events in the microtubule lattice (Gardner et al., 2013).

Stabilised microtubules can be grown *in vitro* by using GMPCPP, a slowly hydrolysable GTP analogue guanylyl α,β -methylene diphosphate (Hyman et al., 1995, Nogales et al., 1998). This analogue binds to the tubulin E-site and promotes spontaneous polymerisation of microtubules. The polymerization rate of these microtubules is very close to that with GTP. However, GMPCPP microtubules have a depolymerisation rate 5000-fold slower than GDP microtubules. GMPCPP also completely suppresses dynamic instability making microtubules stable enough for use in long time course experiments (Hyman et al., 1992). Microtubules are grown *in vitro* by mixing tubulin with GMPCPP or GTP, and magnesium ions at 37°C. Microtubules grown in the presence of GTP can be later stabilised by Taxol (also known as paclitaxel), which binds to a site in β -tubulin on the microtubule's **lumen**, and counteracts the effects of GTP hydrolysis occurring on the other side of the monomer (Amos and Löwe, 1999).

1.2.1 Microtubule accessory proteins

Microtubule associated proteins (MAPs) can be classified into three classes: translocators, regulators of microtubule structure and dynamics, and regulators of microtubule organisation. Some MAPs have features from more than one of these classes. Translocators move in a directed manner along microtubules and use microtubules as tracks for cargo transport. Translocators, such as Kinesin-1 and cytoplasmic dynein, are involved in transport of several cargos including vesicles,

organelles and mRNAs (Allan, 1995, Harada et al., 1998, Burkhardt et al., 1997, Pilling et al., 2006, Lippincott-Schwartz et al., 1995, Zimyanin et al., 2008).

Other microtubule associated proteins act by regulating microtubule structure and dynamics. Some of these proteins increase the rate of microtubule polymerization, slow depolymerisation rate, and decrease the rate of catastrophe, such as tau (Drechsel et al., 1992), or promote catastrophe, such as, Stathmin (Belmont and Mitchison, 1996). Others induce microtubule branching, for example SSNA1 (Basnet et al., 2018). They can also function as microtubule severers, such as Katanin (Yu et al., 2005).

Other microtubule associated proteins regulate the spatial organisation of microtubules. For instance by bundling and cross-linking microtubules, such as MAP65 (Chang-Jie and Sonobe, 1993), or cross-linking and sliding microtubules, for example KLP61F (Sharp et al., 1999).

1.3 Kinesins

Kinesins are ubiquitous among eukaryotes. There are 45 kinesin genes identified in mammals, with alternative splicing expanding the overall number of different kinesins (Miki et al., 2001). Kinesins share a highly conserved motor domain (Vale and Goldstein, 1990). The motor domain consists of ~350 amino acids and is composed of an 8-stranded antiparallel β sheet surrounded by 3 α helices on either side. The ATPase catalytic site is located at the top of the β sheet and consists of four

highly conserved motifs: the Phosphate binding loop (P-loop), Switch I, Switch II, and RXRP. The motor domain contains the microtubule binding site which is composed of the secondary structural elements L8, L11/ α 4 and L12. Other elements L2, α 5, and α 6 are involved to different degrees based on the kinesin family. The motor domain undergoes nucleotide dependent conformational transition which alters its affinity for the microtubule. **Generally**, in the ATP and no nucleotide state the kinesin motor domain is typically tightly bound to the microtubule. Whereas when in the ADP or ADP.Pi state the motor domain is weakly bound to the microtubule (Hackney, 1994, Ma and Taylor, 1997). Interaction with the microtubule stimulates changes in the nucleotide state of the kinesin motor domain, and the interaction with the microtubule is changed in accordance with its nucleotide state. Thus, these cycles are coupled and this is the basis of the various types of behaviour observed for the kinesin superfamily. Near to the motor domain many kinesins contain a domain termed the neck. This domain is essential for motile kinesins as it is responsible for motor domain coordination and movement directionality on microtubules (Endow and Waligora, 1998, Case et al., 1997). The regions outside the motor domain are highly variable between kinesin family members and across kinesin families (Goldstein, 1993). Non motor regions control the multimerisation state of the motor domain, cellular localisation of a kinesin, and attachment to cargo via adapter proteins (Chu et al., 2005, Lee et al., 2010, Tao et al., 2006, Skoufias et al., 1994). Some non-

motor regions contain an additional microtubule binding site that can enhance the processivity of the kinesin (Mayr et al., 2011).

As the size of the kinesin superfamily has grown, due to an increase in the number of identified kinesins, the lack of a unified classification made the naming and categorizing of kinesins unmanageable and inconsistent (Lawrence et al., 2004). To establish a standardized naming system, Lawrence et al. (2004) took the previously identified kinesins and classified them into 14 families based on the amino acid sequence alignment of their motor domains. To be considered as a family, a kinesin group had to have sequences from at least two kingdoms of eukaryotes. A later analysis of 486 kinesin sequences from 19 eukaryotes illustrated that modifications to the Lawrence et al. (2004) were necessary (Wickstead et al., 2010, Wickstead and Gull, 2006). Wickstead et al. (2010) suggested that kinesin superfamily should be classified into 17 families following the same definition of a kinesin family that was proposed by Lawrence et al. (2004). This further analysis of kinesin sequences also suggested to split the Kinesin 12 family into two novel families: Kinesin 15 and Kinesin 16. In addition, they proposed a new family -Kinesin-17- which consists of a cross-kingdom kinesin group, and combined the Kinesin-4 and -10 families into one family, which is known as Kinesin-4/10.

1.3.1 Translocating kinesins

Translocating kinesins may be highly processive; meaning that they can take many steps along microtubule before detaching, or weakly

processive taking just a few steps before dissociating from microtubules. They translocate toward either the plus end or the minus end of microtubules. The majority move towards the plus end and only kinesin-14s move toward the minus end. Some translocating kinesins can show bi-directional movement. The most well characterised plus end directed translocating kinesins are Kinesin-1, Kinesin-2, and Kinesin-3 families. The plus end directed translocating kinesins are exemplified by the kinesin-2 family. Kinesin-2s are generally processive but they are generally slower than Kinesin-1s and Kinesin-3s. Kinesin-2s have two fundamental functions: vesical transport in neuronal cells and intraflagellar transport in cilia and flagella. Kinesin-2s also function in non-neuronal cells, where they are involved in several cargos transport including Golgi vesicles, late endosomes and lysosomes, melanosomes, and mRNA (Scholey, 2013, Messitt et al., 2008). Kinesin-2s are also thought to be involved in pathogenic transport, such as transport of HIV viruses in macrophages (Gaudin et al., 2012). Kinesin-2 consists of a heavy chain (HC) which contains an N-terminal motor domain, followed by a coiled-coil domain, and a C-terminal tail domain. The motor domain is linked to a long coiled-coil domain via a proximal 'neck-coil' dimerization region. The coiled-coil is broken by a hinge region that permits the protein to fold up and the tail domain to inhibit the motor domains when the protein is no cargo present (Hammond et al., 2010). Kinesin-2s can be divided into homodimeric and heterotrimeric members. Homodimeric Kinesin-2s consist of two identical HCs that wrap around each other to form a homodimer, but currently no

associated light chains are identified. Heterotrimeric Kinesin2-s are composed of two non-identical HCs that dimerise via coiled-coil domain, and a KAP3 domain that attaches to the globular C-terminal tail domain of the HCs (**Figure 1.3**). The HCs of heterotrimeric Kinesin-2 comprise a region of opposing charges in the a proximal coiled-coil region that had been thought to drive heterodimerisation, however later it was found that a trigger sequence at C-terminal end of the coiled-coil promotes heterodimerisation (De Marco et al., 2001). In mammals there are four Kinesin-2 variants: KIF3A, KIF3B, KIF3C, and KIF17. KIF17 forms a homodimer while in contrast KIF3A associates with either KIF3B or KIF3C to form heterodimeric KIF3AB and KIF3AC motors. It has been suggested that mechanically heterodimerization of these motors is a way to tune their performance such that they are suited to a specific cellular task (Bensel et al., 2020). A study by Schimert et al. (2019) proposed that scaling of total force generation with the number of motors may happen more efficiently for kinesin-2 motors than in other kinesin subfamilies, suggesting that these motors may be adapted to drive transport in larger teams. It is also possible that heterodimerization of tail domains is important for recruitment of specific cellular cargos.

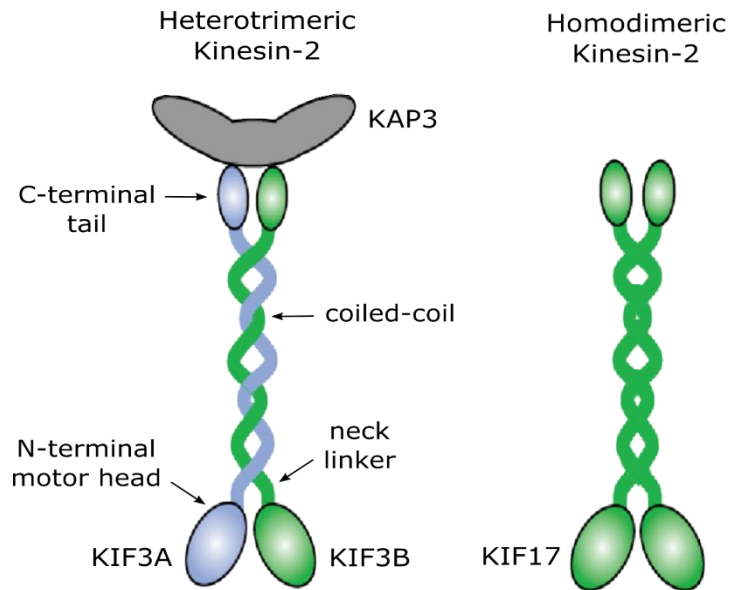


Figure 1.3. Kinesin-2 structure. The family can be divided into two classes: homodimeric and heterotrimeric members, each of which consists of two N-terminal motor domains, joined by a coiled-coil stalk domain, and C-terminal tails. Image was modified from (Brownhill, 2010).

The Kinesin-14 family of translocating kinesins can move toward the minus-end of the microtubule. An example is the kinesin-14, Ncd. Ncd can zip together microtubules at their minus ends in the centrosome-free spindles (Sharp et al., 2000). RNAi depletion of Ncd has been shown to cause a large defect in spindle pole focusing (Goshima and Vale, 2003). The crystal structures of Kinesin-1 and Ncd motor domains are almost identical (Kull et al., 1996, Sablin et al., 1996), and replacing Kinesin-1 motor domain with that of Ncd does not affect the directionality of Kinesin-1 movement (Case et al., 1997). The structural difference in the neck domain was found to be responsible for their opposite directions of movement. Kinesin-1 neck domain composed of two β -strands plus an α -helix, while Ncd neck domain is entirely helical

and form a coiled-coil. The unique neck architectures confer different symmetries to the Ncd and kinesin-1 dimers and position these motors with appropriate orientation on the microtubule (Sablín et al., 1998, Sack et al., 1997).

Some translocating kinesins can walk in a bi-directional manner. For instance, Cin8 and Cut7 which are members of the Kinesin-5 family, a family of homotetrameric proteins that slide apart antiparallel microtubules in mitosis. *In vitro* experiments on purified Cin8 and Cut7 showed that single molecules preferentially moved toward the minus ends of individual microtubules. This directionality of movement was reversed when these motors worked as part of a larger team, either when immobilized on a glass surface at high densities in microtubule gliding experiments or when sliding two antiparallel microtubules relative to each other (Britto et al., 2016, Roostalu et al., 2011). The essential determinant of movement direction is the degree of motor crowding on the microtubule lattice, as with greater crowding the motor converts from minus end-directed to plus end-directed movement (Britto et al., 2016). A single molecule-study on Cin8 showed that it switches frequently between plus and minus-end directed movement along microtubules, demonstrating that the Cin8 head domains are inherently bidirectional. In addition, a tail-less Cin8 shows that the tail controls the switch between plus- and minus-end-directed motility (Düselder et al., 2015). Cut7 was also observed to be inherently bidirectional. A study on Cut7 showed that full length Cut7 is a minus-end-directed motor, whereas a truncation (motor domain with a short

coiled-coil region) is a plus-end one. This suggests that wild type Cut7 is a minus-end-directed motor and also has the plus-end directionality (Edamatsu, 2014).

1.3.2 Kinesins that regulate microtubule dynamics

Kinesins can regulate microtubule dynamics. Regulators of microtubule dynamics may be depolymerisers that antagonise microtubule growth and/or promote shrinkage, such as, the Kinesin-13 family. Unlike translocating kinesins, Kinesin-13s do not move in a directed manner on microtubules. Instead, they undergo stochastic diffusive motion on the microtubule lattice (Helenius et al., 2006). The most extensively studied member of this family is MCAK; mitotic centromere-associated kinesin. This kinesin preferentially binds to and stabilizes the curved tubulin conformations at end of microtubule that are incompatible with lateral tubulin-tubulin bond formation, resulting in eventually removing tubulin subunits from microtubule end (Burns et al., 2014, Asenjo et al., 2013). This depolymerizing activity plays vital roles in spindle formation, correct microtubule-kinetochore attachments and chromosome positioning and segregation (Ems-McClung and Walczak, 2010, Maney et al., 1998, Walczak et al., 2002, Cassimeris and Morabito, 2004). Depletion or inhibition of MCAK activity causes defective spindle maintenance and chromosome misalignment during metaphase and lagging chromosomes during anaphase (Maney et al., 1998, Walczak et al., 2002).

Microtubule regulating kinesins can be polymerisers, promoting microtubule growth. An example is the budding yeast kinesin Kip2. In vitro Kip2 was observed to translocate at a speed that is higher than the rate of microtubule growth. This allows Kip2 to catch up with the growing microtubule end where it promotes microtubule polymerisation and reduces the catastrophe frequency. This leads to a positive feedback: the longer the microtubule, the greater the number of Kip2 molecules that land on it and walk to the plus ends where they reinforce growth and inhibit catastrophe. This, in turn, leads to longer microtubules, which attract more Kip2 and so on (Hibbel et al., 2015). Previous studies have shown that cells with depleted Kip2 have much shorter filaments than wild type cells (Cottingham and Hoyt, 1997, Caudron et al., 2008).

Some microtubule regulating kinesins function as inhibitors of dynamics which antagonise both growth and disassembly of microtubules. For example, Xklp1, a member of the Kinesin-4 family that is essential for organizing central spindle midzone formation. In Xklp1-deficient cells, the central spindle was disorganized, and all midzone-associated proteins failed to concentrate at the midline, instead being dispersed along the loosened microtubule bundles of the central spindle (Kurasawa et al., 2004). In vitro research showed that to keep the antiparallel microtubule overlaps at constant size, Xklp1 is recruited by PRC1, a microtubule binding and bundling protein in vivo and in vitro that associates the mitotic spindle- and is essential for cytokinesis. This recruitment causes local inhibition of both microtubule growth and

catastrophe by Xklp1. Xklp1 reduces both GTP-tubulin on and off-rates showing that it has the property of making microtubules less dynamic by reducing the overall turnover of GTP-tubulin at growing microtubule ends. It was also found to accumulate at microtubule plus end preventing growth (Bieling et al., 2010). See **Table 1** for a summary of the exemplary kinesins for both translocating kinesins and kinesins that regulate microtubule dynamics.

Table 1. Summary table of the translocating kinesins and kinesins that regulate microtubule dynamics.

Kinesin	Family	Organism	Movement pattern	Function
Translocating kinesins				
KIF3A, KIF3B, KIF3C, and KIF17	2	Mammals	Plus-end-directed translocators	Cargo transport
Ncd	14	Insects	Minus-end-directed translocator	Plays a role in spindle focusing, sliding and cross-linking microtubules
Cin8 and Cut7	5	Yeasts	Bi-directional translocators	sliding apart antiparallel microtubules
Kinesins that regulate microtubule dynamics				
MCAK	13	Mammals	Non-translocators (diffusive)	Microtubule depolymerisation
Kip2	8	Yeasts	Plus-end-directed translocator	Microtubule polymerisation
Xklp1	4	Mammals	Plus-end-directed translocator	Inhibition of microtubule growth and catastrophe

1.4 The Kinesin-16 family

The mammalian KIF12 is a member of the Kinesin-16 family. There is no functional data currently available for the Kinesin-16 family.

Phylogenetic analysis of the kinesin superfamily suggests a possible ciliary/flagellar function for kinesin-16s due to their presence only in cilia/flagella building organisms (**Figure 1.4**)(Wickstead and Gull, 2006). This function could be either carrying cargo or regulating microtubule dynamics and length within cilia/flagella.

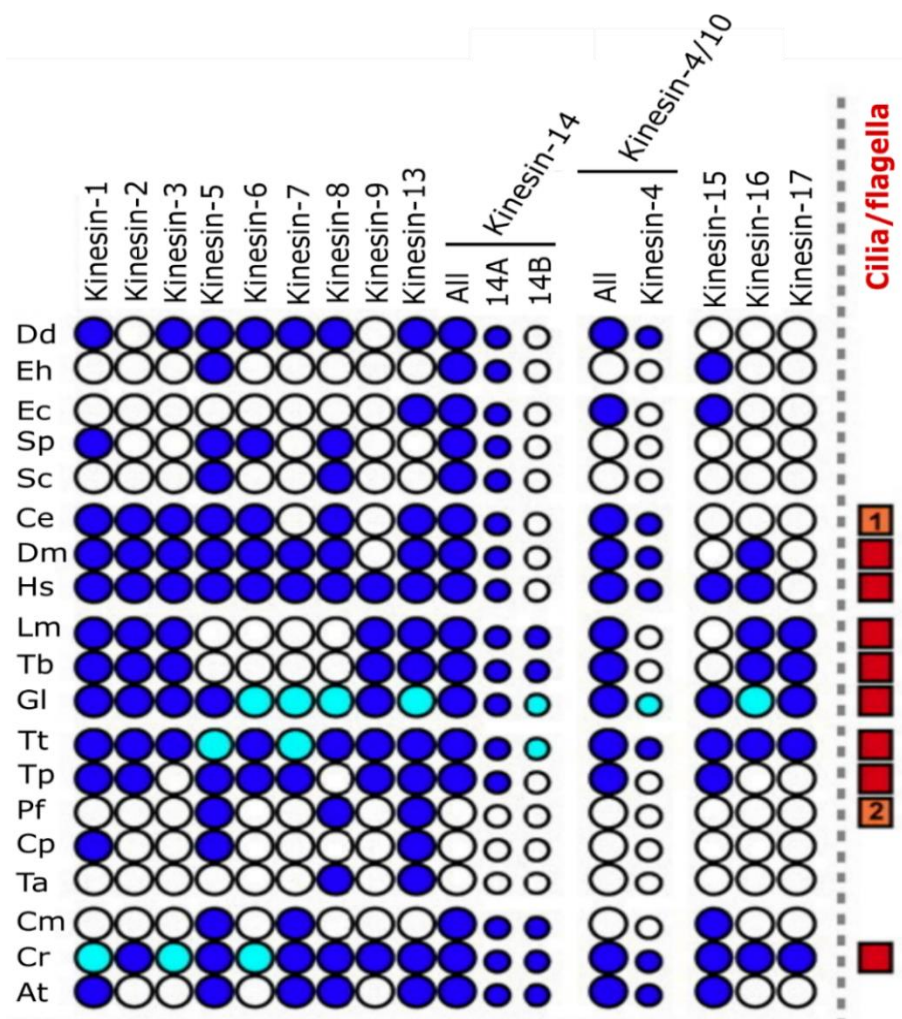


Figure 1.4. Distributions of kinesin families among eukaryotic organisms. The taxonomic distribution of kinesin families can be used as an indicator of kinesin family function. The presence of a paralogue in an organism's genome is shown with a dark blue circle, the absence of a paralogue in an incomplete genome is shown in light blue and absence of a paralogue in a complete genome is shown as a white circle. Subfamilies are represented with smaller circles than families. Organisms that build cilia are indicated by a red/orange square. Organisms with immotile cilia and those that build cilia in the absence of IFT machinery are indicated by a numbered orange box (1 & 2 respectively). Prefixes are as follows: At, *A. thaliana*; Ce, *C. elegans*; Cm, *C. merolae*; Cp, *C. parvum*; Cr, *C. reinhardtii*; Dd, *D. discoideum*; Dm, *D. melanogaster*; Ec, *E. cuniculi*; Eh, *E. histolytica*; Gl, *G. lamblia*; Hs, *H. sapiens*; Lm, *L. major*; Pf, *P. falciparum*; Sc, *S. cerevisiae*; Sp, *S. pombe*; Ta, *T. annulata*; Tb, *T. brucei*; Tp, *T. pseudonana*; and Tt, *T. thermophile*. Image was modified from (Wickstead and Gull, 2006).

The human KIF12 gene encodes a 651-amino acid protein that shares 80.8% total-amino-acid identity with mouse KIF12, with an N-terminal kinesin motor domain corresponds to codon 26-363, followed by regions of coiled coil correspond to codons 381-410 and 420-472 separated by an internal hinge region corresponds to codon 411-419, and a C-terminal tail domain corresponds to the region that is following the coiled coil domain (Katoh and Katoh, 2005, Nakagawa et al., 1997) (**Figure A1.1**). Currently, there is no structure available for KIF12, but sequence similarity suggests that there will be high structural conservation with respect to motor domains from other kinesin families. The domain layout of KIF12 is akin to that of translocating kinesins, which may suggest a cargo carrying function; members of the Kinesin-2 family are known to function in this manner (some examples are discussed in section 1.8), where they transport the components required for the construction and maintenance of cilia and flagella from the site of synthesis in the cell body to the site of growth at the distal tip of the

cilia (Scholey, 2013, Marszalek and Goldstein, 2000). However, other cilium-associated kinesins, such as Kinesin-4, KIF7 function by regulating microtubule dynamics (He et al., 2014, Kobayashi et al., 2011), and it is likely that KIF12 acts as a microtubule-regulating kinesin rather than a translocating one.

The mammalian KIF12 is the only member of Kinesin-16 family for which the physiological role has been studied to date. KIF12 was first identified as a kinesin in a PCR screen of a mouse cDNA library (Nakagawa et al., 1997). This study demonstrates KIF12 is predominantly expressed in the kidney. A more recent study shows that KIF12 is also expressed in pancreatic islet cells (Yang et al., 2014). A quantitative transcriptomics analysis of all major human organs showed that KIF12 RNA is highly expressed in the kidney and at moderately high levels in the pancreas, gall bladder, thyroid gland and small intestine (Fagerberg et al., 2014).

KIF12 is involved in a number of human diseases. The transcription factor hepatocyte nuclear factor-1 β (HNF-1 β) controls expression of KIF12 in the kidney (Gong et al., 2009). Mutations of HNF-1 β lead to a syndrome of inherited renal cysts and diabetes (Bellanné-Chantelot et al., 2004, Horikawa et al., 1997). Consistent with this, a study on mouse model of polycystic kidney disease (PKD) shows that KIF12 is implicated as a candidate genetic modifier that modulates the severity of the disease phenotype (Mrug et al., 2015, Mrug et al., 2005). In this model, mice showed renal and biliary cysts similar to that observed in human PKD. The mouse model (B6) harbours a mutation in its cystin

gene (Cys1cpk) which encodes for a truncated protein compared to wild type (Yoder et al., 2002, Hou et al., 2002). When B6 was crossed with the CAST/Ei mouse line (an inbred strain derived from the wild strain *Mus mus castaneus*), hybrids screened for Cys1cpk homozygous showed varying expression and severity of disease caused by genetic background. The severity of renal and biliary disease was only weakly correlated in the PKD mouse model hybrids (Mrug et al., 2005). Genome scanning identified a major effect quantitative trait loci (QTL) complex for renal severity, and Kif12 was found to be the strongest modifier gene present. Kif12 alleles from B6 and CAST/Ei mouse models were sequenced, and CAST/Ei Kif12 was found to possess an extra five amino acids compared with B6 Kif12. CAST/Ei contains the additional PPGGG, predicted to be in loop-2 of the microtubule binding site of the kinesin motor domain. CAST/Ei x B6 mice showed more severe PKD in individuals possessing the CAST/Ei Kif12 allele compared with the B6 Kif12 allele (Mrug et al., 2005). Kif12 strain-specific haplotypes and Kif12 expression levels strongly correlated with the severity of renal disease phenotype in these intercross mice. The Mrug et al. (2015) study provides a further evidence for KIF12 as a PKD modifier gene as it shows that KIF12 localises to the primary cilia in mouse kidney IMCD3 cell line (**Figure 1.5**), as the primary cilia is the same location of Cys1 and most genes that are involved in cystic renal disease (Guay-Woodford et al., 2000). The expression of Kif12 and Cys1 in IMCD3 cell line are strongly correlated (Mrug et al., 2015).

The localisation of Kif12 to the primary cilia in IMCD3 cell line also supports the ciliary role of Kinesin-16s.

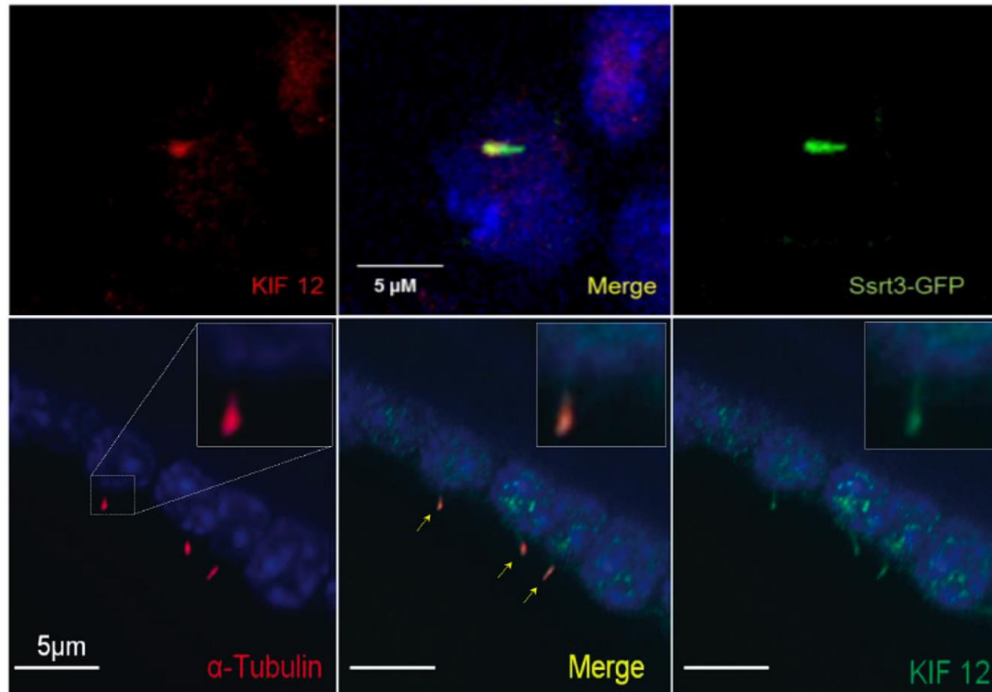


Figure 1.5. KIF12 localises to the primary cilium. Upper panel: Immunofluorescence images of KIF12 (red) and a green fluorescent protein (GFP)-tagged primary cilium marker, somatostatin receptor 3 (green) co-localisation in a mIMCD cell line. Lower panel: KIF12 (green) co-localised with α -tubulin (red), another primary cilium marker. Mrug 2015 PLOS One.

KIF12 also seems to play a role in glucose metabolism and control of blood sugar levels. KIF12 knockout mice suffer from glucose intolerance due to reduced insulin secretion (Yang et al., 2014). A study of KIF12 knockout mice indicates a role in the regulation of glucose metabolism, possibly via an influence on insulin secretion, suggesting that dysfunction of KIF12 may be involved in the progression of certain types of diabetes (Yang et al., 2014). This is supported by a study of Type 2 diabetes in the Qatari population which shows that *KIF12* gene was

among six genes found to harbour potentially deleterious low- frequency mutations (O'Beirne et al., 2018). Mutations in the *KIF12* gene have also been shown to be strongly correlated with paediatric cholestatic liver disease (Maddirevula et al., 2019, Ünlüsoy Aksu et al., 2019). This is a disease characterised by decreased bile flow due to impaired secretion by hepatocytes. The suggested association of KIF12 dysfunction with conditions such as cholestatic liver disease and reduced insulin secretion, together with its tissue distribution and localisation to the primary cilia, may indicate a general role for KIF12 in the function of secretory cells.

1.5 Cilia/Flagella

Cilia and flagella are membrane-bound organelles that protrude from the surface of cells and are found on most types of eukaryotic cells. Cilia and flagella are structurally conserved; however, they differ in length and/or function (Haimo and Rosenbaum, 1981). Flagella tend to be longer than cilia, always motile, and usually one per cell. Flagella have a function in cell locomotion; for example the flagellum of the sperm which provides a whip-like movement in order to move it forwards. Cilia are shorter and either motile, which usually exist in multiples on the cells, or non-motile (primary cilia) which usually present as single cilia. The function of the cilia depends on whether it is a motile or non-motile cilia. Motile cilia assist movement; one example for that exists in the epithelial cells that line the human respiratory tract, where cilia constantly move mucus up from the lungs to the back of the throat;

another exists in the fallopian tubes, where cilia move the eggs down the tube toward the uterus. Primary cilia and most motile cilia are function as sensors for mechanical and chemical environmental signals, which helps in regulating cellular physiological processes, such as tissue homeostasis and development (Plotnikova et al., 2009).

Cilia form from the basal body which provides a template for the formation of the axoneme. Axoneme consists of nine microtubule doublets (A and B tubules); A- tubule is a complete as it consists of 13 protofilaments, while B- tubule is incomplete where it is composed of 10 protofilaments. The outer doublets either surround a central pair of microtubules (9 + 2 pattern) as in motile cilia, or lack the central pair (9 + 0 pattern) as in primary cilia. The central microtubule pair are complete separate tubules rather than a doublet. Motile cilia also have dynein arms and radial spokes. The movement of motile cilia is powered by dynein arms, motors that hydrolyse ATP to generate sliding interactions between the microtubules of the outer doublets. Radial spokes are T-shaped structures that are visible as regularly distributed groups consist of three elements: RS1, RS2, and RS3. They are anchored perpendicularly to the A-tubule by the so-called stalk and extend the head toward the central pair. The stalk and head are connected by the so-called neck. Radial spoke are composed of at least 23 polypeptides (radial spoke proteins, RSP1–23) that function as a mechanochemical transducers between the central pair and the outer microtubule doublets (Yang et al., 2006, Pigino and Ishikawa, 2012).

The structure of cilia, motile and non- motile, is schematically depicted

in **Figure 1.6**. The ciliary structure described here will be focused on that of the primary cilium since *KIF12*, localises to the primary cilium.

1.5.1 Basal body and transition fibres

Primary cilia forms when the basal body (derived from the mother centriole) docks at the apical cell membrane via transition fibres and serves as a nucleation site for the growth of the axoneme microtubules (Reiter et al., 2012). The transition fibre is comprised of at least five proteins. These include CEP164, CEP83 (CCDC41), CEP89 (CCDC123 or Cep123), SCLT1 (sodium channel and clathrin linker 1) and FBF1 (Fas (TNFRSF6) binding factor 1). CEP83 is required for the localization of CEP89 and SCLT1 to centrioles, and the latter is required for localizing FBF1 and CEP164 (Tanos et al., 2013). All of these five transition fibres components are essential for basal body docking to a membrane and ciliogenesis (Tanos et al., 2013, Schmidt et al., 2012). The core of the basal body comprises a nine-fold microtubule-triplet cylindrical structures. Each triplet consists of three tubules; A-tubule being a complete microtubule with 13- protofilaments, B- and C- tubules are incomplete microtubules with only 10-protofilaments (Nicastro et al., 2011). The A- and B- tubules extend to form a transition zone (TZ) and, ultimately, the axoneme (**Figure 1.6**).

1.5.2 Transition zone

Transition zone (TZ) represents a structural junction between the basal body and the axoneme, and is part of a "ciliary gate" that controls protein entry and exit from this organelle. TZ is characterised by Y-

shaped linkers that extend from the outer microtubule doublets of the TZ to the ciliary membrane, and the ciliary necklace, a specialized membrane domain represented by rows of membrane particles encircling the base of the axoneme (Craigie et al., 2010, Reiter et al., 2012) (**Figure 1.6**).

1.5.3 Ciliary gate

Ciliary gate or “ciliary partitioning system” consists of a terminal plate, where the basal body C- tubule terminates (**Figure 1.6**), and it serves as a cytosolic “ciliary pore complex” (CPC). The gate also has a membrane region that serve as a diffusion barrier. The CPC is a plate-shaped structure containing nine pores via which the microtubule doublets of the basal body extend. Each pore expands from the doublet B-tubule into an opening well suited for filtering the passage of cytosolic material into and out of the cilia. The membrane diffusion barrier includes an extended region of periciliary membrane (ciliary pocket) and a ring complex that connects the CPC to the membrane (Ounjai et al., 2013, Ishikawa and Marshall, 2011).

1.5.4 Axoneme

The axoneme is the main extracellular part of the cilia in eukaryotes. It consists of nine microtubule doublets extended from A- and B- tubules of the basal body triplets (**Figure 1.6**). Microtubule doublets are crucial for the formation and function of cilia, where they form scaffolds for ciliary compartment. In addition, the length of the microtubule doublets controls that of cilia which is a determinant of the signalling capabilities of

cilia. Furthermore, they serve as tracks for transporting ciliary proteins necessary for the formation of functional cilia (Hu et al., 2015).

Microtubule doublets, like cytoplasmic microtubules, possess polarity with the plus end being the site of greater dynamism (Cassimeris et al., 1987, Marshall and Rosenbaum, 2001). Due to the unsynchronised nature of microtubule dynamics the microtubule doublets will differ in length towards the distal tip of the axoneme. For the same reasons, at the ciliary tip it is likely that many of the “doublets” will have become singlet structures.

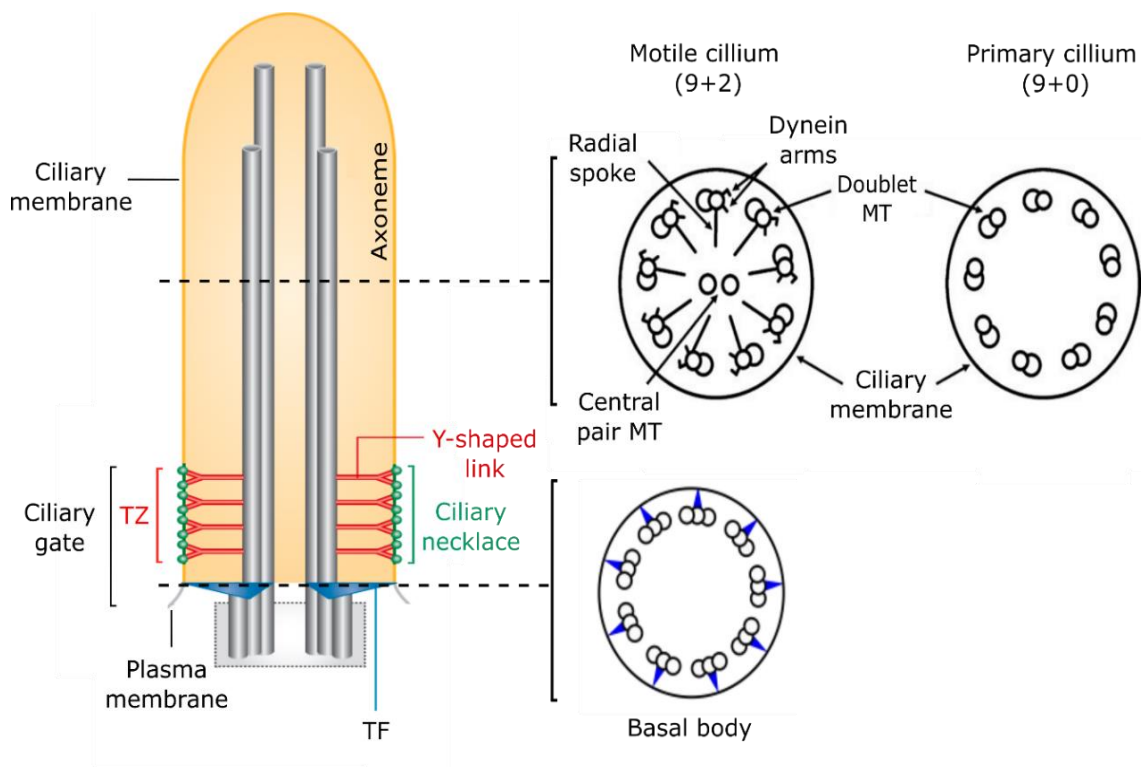


Figure 1.6. The structure of a cilium. Both types of cilia; motile or primary cilia are formed from the basal body. Transitional fibres (blue) attach the basal body to the base of the ciliary membrane. The area above the transition fibres is called transition zone (TZ) which contains Y-shaped proteins (red) that links the axoneme to the ciliary membrane. These proteins are decorated with the ciliary necklace (green). The TZ and a small region of the basal body is the site of the ciliary gate, a diffusion barrier that separate the cilium from the cytoplasm. For simplicity, the depiction of the cilium in the left panel only shows two outer doublet microtubules (grey tube) in the cilium axoneme and transition zone and two triplet microtubules (grey tubes) in the basal body. Right panel are cross-sectional diagrams showing views of motile and primary cilia and the basal body. A motile cilium usually contains one central pair of microtubules surrounded by nine outer microtubule doublets whereas primary cilium lacks the central pair microtubules. The doublets all vary in size with some becoming microtubule singlets towards the ciliary tip. Besides the central pair, motile cilia possess pairs of dynein arms and radial spokes, structures that assist in motility. The basal body has nine triplet microtubules each attached to a transition fibre. Image was modified from (Reiter et al., 2012, Deane and Ricardo, 2012).

1.6 Ciliogenesis

When a cell exits the cell cycle, mother centrioles are differentiated into basal bodies which dock onto the plasma membrane through transition fibres to nucleate the cilium. While migrating toward the cell membrane basal bodies attach to membrane vesicles and the basal body membrane vesicle complex eventually fuses with the plasma membrane of the cell. This fusion is likely what forms the ciliary membrane compartment. The axonemal microtubule doublets elongation is then initiated from the basal bodies beneath the developing membrane of the cilium. As primary cilia have no protein synthesising machinery, components required for building the axoneme, such as tubulin, must be transported from cytoplasm to the cilium. The process of selectively importing ciliary structural components to the cilia and delivering them

to the tip of the cilium is termed “intraflagellar transport”, which is a molecular motor-driven process discussed below (Ishikawa and Marshall, 2011, Kobayashi and Dynlacht, 2011). Ciliary growth is highly dynamic as when the elongation of microtubule doublets is completed new tubulin is continuously incorporated at the ciliary tip in steady-state (Marshall and Rosenbaum, 2001), however the doublets do not elongate further because the assembly is balanced by ongoing turnover (Marshall and Rosenbaum, 2001, Stephens, 1997, Song and Dentler, 2001). Disassembly of doublets at the tip is not likely to occur via spontaneous depolymerization but rather requires an active mechanism, which involves molecular motors, such as Kinesin-13s (Miyamoto et al., 2015).

1.7 Intraflagellar transport (IFT)

As mentioned above, the transport of ciliary proteins from the cytoplasm to the tip of the cilia is mediated by IFT, the bidirectional movement of multi-protein complexes, termed IFT particles or IFT trains, along the axoneme (Pedersen and Rosenbaum, 2008, Hao and Scholey, 2009).

1.7.1 Intraflagellar trains

IFT trains have been observed by electron microscopy to consist of a varying number of particles assembled into linear arrays that appear to contact the outer doublet B- tubules and the ciliary membrane (KozMINSKI et al., 1993, Kozminski et al., 1995) (**Figure 1.7**). They have been classified into two different groups; one group of relatively long IFT train, around 700nm in length, and another group of short train with a length of 250nm. These long and short IFT trains were proposed

to be involved into anterograde (from base to tip) and retrograde (from tip to base) transport, respectively, as the short trains were observed to disappear in a retrograde IFT mutant (Pigino et al., 2009). Direct imaging revealed that proteins of the ciliary matrix, membrane, and axoneme including tubulin, the major structural protein of cilia, transport through IFT trains (Lechtreck, 2015).

1.7.2 Intraflagellar motors

Movement of cargo proteins along microtubules is mediated by kinesin and dynein motor proteins either towards the plus end or towards the minus end of microtubule doublet. Members of the Kinesin-2 family carry IFT trains to the ciliary tip and they are returned to the cell body by cytoplasmic dynein 2 (Pedersen and Rosenbaum, 2008, Rosenbaum and Witman, 2002) (**Figure 1.7**).

1.7.3 Intraflagellar complex proteins

IFT complex proteins can be divided into two classes; IFT complex A and complex B (Piperno and Mead, 1997, Cole et al., 1998). IFT particles are consist of at least 20 proteins; six proteins were identified as IFT complex A particles, and 14 were found to belong to proteins IFT complex B (Hao and Scholey, 2009, Pedersen and Rosenbaum, 2008). The two IFT complexes play complementary but unique roles in the transport of ciliary proteins. IFT complex B plays a role in an anterograde transport and is fundamental for the assembly and maintenance of cilia and flagella (Qin et al., 2007, Pazour et al., 2000, Deane et al., 2001, Follit et al., 2006). By contrast, IFT complex A is

required for retrograde transport but it does not seem to be necessary for ciliary assembly (**Figure 1.7**) (Tsao and Gorovsky, 2008, Iomini et al., 2009, Tran et al., 2008). Additional proteins were found to interact with IFT complex and classified as IFT complex accessory proteins. For instance; proteins Bardet–Biedl syndrome (BBS) proteins (**Figure 1.7**). Loss-of-function mutations in these proteins were found to cause structural and functional ciliary defects. This could be because these mutations cause combined IFT particles to fragment into separate IFT complexes A and B, which are then transported separately by Kinesin-2 motors (Blacque et al., 2004, Ou et al., 2005). Although it remains unclear why separate transport of complexes A and B would cause ciliary defects, it was suggested that interaction between the two complexes may regulate some aspects of cargo transport.

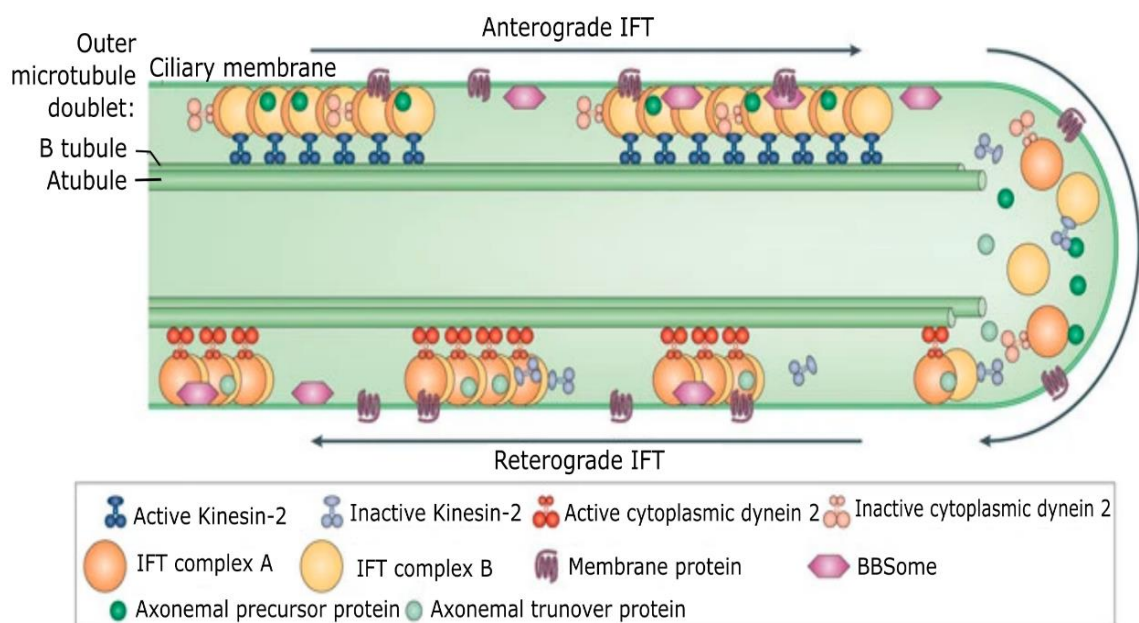


Figure 1.7. Intraflagellar transport (IFT) machinery. The anterograde intraflagellar transport (IFT) motor, heterotrimeric Kinesin-2, transports IFT complexes A and B, axonemal proteins and cytoplasmic dynein 2 to the tip of cilium. During this anterograde movement, Kinesin-2 is active and the retrograde motor, cytoplasmic dynein 2, is somehow kept inactive to allow smooth processive anterograde transport. At the tip of cilium, anterograde IFT trains release axonemal proteins and rearrange their conformation for retrograde IFT. Cytoplasmic dynein 2 is activated and moves retrograde IFT trains to the cytoplasm. Subsets of IFT trains are involved in transporting membrane proteins and the BBSome (a complex comprised of at least seven Bardet-Biedl syndrome proteins). Image is from (Ishikawa and Marshall, 2011).

1.8 Ciliary Kinesins

Several kinesins are involved in primary cilia-specific functions. The heterotrimeric Kinesin-2 motor appears to be the 'core' IFT motor for both generation and maintenance of cilia structure as disruption of Kinesin-2 function results in the loss of cilia in *Chlamydomonas*, *Tetrahymena*, *Drosophila*, *Xenopus*, sea urchin, trypanosomes and mouse (Rosenbaum and Witman, 2002, Scholey, 2008). The heterotrimeric Kinesin-2 that is composed of KIF3A and KIF3B associated with the accessory subunit KAP3 was found to mediate anterograde IFT through interactions with IFT-B complexes (Scholey, 2013, Nakayama and Katoh, 2018). The homodimeric Kinesin-2, KIF17, was shown to mediate anterograde IFT along the distal singlets of microtubules within the sensory cilia of the worm, and to be required for the assembly of this singlet region (Snow et al., 2004). KIF17 is also implicated in the delivery to the cilium of several membrane proteins with crucial functions in signalling. For instance, targeting of CNG channels and dopamine receptors to primary cilia of MDCK cells and

IMCD3 cells, respectively (Jenkins et al., 2006, Leaf and Von Zastrow, 2015).

In addition to their role in IFT, several kinesins have more recently been shown to function in regulating the length of the axoneme or in the disassembly of the axoneme during cell cycle re-entry. For instance, Kinesin-4, KIF7 which is a conserved regulator of the Hh signalling pathway in mammalian cells. KIF7 localizes to the cilium tip, the site of microtubule plus ends, where it limits cilium length and controls cilium structure. In vitro, purified recombinant KIF7 binds the plus ends of growing microtubules, where it reduces microtubule growth rate and increases the frequency of microtubule catastrophe. KIF7 is not required for intraflagellar transport of Hh pathway proteins into cilia. Instead, a central function of KIF7 in the mammalian Hh pathway is to control cilium architecture and to create a single cilium tip compartment, where Hh proteins activity can be correctly regulated (He et al., 2014). Other examples include Kinesin-13, KIF2A which was shown to be involved in the disassembly of primary cilia upon cell cycle entry via its depolymerisation activity at the mother centriole (Miyamoto et al., 2015). KIF24 which was shown to play a role in regulating centriolar length and ciliogenesis by possessing a microtubule depolymerising activity specific to centriolar microtubules (Kobayashi et al., 2011).

Klp10A which is a kinesin-13 of *Drosophila melanogaster* that acts as a microtubule depolymerase on centriolar microtubules to regulate centriole length (Delgehyr et al., 2012).

Aims

To explore the cellular function of *KIF12*, I expressed and purified a truncated version of *KIF12*, as full-length *KIF12* was found insoluble, and characterised its interaction both with microtubules and with nucleotide by using microtubule- and nucleotide- based assays explained in Chapter 2. I started by looking at translocating, microtubule- depolymerising, and microtubule dynamics regulating activities of *KIF12 in vitro*, and I also looked at the ATP turnover as shown in Chapter 3. To see if *KIF12* tail has a role in the interaction of *KIF12* with microtubules I expressed, purified, and characterised *KIF12* tail using a microtubule-based assay as shown in Chapter 3. I also tried to characterise the ATP cycle of *KIF12* in the presence of both unpolymerised tubulin and microtubules as show in Chapter 3. To determine the impact of a deletion mutation (Δ PPGGG) which is located in *KIF12* motor domain on *KIF12* activity I expressed, purified, and characterised *KIF12* with this mutation as shown in Chapter 4. In Chapter 5, I transfected full-length *KIF12* in mammalian cell line in an attempt to obtain a soluble full length protein and used it in *in vitro* assays used to characterise the truncated version. This chapter also shows my attempt to confirm the translocating activity seen for *KIF12 in vitro* by comparing it to that seen in cells, and my attempts to see *KIF12* localisation in cell and measure the impact of *KIF12* on microtubule dynamics.

Chapter 2 Methods

2.1 Cloning using USER™ (uracil-specific excision reagent)

The power of USER cloning lies in the ability to generate long, complementary overhangs in both PCR product and vector. These overhangs can anneal to each other to form a stable hybridization product that can be used to transform bacterial cell without prior ligation. Most importantly, the overhangs on the PCR fragments are custom-made and their generation is not dependent on the introduction of restriction sites. To create constructs of KIF12-472, KIF12 tails [434-651], KIF12 tail [478-651], and full length KIF12 with visualisation and purification tags USER primers were required (Integrated DNA Technologies). USER primers contain a short (~8 nt) sequence that ends in a single deoxyuridine residue is included as an upstream extension in each primer used to amplify the target DNA (Nour-Eldin et al., 2010), see **Appendix 2**. PCRs were carried out using PfuTurbo Cx Hotstart DNA Polymerase (Agilent Technologies) in PfuTurbo Cx reaction buffer containing a final concentration of 2 ng/μl double stranded pFastBac containing the DNA template, 2 ng/μl forward primer, 2 ng/μl reverse primer, 0.2 mM dNTP mix, 2 % (v/v) DMSO. Control reactions without primers and without polymerase were also set up. The reactions were started at 95 °C for 5 minutes and then went through 25 cycles of 95 °C for 30 seconds, 55 °C for 1 minute and 3 minutes at 72 °C. At the end of the cycles the reaction was held at 4°C. To each PCR reaction DpnI (New England Biolabs) was added to a final concentration of 2 U/μl, and incubated for 1 hour at 37°C to digest the original plasmid DNA

template. DpnI was inactivated by heating to 80°C for 20 minutes. The PCR product size was checked by running the digested PCR products on a 1% agarose gel. Plasmids for cloning (pFastBac10/pFastBac11 /pFB-Skin0-GFP/PCMV) were linearized by adding 1µl XbaI to 5µg plasmid DNA in NEBuffer, and the reaction was incubated overnight at 37°C. Next, a further 0.5µl XbaI was added to the reaction, then 1µl Nt.BbvCI was added and the reaction was incubated for 2 hours at 37°C to nick the XbaI-linearized vector. Digested vectors were purified using the QIAquick PCR Purification Kit.

USER reaction was initiated by mixing 10µl of each DpnI-digested PCR product with 1µl open plasmid (pFastBac10/pFastBac11/pFB-Skin0-GFP/PCMV) (20 ng) and 0.5µl USER enzyme (1000 u/ml), and incubating for 15 minutes at 37°C. USER reactions were incubated for 15 minutes at room temperature. 2µl of each reaction was added to 50µl XL10 Gold competent cells (made using the Inoue method (Inoue et al., 1990)), incubated on ice for 30 minutes, heat shocked at 42°C for 40 seconds then incubated on ice for 2 minutes. 0.5ml LB (Luria-Bertani) was added to each mixture and incubated at 37°C with shaking at ~225rpm for 1 hour, spun down at 2000rpm for 5 minutes, 350µl was removed from supernatants, cell pellet was resuspend in remaining supernatants. Cells were plated on ampicillin containing LB-agar plates and incubated overnight at 37°C. A single colony was grown up in 5ml LB- broth containing ampicillin (0.1 mg/ml) with shaking at 225 rpm for overnight at 37°C. The cells were centrifuged at 4000rpm for 5 minutes and the supernatant was removed. The DNA was extracted from the cell pellet

using the QIAPREP SPIN Miniprep kit (Qiagen) and sequenced. DNA sequencing was carried out by Source-BioSciences.

2.2 Cell culture and protein expression in insect Sf9 and HEK293a cells

2.2.1 Sf9 Cell culture

Spodoptera frugiperla (Sf9) cells were grown in Insect-XPRESS™ protein-free insect cell medium (Lonza), supplemented with 200 units/ml penicillin, 0.2 mg/ml streptomycin and 10 % (v/v) fetal bovine serum (FBS), in suspension incubated at 27°C with an orbital shaking at 150 rpm.

2.2.2 Transformation of DH10Bac

Recombinant pFastBac10 with KIF12-472, pFastBac10/pFastBac11/pFB-Skin0-GFP each with KIF12 tail [434-651]/KIF12 tail [478-651] were transformed into DH10Bac cells. The pFastBac has the *Autographa californica* multiple nuclear polyhedrosis virus (AcMNPV) polyhedrin promoter which permits high levels of protein expression in Sf9 cells, and is flanked by Tn7. DH10Bac cells contain bacmid with an *attTn7* target site and a helper plasmid. When pFastBac plasmid was transformed into DH10Bac cells, transposition occurs between the Tn7 site on pFastBac vector and the *attTn7* target site on the bacmid with the help of transposition proteins including transposase generated by the helper plasmid. This produces a recombinant bacmid with the desired gene, which is then purified. The bacmid DNA was then transfected into Sf9 insect cells to generate recombinant baculovirus

which contains the gene of interest, and then used to infect Sf9 cell culture to produce the desired KIF12 constructs. Insect cells have chaperones which assist KIF12 correct folding and also possess the ability to modify the proteins post-translationally.

In brief, 1 μ l of the each recombinant vector was added to 50 μ l of DH10Bac cells, the mixture was incubated on ice for 30 minutes, heat-shocked the by transferring to 42°C water bath for 45 sec, chilled on ice for 2 minutes. 900 μ l room temperature LB media was added to the mixture, incubated at 37°C with shaking at 170 rpm for 4 hours. The cells were spun down for 10 minutes at 1300 rpm to pellet the cells, the supernatant was poured off and cells were resuspend in remaining medium, and spread all onto the LB agar plates containing 30 μ g/ml kanamycin, 7 μ g/ml gentamicin, 10 μ g/ml tetracycline, 100 μ g /ml 5-bromo-4-chloro-3-indolyl- β -D-galactopyranoside (X-gal) and 40 μ g/ml isopropyl β -D-1-thiogalactopyranoside (IPTG). The plates were incubated for 72 hours at 37°C. White large colonies (containing the recombinant bacmid) were picked and restreaked onto a fresh plate and incubated overnight at 37°C to confirm the phenotype as the restreaking showed no blue colonies. From each restreaked colony a 5ml overnight culture was made, these cultures were used to prepare glycerol stocks by adding glycerol to give a final glycerol concentration of 15% (v/v), and they were stored at -80°C.

2.2.3 Baculovirus production

A 5ml overnight culture was made from glycerol stocks of transformed DH10Bac cells, and bacmids were isolated using Zymo ZR BAC DNA Miniprep kit and stored at 4°C overnight. 2 ml of Sf9 cells at 0.5×10^6 cells/ml were transferred into each well of a 6 well plate and left to adhere for 1 hour. Meanwhile, 5µl of bacmid was diluted into 500µl Xpress media (serum and antibiotic free), and 5µl of Escort IV transfection reagent (Sigma L-3287) was diluted into 500µl of Xpress media (serum and antibiotic free) for each transfection. The Escort IV mix was then added to the bacmid mix and incubated for 15-45 minutes at room temperature. The media of the plated cells was removed and cells were washed with 1 ml of fresh Xpress media, the transfection mix (bacmid and Escort IV) was added to the cells, and incubate for 5 hours at 27°C. After 5 hours the transfection mix was removed and replaced with 3ml supplemented Xpress media containing 2% (v/v) FBS and 2% (v/v) antibiotic, the plate was incubated at 27°C for 5 days (transfected cells showed up bright green under fluorescent microscope). After that, the cell suspension was removed and spun down at 1300 rpm for 5 minutes and 1 ml of the supernatant was used to infect 50 ml Sf9 cell suspension at 0.5×10^6 cells/ml in media containing 2% antibiotic. The cells were monitored to harvest them at a point when they made a large amount of the virus but had not lysed. To accomplish this, cell number and diameter were measured at 24 and 42 hours using MOXI cell counter. When the mean diameter of the transfected cells reached 17-18µm compared to uninfected cells (15-16 µm), cells were spun down at

1500rpm for 5 minutes, resuspended in 2.5 ml of Xpress media supplemented with 10% DMSO and 2% antibiotic, aliquoted in 500 μ l aliquots in cryotubes, frozen down in a -80 $^{\circ}$ C freezer using a -1 $^{\circ}$ C/minute cooling rate rack (Mr Frosty), and transferred to LN₂ for long term storage. This is referred to as a BIIC (Baculovirus infected insect cell) stock.

2.2.4 Protein expression

KIF12-434/ KIF12 -434 Δ PPGGG / KIF12-472/ KIF12 tail [434-651]/ KIF12 tail [478-651] each was expressed by adding 100 μ l of baculovirus infected insect cells (BIIC stocks for KIF12-434 and KIF12 Δ PPGGG-434, supplied by C. Friel) to 300ml of the cell suspension at $\sim 1 \times 10^6$ cells/ml in a media containing 2% (v/v) antibiotic. After incubation for 72 hours at 27 $^{\circ}$ C with shaking at 150 rpm, cells were harvested by centrifugation at 4000 rpm for 10 minutes, resuspended in 2ml cold lysis buffer (50 mM Tris pH 7.5, 300 mM NaCl, 10 % glycerol, 5 mM MgCl₂, 0.1 % Tween 20, 10 mM Imidazole, 1 mM DTT, and 1 mM ATP)/ g cell wet weight and frozen as drops in liquid nitrogen to form cell pearls, which were stored at -80 $^{\circ}$ C.

2.2.5 Protein solubility

To compare the solubility of KIF12-434 Δ PPGGG to that of wild type KIF12-434, 0.5g of the cell pellet was dissolved in 6ml lysis buffer (50mM Tris pH 7.5, 300mM NaCl, 10% glycerol, 5mM MgCl₂, 0.1% Tween 20, 10mM Imidazole, 1mM DTT, 1mM ATP, 5 μ g/ml Leupeptin, 0.7 μ g/ml Pepstatin A, 18 μ g/ml PMSF). The lysed cells were incubated at

4°C for 30 minutes, and 10µl was removed for SDS-PAGE analysis. The lysed cells were then centrifuged at 20000 rpm for 1h at 4°C. 10µl of each sample: cell lysate, cleared lysate, and cell pellet were prepared for SDS-PAGE and gel running were carried out as described in (2.4) except that the samples were boiled for 30 minutes before loading onto the gel.

2.2.6 HEK293a cell culture

HEK293a cells (supplied by A. Hume) were propagated in 75cm² TC flask in Gibco Dulbecco's Modified Eagle Medium (DMEM) (Thermo Fisher), supplemented with 10% (v/v) FBS and 2 % (v/v) penicillin/streptomycin, 4mM L-Glutamine in a humidified incubator at 37°C, supplemented with 5% CO₂.

2.2.7 HEK293a cell transfection and protein expression

At ~50% confluency cells were washed with 8ml prewarmed Dulbecco's Phosphate Buffered Saline (DPBS) (Sigma), and replaced with 8ml prewarmed Gibco Opti-MEM™ I Reduced Serum Medium (Thermo Fisher) 30 minutes before transfection. Meanwhile, all reagents required for the transfection were warmed to room temperature. Two aliquots of 2ml Opti-MEM were made (A and B). To tube (A) 55 µl of Lipofectamine 3000 reagent was added, and to tube (B) 18µg plasmid DNA (full length KIF12-pCMV) was added then 48 µl of P3000 enhancer reagent, both tubes were briefly vortexed, and spun down. All the contents of tube B were added to tube A, mixed by brief pipetting, and incubated for 20 minutes. This mixture was added to the cells in a dropwise manner, and

incubated at 37°C and 5% CO₂. 24 hours post- transfection, Opti-MEM media was replaced by 16ml DMEM, supplemented with 10% (v/v) FBS and 2% (v/v) penicillin/ streptomycin, and 4mM L-Glutamine. 2 days post-transfection cells were washed with 1x DPBS, detached with 0.05% trypsin and collected in PBS. To remove trypsin, cells were washed once more with 1x DPBS and cold centrifuged. Cell pellet was stored at -80 °C.

For still- and live-cell imaging, HEK293a cells were seeded onto glass-coverslip placed into a well of a 6-well plate and glass-bottomed dishes (MatTek), respectively. For still- cell imaging, cells were either transfected with a plasmid for expression of KIF12-GFP or for only GFP as a control. For live- cell imaging, cells were co-transfected with plasmids for expression of mCherry-tubulin (supplied by S. Wheatley) and KIF12-GFP. Transfection was carried out as described above for protein expression except that the volumes of the required reagents were scaled down. At ~50% confluency cells were washed with 2ml prewarmed 1x DPBS, and replaced with 2ml prewarmed Opti-MEM 30 minutes before transfection. Two aliquots of 125µl Opti-MEM were made (A and B). To tube (A) 6 µl of Lipofectamine 3000 was added, and to tube (B) 5µg plasmid DNA (for co-transfection 2.5 µg of KIF12-GFP and 2.5 µg of mCherry-tubulin plasmid DNAs were mixed) was added, followed by adding 6 µl of P3000 enhancer, both tubes were briefly vortexed, and spun down. All the contents of tube B were added to tube A, mixed by brief pipetting, and incubated for 20 minutes. This mixture was added to the cells in a dropwise manner and incubated for

overnight at 37°C and 5% CO₂. Opti-MEM media was then replaced by 2ml DMEM supplemented with 10% (v/v) FBS and 2% (v/v) penicillin/streptomycin, and 4mM L-Glutamine and incubated at 37°C and 5% CO₂ for overnight. Cells seeded onto glass-bottomed dishes were then live-imaged, and those seeded onto glass-coverslip were washed with 1x DPBS prior to cell fixation.

Live-cell imaging was carried out as using an inverted total internal reflection super-resolution microscope (Elyra) equipped with EMCCD AndorPALM camera, an alpha-Plan-Apochromat 100x1.46 N.A. oil immersion DIC M27 objective, HD diode 488nm and HD DPSS 561nm lasers. The TIRF angle was adjusted for maximum penetration for the evanescent field into the cells. Images were acquired using ZEN 2012 SP5 software in both 488nm and 561nm channels every 200ms for 60 seconds.

2.2.8 Cell fixation

Cells seeded onto glass-coverslip and washed with 1x DPBS were incubated with 4% (v/v) paraformaldehyde (MP Biomedicals) in 1x DPBS for 15 minutes, washed three times with 1x DPBS, and coverslip was immersed in 50mM NH₄Cl for 10 minutes. Cells were then mounted onto glass slide using ~6µl of mounting medium (GeneTex), and incubated for 1 hour at room temperature to give the mounting medium time to harden, then stored at 4°C. Cells used for live-cell imaging were also fixed following the same method up to incubating in 50mM NH₄Cl. Confocal imaging was performed using super-resolution microscope

(ZEISS Elyra) equipped with EMCCD camera, an alpha-Plan-Apochromat 63x/1.4 N.A oil DIC M27 objective and 488nm and 561nm lasers.

Images were acquired using ZEN 2012 SP5 software in both 488nm and 561nm channels.

2.3 Protein purification

2.3.1 One step purification of KIF12-His6 proteins

KIF12-434, KIF12-434 Δ PPGGG, KIF12-472 and KIF12 tail [434-651] were purified using a **nickel** affinity chromatography column.

Approximately 5g of cell pearls were lysed by adding 15ml lysis buffer (50mM Tris pH 7.5, 300mM NaCl, 10% glycerol, 5mM MgCl₂, 0.1% Tween 20, 10mM Imidazole, 1mM DTT, 1mM ATP, 5 μ g/ml Leupeptin, 0.7 μ g/ml Pepstatin A, 18 μ g/ml PMSF), and incubating at 4°C for 30 minutes on a roller. The cell lysate was centrifuged at 20,000 rpm for 60 minutes, and cleared lysate was loaded onto a **nickel** affinity column (Biorad). The column was washed with 60mM Imidazole nickel affinity buffer (50mM Tris pH 7.5, 300mM NaCl, 10% glycerol, 1mM MgCl₂). The protein was eluted with 200mM Imidazole **nickel** affinity buffer, and collected in fractions of \sim 500 μ l. The protein aliquots were snap frozen in liquid nitrogen and stored at -80 °C until further use.

Full length KIF12 was purified using Ni-NTA Agarose beads (QIAGEN).

Cells were resuspended in 800 μ l cold lysis buffer (50mM Tris pH 7.5, 300mM NaCl, 10% glycerol, 5mM MgCl₂, 0.1% Tween 20, 10mM Imidazole, 10mM DTT, 1mM ATP) supplemented with protease inhibitors; 5 μ g/ml Leupeptin, 0.7 μ g/ml Pepstatin A, 18 μ g/ml PMSF or

proteases inhibitor cocktail tablet (Roche)), and incubated on ice for 15 minutes with occasional pipetting to break cells. The lysate was centrifuged at 18,500g for 15 minutes at 4 °C. The supernatant was added to 250 µl pre-equilibrated Ni-NTA Agarose beads with lysis buffer and incubated for 45 minutes at 4 °C by slow rotation. The beads were washed 3 times in 60mM Imidazole **nickel** affinity buffer. The protein was eluted with 100–250 µl 200mM Imidazole **nickel** affinity buffer. Eluted protein was aliquoted, snap-frozen in liquid nitrogen and stored at -80 °C.

The purity of the proteins were assessed using SDS-PAGE. The concentration of the proteins were determined by making serial dilutions of the protein in the elution buffer, and measuring the absorbance at 488nm using spectrophotometer as all proteins were GFP-labelled. The absorbance was plotted against dilution. The linear part of the data was fit to a line and used to calculate the absorbance of the undiluted protein stocks. To convert absorbance into molar concentration of the protein stock the following equation was used:

$$C=A / (\epsilon \times I)$$

Where, c=concentration; A= absorbance; ϵ = the extinction coefficient for GFP= 56,000 M⁻¹cm⁻¹; I = path length of the cuvette (1cm).

2.3.2 Two step purification of KIF12-His6 and StrepII/SBP proteins

KIF12 tail [434-651] and tail [478-651] were purified by **nickel** and StrepTactin affinity chromatography. **Nickel** affinity chromatography based purification was carried out as described above for KIF12-434,

KIF12 Δ PPGGG-434 and KIF12-472. Proteins eluted from **nickel** affinity purification incubated with 0.5ml pre-washed StrepTactin Sepharose High Performance beads (GE Healthcare) for 1 hour, transferred into a gravity column, and the supernatant was allowed to flow through. The beads were washed with 5ml BRB20, 75mM KCl, 0.1% Tween 20, and the proteins were eluted in BRB20, 75 mM KCl, 0.1% Tween 20, 10% glycerol, 5mM d-Desthiobiotin, aliquoted, snap frozen, and stored in -80°C.

2.4 Expression of Kinesin-1

Kinesin-1 (rKIN430GFP) in pET-17b was supplied by Stefan Diez, Centre for Biomolecular Engineering TU Dresden, Germany. Glycerol stock of *E.coli* BL21 transformed with the plasmid was used to grow single colonies on LB agar plate containing ampicillin (0.1 mg/ml) incubated at 37 °C overnight. A 5 ml LB culture containing 50 μ M ampicillin was made from a single colony and incubated at 37 °C overnight. LB supplemented with 100 μ g/ml ampicillin was inoculated with transformed BL21 cells and incubated overnight at 37 °C. This culture was then spun down at 4000rpm and resuspended in 700ml of fresh LB containing 50 μ M ampicillin and incubated at 37 °C with 220 rpm shaking to an OD of 0.6. The cells were cooled to 18 °C and induced by adding 1 mM isopropyl- β -d-thio galactopyranoside (IPTG), and grown for additional ~16 h at 18 °C with shaking at 220rpm. The cells were harvested by centrifugation for 10 minutes at 4000rpm, the pellet was collected, snap frozen in liquid nitrogen and stored at -80°C.

2.5 Purification of Kinesin-1

The cell pellet was resuspended in a 100 ml lysis buffer 50 mM Sodium phosphate buffer (Na_2HPO_4 and NaH_2PO_4 titrated to pH 7.5), 100 mM NaCl, 1 mM MgCl_2 , 5 mM 2-mercaptoethanol (BME), 10 μM ATP, and protease inhibitor cocktail tablet (Roche). The cells were lysed by passing through a cell disrupter (Constant Systems) at 35 kpsi. Cell lysate was centrifuged at 75,000g for an hour. The cleared lysate was loaded onto a prepacked Hi Trap Q column (GE Healthcare), and washed with 10 ml with ion exchange buffer (50 mM PIPES pH 6.9, 5 mM MgCl_2 , 1 mM DTT). The column was then washed with 100 mM NaCl ion exchange buffer, and the protein was eluted in 10 ml 200 mM NaCl ion exchange buffer. The elution was loaded onto a HisTrap HP column (GE Healthcare). The column was washed with 10 ml 75 mM Imidazole **nickel**-affinity buffer (50 mM Sodium phosphate buffer pH 7.5, 300 mM KCl, 5% glycerol (v/v), 1 mM MgCl_2 , 10 mM BME, 0.1 mM ATP). The protein was eluted in 4ml 300 mM Imidazole **nickel**-affinity buffer with 10 mM ATP and 10% (w/v) sucrose, and collected in fractions of approximately 300 μl , snap frozen, and stored at -80°C . The purity of the fractions was evaluated using SDS-PAGE (see SDS-PAGE section). The concentration of rKIN430GFP was determined using the Bradford assay.

2.6 Sodium dodecyl sulphate polyacrylamide gel electrophoresis (SDS-PAGE)

Protein samples were mixed with an equal volume of sample buffer (0.16 M Tris HCl pH 6.8, 4% (w/v) SDS, 20% (v/v) glycerol, 5% (v/v) β -mercaptoethanol), incubated for 10 minutes at 70°C, and separated by electrophoresis using a 10% polyacrylamide gel (Sure-Page, Bis-Tris, 10×8) and TRIS-MOPS running buffer (50mM MOPS, 50mM TrisBase, 0.1% SDS, 1mM EDTA, pH 7.7). Gels were run at 150 V for ~1 hour, and stained with Instant Blue (Expedeon).

2.7 Preparing tubulin

2.7.1 Cycling tubulin

To prepare tubulin that was both polymerisation and depolymerisation competent, 4ml purified tubulin (supplied by C. Friel) was polymerised in BRB80, 30% glycerol (v/v), 1mM GTP, 4mM MgCl₂ at 37°C for 1 hour. The polymerised microtubules were centrifuged through a cushion of 60% glycerol in BRB80 (v/v) at 50,000 rpm for 1 hour at 37°C. Supernatant and cushion were removed, and pellet was rinsed with BRB80 and incubated on ice in the minimum volume of BRB80 with 0.1% BME for 20minutes to depolymerise the microtubules. The pellet was then resuspend by pipetting and centrifuged at 50,000 rpm for 15 minutes at 4°C. The supernatant was collected, aliquoted, snap frozen, and stored at -80 °C. Tubulin concentration was measured on a spectrophotometer, using $\epsilon=115,000 \text{ M}^{-1} \text{ cm}^{-1}$ (Desai and Mitchison, 1998).

2.7.2 Labelling tubulin

Rhodamine labelled tubulin was provided by C. Friel.

2.8 Assembling microtubules

2.8.1 Microtubules for microscopy

2.8.1.1 GMPCPP stabilised microtubules

Microtubules were prepared by mixing 10 μ M tubulin (25 % rhodamine labelled), 1 mM GMPCPP and 1 mM MgCl₂ in BRB80 (80mM PIPES/KOH pH 6.9, 1mM MgCl₂, 1 mM EGTA) in a total volume of 50 μ l. The mixture was incubated on ice for 5 minutes, followed by 2 hours at 37 °C. The polymerized microtubules were diluted in 200 μ l BRB80, and centrifuged through a cushion of 40% glycerol in BRB80 in an airfuge (Beckmann Coulter) at 10 psi (90,000 rpm) for 10 minutes, and the pellet resuspended in 400 μ l BRB80.

Microtubule seeds for microtubule dynamic assay were prepared in the same way as for GMPCPP microtubules except that 10 μ M tubulin (5% rhodamine-labelled tubulin, 4% biotinylated tubulin) was used.

2.8.1.2 Taxol stabilised microtubules

~32 μ M tubulin (5% rhodamine labelled) was mixed with 1mM GTP, 4mM MgCl₂, and 5% DMSO in BRB80 (final volume of 12.5 μ l), and incubated at 37°C for 30 minutes. 5 μ l of 1mM Taxol in DMSO was added to 495 μ l BRB80, then 5 μ l of this solution was removed. At the completion of polymerization time, 5 μ l of the polymerised microtubules was added to the 10 μ M Taxol solution (495 μ l), immediately vortexed for 5 second, and spun in the airfuge (Beckman) at 30psi for 5 minutes.

The supernatant was removed, and microtubules were resuspended in 200µl 10µM Taxol- BRB80.

2.8.2 Double-cycled freezable microtubules

20 µM tubulin was mixed with 1mM GMPCPP BRB80, incubated on ice for 5 minutes, then at 37 °C for 30 minutes. The microtubules were spun in an airfuge at 90000 rpm for 5 minutes at 25°C. The pellet was resuspended in 720ul BRB80 and incubated on ice for 20 minutes.

Microtubules were centrifuged at 13000rpm for 2 minutes at 25°C and 80 µl 1mM GMPCPP was added. The mixture was incubated on ice for 5 minutes, then at 37°C for 30 minutes. Microtubules were spun in the airfuge at 90000 rpm 5 minutes at 25°C, and resuspended in 420µl BRB80, aliquoted, snap frozen, and stored in liquid nitrogen. The concentration of tubulin was calculated by measuring the absorbance at 280nm using a spectrophotometer and the extinction coefficient $\epsilon=115,000 \text{ M}^{-1} \text{ cm}^{-1}$ (Desai and Mitchison, 1998).

2.9 Silanisation of coverslips

Glass coverslips were initially soaked in acetone with sonication for 20 minutes, then in methanol with sonication for 20 minutes, and washed with nanopure water. This was followed by cleaning in KOH where the coverslips were soaked in 1M KOH with sonication for 1 hour, washed repeatedly with nanopure water, soaked in acetone with sonication for 20 minutes, then in methanol with sonication for 20 minutes, and rinsed in nanopure water. Thereafter, the coverslips were soaked in 5M KOH with sonication for 1 hour, rinsed repeatedly with nanopure water, and

blow-dried using N₂ prior to silanization in 0.05% dichlorodimethylsilane in trichloroethylene for 1 hour. The silanized coverslips were submerged in methanol with sonication for 5 minutes, then in a fresh methanol with sonication for 15 minutes, then in a fresh methanol with sonication for 30 minutes, and blow-dried using N₂.

2.10 Microtubule gliding assay

Flow-chamber was constructed using 18mm x 18mm and 22mm x 22mm silanized coverslips separated by typically four stripes of double-sided tape (Scotch 3M) to define three channels (0.1mm thick, 3mm wide and 18mm long) as shown in **Figure 2.1**.

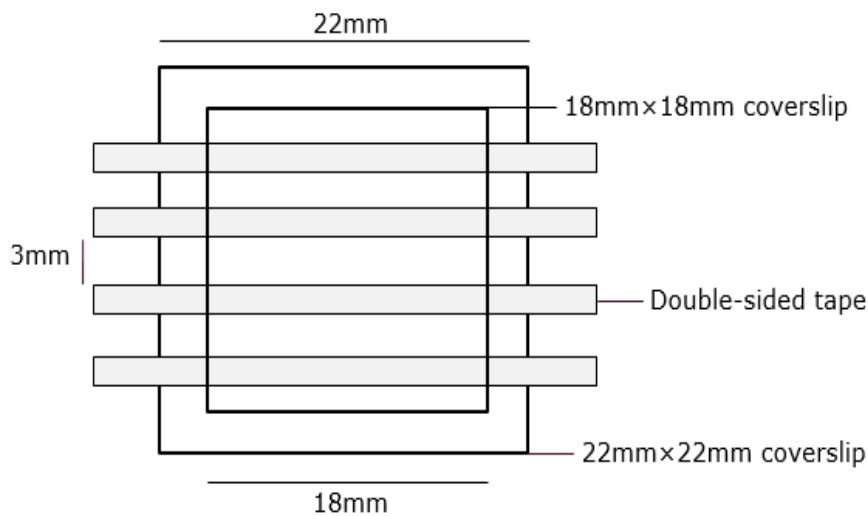


Figure 2.1. Construction of channels for microtubules gliding assay. An 18mm x 18mm silanized coverslip is stuck on a silanized 22mm x 22mm coverslip by strips of double-sided tape laid in between to form flow channels.

Flow channels were incubated with 20 μ l 20 μ g/ml penta-His antibodies (Sigma, 1:100 in BRB80) for 5 minutes (**Figure 2.2 A**), then 20 μ l blocking buffer (0.2% Tween in BRB80) for 5 minutes (**Figure 2.2 B**), followed by 20 μ l 52 μ M His tagged KIF12-434 diluted 1 in 10 in reaction buffer (BRB80, 0.2% Tween 20, 1 mM ATP/Mg²⁺, 0.1 mg/ml bovine serum albumin, 40 mM α -D-glucose, 40 μ g/ml glucose oxidase, 16 μ g/ml catalase, 1% 2-mercaptoethanol) for 5 minutes (**Figure 2.2 C**). 20 μ l GMPCPP stabilized microtubules polymerized as described in (2.8.1) in reaction mix were then added (**Figure 2.2 D**) and incubated until they were observed in a density that was suitable for the subsequent analysis then washed with 20 μ l reaction mix. Imaging was carried out by Zeiss 200M equipped with a CoolSNAP MYO camera and 100x (1.46 NA) oil-immersion objective and TRITC filter was used. Images were taken at a frame every 5 second for 7 minutes. From these image stacks kymographs were produced. Kymographs show an individual microtubule over time, allowing the change over time to be shown in a single 2D image. The microtubule is shown at the top of the image and the same slice from a time series of images is shown underneath. Kymographs were generated to show how KIF12-434 interacting microtubules behaved as they did not show directional motility as Kinesin-1 interacting ones.

The velocity of microtubule movement by kinesin-1 was measured using a maximum intensity projection method via image-processing Fiji software. Analysis included production three-colour overlay of maximum intensity (depicts the trajectories of gliding microtubules), first frame,

and last frame of a stack. The velocity was indirectly measured by dividing the microtubule travelled distance by the time between the first frame and last frame (Gell et al., 2010). The average of the obtained velocities was calculated using IGOR PRO 7.04 software.

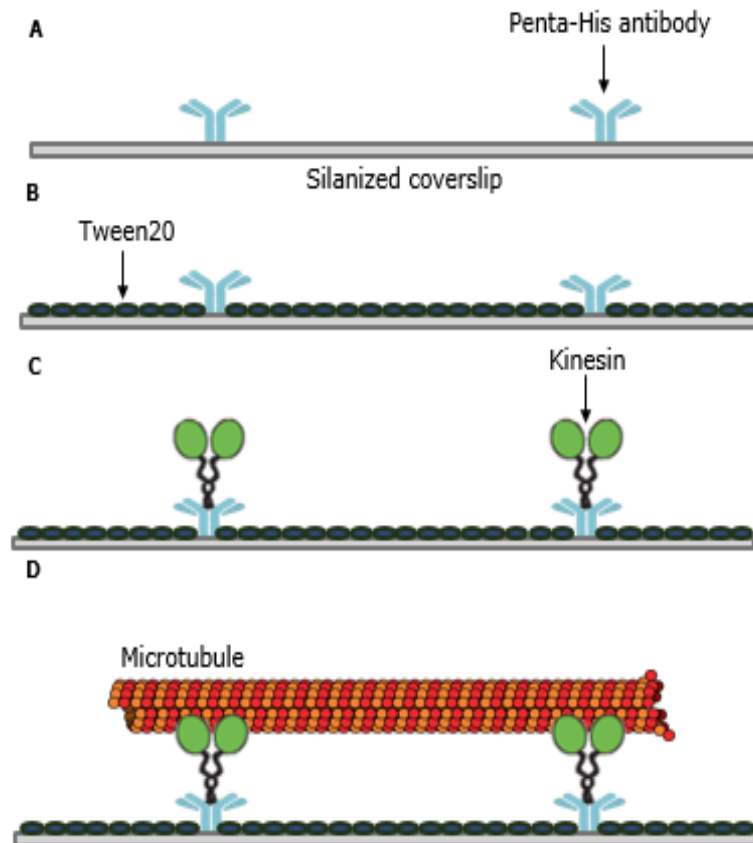


Figure 2.2. Gliding assay setup. A) 20 μ g/ml penta-His antibodies in BRB80 were first added to the constructed channel made of silanized coverslip, followed by; B) 0.2% Tween 20 in BRB80, C) reaction mix (BRB80, 0.2% Tween 20, 1 mM ATP/Mg²⁺, 0.1 mg/ml bovine serum albumin, 40 mM α -D-glucose, 40 μ g/ml glucose oxidase, 16 μ g/ml catalase, 1% 2-mercaptoethanol) containing his tagged KIF12-434, reaction mix wash, and D) reaction mix containing rhodamine-labelled microtubules.

2.11 TIRF microscopy for stepping assay

The flow channels were constructed in the same way as with the microtubule gliding assay (**2.10**). Flow cell was first incubated with 20 μ l anti- β tubulin antibody (Sigma, mouse, 1:200 in BRB80) for 5 minutes (**Figure 2.3 A**), washed with 20 μ l BRB80, then with 20 μ l blocking buffer (0.02% Tween 20 in BRB80) incubated for 5 minutes (**Figure 2.3 B**), 20 μ l GMPCPP-stabilised microtubules grown as described in (**2.8.1**) were then added to the channel and incubated for 5 minutes, then washed with 20 μ l reaction mix (BRB20, 0.2% Tween 20, 1 mM ATP/Mg²⁺ or AMP-PNP, 0.1 mg/ml bovine serum albumin, 40 mM α -D-glucose, 40 μ g/ml glucose oxidase, 16 μ g/ml catalase, 1% 2-mercaptoethanol) (**Figure 2.3 C**). 20 μ l GFP-tagged KIF12-434 in reaction mix at a concentration of 0.3 or 1.6 nM was then added to the channel (**Figure 2.3 D**). The imaging was conducted using Zeiss Observer Z1 microscope with a Zeiss TIRF 3 module, QuantEM 512SC EMCCD camera (Photometrics), Zeiss filter sets 20 and 38, and using a 100 x objective lens (Zeiss, alphaPlanApo/ 1.46NA oil). The frame rate was a frame every 100ms for 20 seconds. From these frame stacks kymographs were produced. Analysis of the kymographs was performed using Fiji software. For Kinesin-1 kymographs show the traces of single molecules moving along microtubules. A trace was defined as the discrete trajectory of a single motor between appearance and disappearance of a fluorescent spot on a microtubules. The length of trace is equivalent to the travelled distance by a single molecule. The distance was calculated and divided by the time to obtain the velocity.

For KIF12 kymographs were used to quantify GFP signal intensity on microtubules.

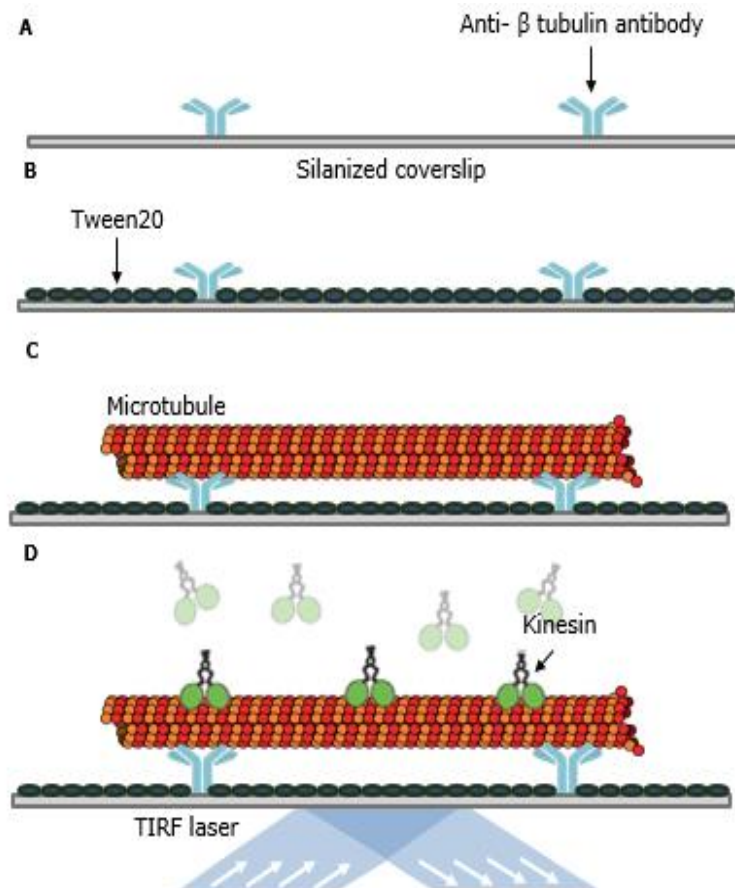


Figure 2.3. TIRF assay experimental setup. A) Anti β-tubulin antibodies in BRB80 were first injected to the channel, followed by B) 0.2% Tween 20 in BRB80, then C) reaction mixture (BRB20, 0.2% Tween 20, 1 mM ATP/Mg²⁺ or AMP-PNP, 0.1 mg/ml bovine serum albumin, 40 mM α-D-glucose, 40 μg/ml glucose oxidase, 16 μg/ml catalase, 1% 2-mercaptoethanol) containing rhodamine-labelled microtubules, then wash with reaction buffer, and C) GFP- labelled KIF12-434 diluted in the reaction mixture was added. The illumination comes from an angled laser which is totally internally reflected, producing a thin layer of illumination near the surface of the glass (<200nm), thus only molecules close to the surface are illuminated.

2.12 Microtubule depolymerisation assay using microscopy

Flow channels were constructed and treated in the same way as with the microtubule gliding assay (**2.10**) except that GMPCPP-labelled microtubules were added to the channel in 20µl reaction buffer (BRB20, 0.2% Tween 20, 1 mM ATP/Mg²⁺, 0.1 mg/ml bovine serum albumin, 40 mM α-D-glucose, 40 µg/ml glucose oxidase, 16 µg/ml catalase, 1% 2-mercaptoethanol) and incubated for 5 minutes, the channel was washed with 20µl reaction buffer, and 32 nM KIF12-434 in 20µl reaction buffer was then added. Images were acquired every 5 seconds for 30 minutes using a Zeiss TIRF microscope equipped with quant EM camera, and 100x (1.46 NA) oil-immersion objective. FIJI software (Schindelin et al., 2012) was used to measure the lengths of individual microtubules through successive frames. These lengths were then plotted and the initial rate of the change of length over time was measured by fitting using Igor Pro.

2.13 Microtubule dynamic assay

Flow channels were constructed in the same way as with the microtubule gliding assay (**2.10**). The channel was incubated with anti-biotin **antibody** (Sigma, diluted 1:100 in BRB80) for 5 minutes, then with 20µl 0.2% Tween 20 in BRB80 for 5 minutes. 20µl 5% rhodamine labelled, 4% biotinylated microtubule seeds (polymerised as described in (**2.8.1**)) was added and incubated for 2 minutes, washed with 20µl BRB80 0.2% Tween20, then with 20µl reaction buffer containing 1mM GTP. Microtubule growth was initiated by adding 12.5µl 20uM 10%

rhodamine labelled tubulin in reaction buffer containing 1mM GTP (extension mix). The assay was first carried out in the absence of KIF12-434 (as a control), then to see the impact of KIF12-434 on microtubule growth dynamics 300nM GFP tagged KIF12-434 in the extension mix was added to the seeds. Time-lapse images were acquired using Zeiss Elyra super resolution microscope equipped with EMCCD camera, objective 100x 1.46NA (+1.6 optovar), 651nm and 488nm filter cube. Macro for movie: 5s interval, 200 cycles. Microtubule dynamics were analysed by generating kymographs. The plus ends of the microtubules were distinguished from the minus ones by comparing their growth rates; the faster growing ends were classified as the plus ends and the slower ones as the minus ends. The parameters of the microtubule dynamics were determined as follows; the growth length was measured by calculating the difference in distance between the start and the end of individual growth event. The growth rate was determined by dividing the growth length by the time between the start and the end of a growth event. Catastrophe frequency was acquired by dividing the total number of catastrophes observed by the total time microtubule spent in growth (Zanic, 2016).

2.14 Competition assay

Flow channels were prepared as described in (2.10), and same setting as for microtubule dynamic assay were used (2.13) with the exception that the reaction buffer for these experiments was not supplemented with GTP to avoid microtubule growth. Tubulin was diluted in a reaction

buffer to the desired final concentration. 200nM/300nM GFP labelled KIF12-434 and tubulin were premixed and incubated for 3 minutes on ice. The mixture was brought to room temperature prior to adding to the channel and incubated for 2 minutes, then snap images were acquired using Elyra super resolution microscope with EMCCD camera, objective 100x 1.46NA (+1.6 optovar), 651nm and 488nm filters. To determine the affinity of KIF12-434 for tubulin, various tubulin concentrations have been tried ranging from 0 μ M to 27 μ M. The integrated GFP signal intensity of the KIF12-434 on the microtubules was measured using Fiji, and plotted against tubulin concentration using Igor pro.

2.15 Microtubule affinity assay

Flow channels were constructed as described in (2.10), and treated as described for TIRF stepping assay (2.11) with the exception that to measure the affinity of KIF12-434 for microtubules, GFP tagged KIF12-434 was added at various concentrations ranging from 0 nM to 300 nM, and still imaging was executed as described for competition assay. KIF12-434 GFP signal intensity on the microtubules was quantified using Fiji, and plotted against KIF12-434 concentration using Igor pro.

2.16 ATPase assays

2.16.1 Discontinuous assay with ADP production monitored by HPLC

A reaction mix (150 μ l) of 2 mM ATP/Mg²⁺ and 9 μ M KIF12-434 in BRB20, 75 mM KCl, 0.05% Tween 20 (v/v), 1 mM DTT was incubated at 25°C. Then, samples were taken every 3 minutes, and the reaction was

quenched with an equal volume of 0.6 M perchloric acid (PCA), before neutralization by addition of 6M KOH. The samples were clarified by centrifugation at 13,000 rpm for 10 minutes, then mixed with an equal volume of HPLC running buffer (100 mM potassium phosphate pH 6.5, 10 mM tetrabutylammonium bromide, 12% acetonitrile). ADP and ATP were separated by HPLC system (Gilson) on a C18 column (Phenomenex) using isocratic flow, and the nucleotides were detected by absorbance at 259nm. The ADP fraction was calculated by dividing the area under the ADP peak by the sum of the areas under ADP and ATP peaks. The gradient of a graph of change in ADP fraction over time was then multiplied by the total nucleotide concentration (2000 μM), then divided by the concentration of KIF12 motor domains (9 μM) to give the number of ATP molecules cleaved per motor domain per second (the ATPase rate).

2.17 ADP dissociation

KIF12-434 was loaded with mADP (Jene Bioscience) by mixing with 25-fold excess of mADP (2 μM KIF12-434:50 μM mADP) and incubating at 25 °C for 30 minutes. The free nucleotides were removed by loading the mixture (0.5ml) on NAP-5 column after equilibration with a reaction buffer consisting of BRB20, 75 mM KCl, 0.05 % (v/v) Tween 20, 1 mM DTT, the protein was then eluted in 1 ml reaction buffer and kept on ice. Dissociation of mADP from KIF12-434 was measured by rapidly mixing 1:1 (v/v) with 100 μM unlabelled ATP (+ where indicated 10 μM tubulin or 5.7 μM microtubules – chosen to give a comparable number of ends

to 10 μM microtubules in ATPase assay) in an SX20 stopped-flow fluorimeter (Applied Photophysics). The fluorescence of mant group was excited at 365nm, and the emitted light was collected between 395 nm and 495 using BP445/50 filter (Zeiss). The data was collected in the form of overlying traces which represent fluorescence transients over a time scale of 100s at 25 °C. For each independent experiment, 5 measurements (traces) were obtained and were fitted to an exponential with the fewest terms required to adequately describe the curve (fitting of mADP dissociation data has been described previously (Patel et al., 2014)). The fluorescence transients were fit to a single exponential function plus a line of constant negative slope to account for photobleaching using **Equation 2.1**:

$$\text{Fluorescence} = A_0 \cdot \exp(-k_{\text{obs}} \cdot t) + (m \cdot t + c)$$

Where A_0 is the amplitude of the exponential decay, k_{obs} is the observed rate constant, and $(m \cdot t + c)$ is a linear term to account for photobleaching of mant group. When a single exponential was not able to adequately describe the curve, a double exponential was used (**Equation 2.2**):

$$\text{Fluorescence} = A_{\text{fast}} \cdot \exp(-k_{\text{fast}} \cdot t) + A_{\text{slow}} \cdot \exp(-k_{\text{slow}} \cdot t) + (m \cdot t + c)$$

This gives two k values, which are termed k_{fast} for the larger value and k_{slow} for the smaller value.

The data for each of the five fluorescent traces in each experiment were averaged and then fitted to the relevant exponential equation. Three

independent experiments were performed. Averages and standard deviations were calculated for the k values and A from each experiment.

2.18 Statistical tests

Whether a difference between measured parameters was statistically significant was determined using unpaired t-test. Values of $p < 0.05$ were considered statistically significant.

Chapter 3 In vitro characterisation of the activity of

KIF12

KIF12 is a member of the Kinesin-16 family that is found only in organisms that have cilia or flagella. The activity of KIF12 in relation to microtubules has not yet been defined. Knowing how KIF12 interacts with microtubules would help to determine its function within the primary cilium whether contributing in axoneme building or in intra-flagellar transport (IFT). Therefore, I decided to study the activity of KIF12 in *in vitro* microtubule- based assays; to achieve this it is necessary to express and purify KIF12 protein.

3.1 Expression and purification of KIF12

Bacterial expression of protein is quicker, simpler, and cost effective when compared to other protein expression systems. However, the solubility of the protein produced is not always guaranteed. This is because of protein misfolding that may occur due to the lack of more complex protein folding machinery available in eukaryotic systems. Add to that, for kinesins the presence of long coiled-coil region, which has proven to cause insolubility issues **when expressed in bacteria**.

Therefore an insect cell system (*Spodoptera frugiperda* (Sf9)) was used for expression of KIF12. Previous work carried out to express full length KIF12 and the motor domain only (KIF12 [1-363]) in Sf9 cells showed the full length was not soluble but the motor domain was. The position of the GFP tag is also important even for the motor domain only, when GFP was on the N-terminus the motor domain was insoluble, but when

GFP was located on the C-terminal end the KIF12 motor domain was soluble (Littledale, 2017). As the coiled-coil domain is required to allow the dimerization of the motor domains which is often required to allow kinesins to fulfil their functional duties, a set of truncation mutants with different coiled coil lengths were tested, to see if a soluble but likely dimeric construct could be found. To achieve this, the predicted coiled-coil region of KIF12 was compared with DmKHC (Kinesin-1) known dimeric constructs and predicted coiled-coil region, and based on this four truncation mutants were designed; KIF12-[1-393], KIF12-[1-415], KIF12-[1-434], and KIF12-[1-472] (all constructs were supplied by C. Friel except KIF12-[1-472]) (**Figure 3.1**).

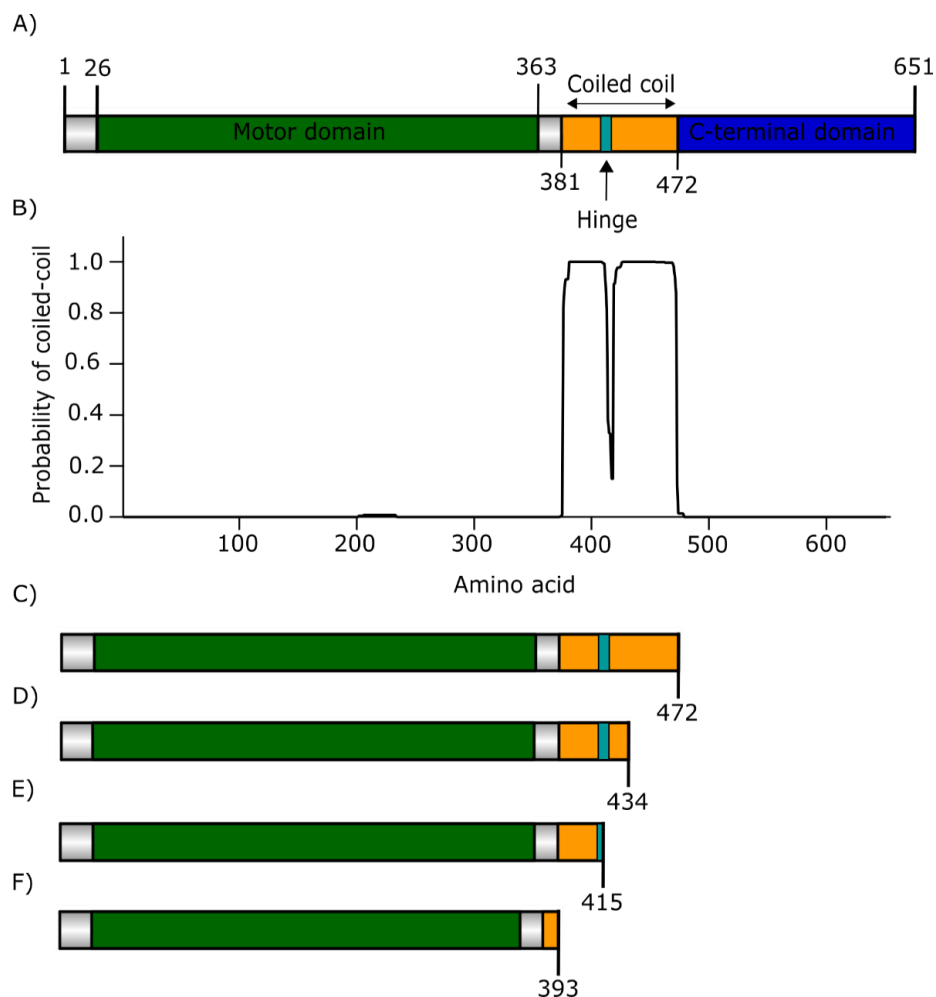


Figure 3.1. Domain layout for the wild type mammalian KIF12. A) Ribbon diagram showing the predicted domain layout of KIF12, numbered according to the amino acid sequence of human KIF12, B) probability of coiled-coil formation of the primary sequence of human KIF12, predicted using COILS v2.1, C-F) KIF12 truncations [1-472], [1-434], [1-415], and [1-393], respectively.

All the four truncated versions of KIF12 were tagged with C-terminal GFP and 7xhis, and expressed in Sf9 cells using bac-to-bac expression system as previously described (2.22.2.2 to 2.2.4). All the truncations were found to be soluble, except the longest one, KIF12-[1-472], and so the longest soluble construct, KIF12 [1-434], was chosen to progress as this is most likely to form a dimer. KIF12-434 was then purified using **nickel** affinity chromatography (2.3.1); as shown in **Figure 3.2**.

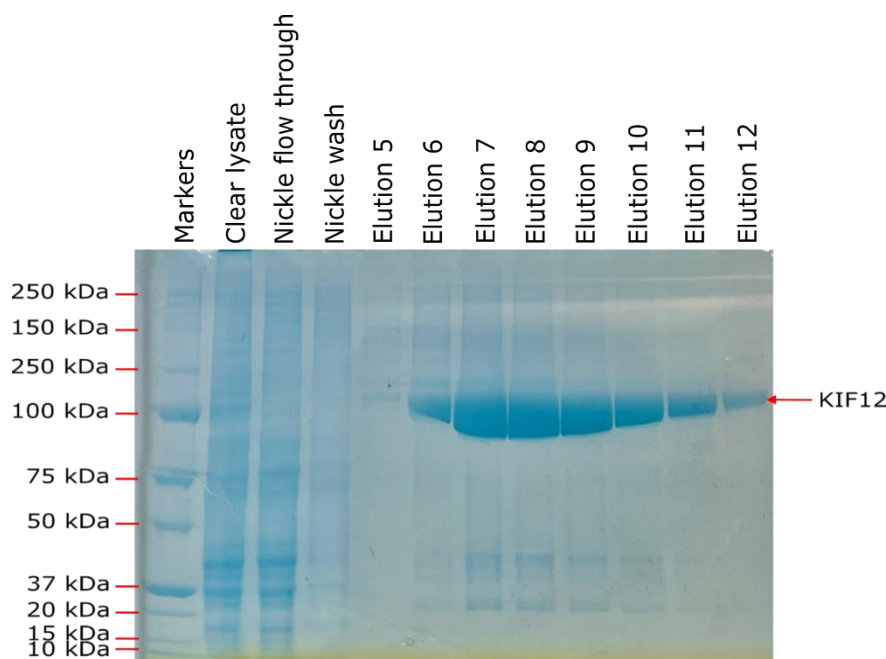


Figure 3.2. Purification of KIF12-434. Instant blue stained SDS-PAGE gel of the progression of wild type KIF12-434 tagged with C-terminus GFP and 7his purification. Markers: protein standards, Clear lysate: the cleared lysate, **nickel** flow through: flow through from clear lysate applied to **nickel** affinity column, **nickel** wash: wash with 60mM imidazole, elutions 5-12: protein eluted in 200mM imidazole. The expected molecular weight of KIF12-434-GFP-7h is 77kDa.

The oligomeric state of the purified KIF12-434-GFP sample was assessed using analytical ultracentrifugation (AUC). The centrifuge uses centrifugal acceleration to sediment protein species out of the solution. The sedimentation process was monitored with absorbance detection at 395 nm at gradient protein concentrations. Sedimentation coefficient distribution for KIF12-434-GFP shows a monomer peak at ~ 2.6 S, and a dimer peak at ~ 4 S, and the comparison of the height of the two peaks shows that approximately one-third of the protein sample was dimeric, $\sim 27\%$ dimer compared to $\sim 73\%$ monomer (see **Appendix 3**). These data suggest that this protein exists as a mixed population of monomer and dimer, and no further steps were taken to separate dimer from monomer. Therefore, in all the experiments described the protein studied is likely to be a combination of monomers and dimers.

3.2 KIF12-434 does not act as a translocating kinesin

Sequence analysis of KIF12 shows that it has an N-terminal motor domain (Kato and Kato, 2005) (**Figure 3.1 A**), similar to known plus end directed translocating kinesins, such as Kinesin-1. Thus, we hypothesized that KIF12 is a translocating kinesin and may function as a cargo carrying kinesin within the primary cilia, similar to Kinesin-2 family (Cole et al., 1998). To test this hypothesis, a microtubule gliding assay was carried out. In this assay, kinesin motility activity can be detected by observing microtubule directional motion generated by surface-immobilized kinesin molecules as detailed in Section **2.10**. As a positive control when setting up this assay, I expressed and purified

conventional Kinesin-1 since it is a well-known translocating kinesin (Hirokawa et al., 2009, Kanai et al., 2004).

3.2.1 Expression and purification of Kinesin-1

The Kinesin-1 (rkin430-GFP-6his) construct was generously supplied by Stefan Diez, Max Plank Institute of Molecular Cell Biology and Genetics, Dresden (Leduc et al., 2007). The kinesin-1 was expressed in *E.coli* BL21 as described in Section (2.4), and purified using Ion exchange chromatography followed by **nickel** affinity chromatography (Section 2.5), as shown in **Figure 3.3**.

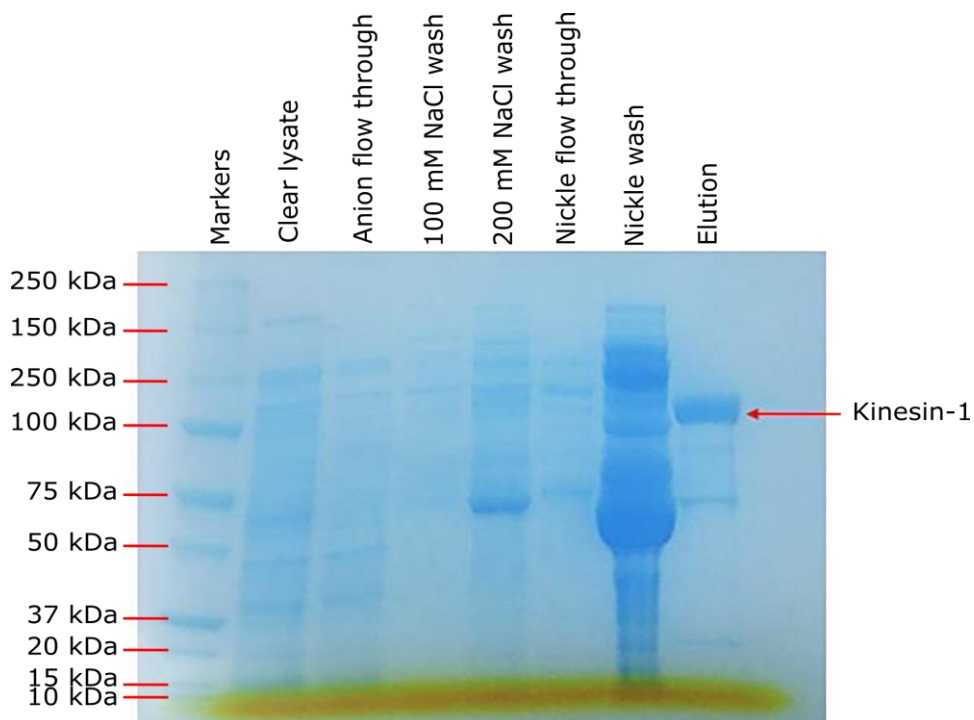


Figure 3.3. Purification of Kinesin-1. Instant blue stained SDS-PSGE gel showing the purification steps of rkin430-GFP-6his. Markers: protein standards, clear lysate: cell lysate after centrifugation, anion flow through: flow throw from cleared lysate applied to anion exchange column, 100mM NaCl wash: wash with 100mM NaCl, 200mM NaCl wash: wash with 200mM NaCl, **nickel** flow through: flow throw from 200mM NaCl elution applied to **nickel** affinity column, **nickel** wash: wash with 75mM Imidazole, elution: protein was eluted from **nickel** affinity column in 300 mM imidazole. The expected molecular weight of rkin430-GFP-6h is 75 kDa.

3.2.2 Kinesin-1 microtubule gliding assay

A gliding assay was performed using kinesin-1, and the result shows that kinesin-1-attached microtubules moved in a directional manner (**Figure 3.4 A-C**). The velocity of the moving microtubules was then measured as described (**2.10**), as shown in **Figure 3.4 (D)**, and the average velocity was found to be 663.36 ± 48 nm/s which is comparable to another literature value (680 nm/s) measured by Leduc et al. (2007).

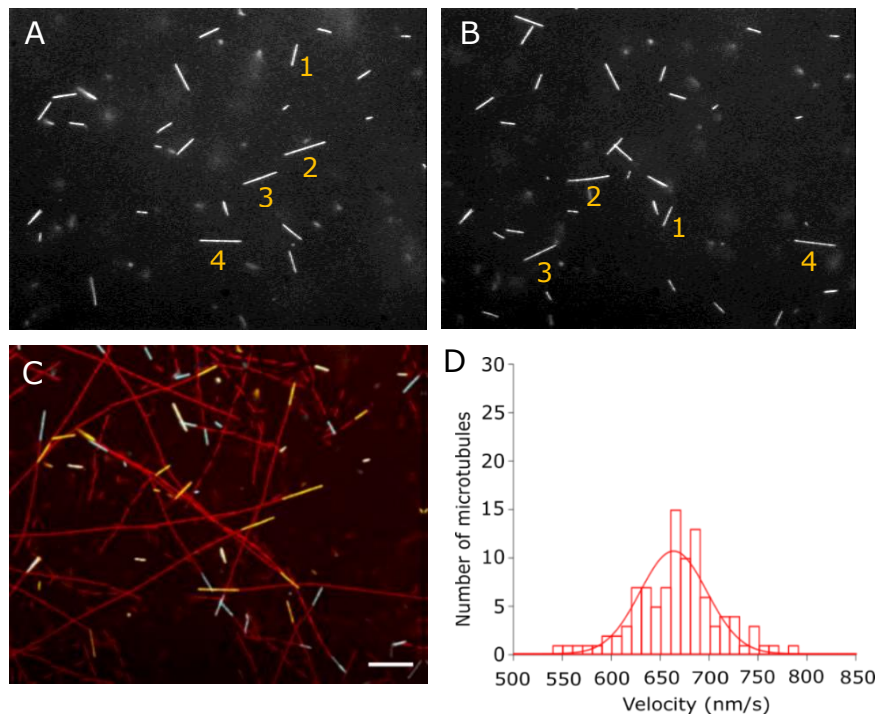


Figure 3.4. Kinesin-1 moves microtubules in a directional fashion. A & B) Frames from a movie of a microtubule gliding assay using *rkin430*, (A) at 0s and (B) at 10s. Numbers represent the same individual microtubules in each frame. (C) A composite of the first frame (yellow), maximum intensity (red), and final frame of the movie (cyan). (D) Histogram shows the distribution of velocities calculated for individual microtubules. Two sets of gliding assay experiments were carried out, and the average velocity was 663.36 ± 48 nm/s (mean \pm SD, $n=100$). Bin size; 50 nm/s. Scale bar $2\mu\text{m}$.

3.2.3 KIF12-434 does not act as a translocating kinesin

To test the ability of KIF12-434 to translocate along microtubules I tested it in a gliding assay. No directional movement of microtubules was observed, as would be expected if KIF12-434 displayed directed translocation along microtubules. Microtubules were either static or showed back and forth motion over a range of ~ 1 -2 microns (**Figure 3.5 A**). To determine whether this movement results from a diffusive interaction with microtubules, a gliding assay was carried out using the Kinesin-13, MCAK (**Figure 3.5 B**), which has been shown to interact with microtubules in a purely diffusive fashion (Helenius et al., 2006). MCAK was observed to move microtubules in a way similar to KIF12-434, and this indicates that KIF12-434 is a diffusive kinesin rather than a translocating kinesin.

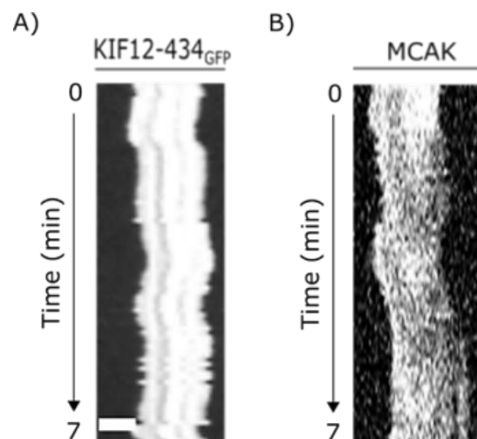


Figure 3.5. KIF12-434 does not move microtubules in a directional manner. A) and B) Representative kymographs showing the motility of rhodamine-labelled GMP-CPP stabilised microtubules (shown in grey scale) driven by surface-bound KIF12-434 or MCAK in the presence of 1mM Mg-ATP. Images were recorded every 5s (frame rate was 1 frame per 5 s). Horizontal scale bar, $2\mu\text{m}$, vertical scale bar, 400s. Data sets from four independent experiments for KIF12-434 and one experiment for MCAK.

3.3 Stepping assay confirms that KIF12-434 dose not translocate on microtubules

3.3.1 Kinesin-1 stepping assay

To further investigate the interaction of KIF12-434 with microtubules, a stepping assay was then performed (as described in Section **2.11**).

Briefly, microtubules were immobilised on a silanized coverslip surface by anti- α tubulin antibodies, reaction buffer containing kinesin at low concentration (low nM) to allow detection of single molecule behaviour on microtubules was then added, and imaging was carried out using TIRF microscopy. rkin430-GFP was first used as a control, and was observed moving along microtubules in a directed manner as shown by the diagonal traces (**Figure 3.6 A**), the mean velocity was measured as described (**2.11**) (**Figure 3.6 B**), where it was 714 ± 258 nm/s (mean \pm SD) which is similar to previously measured velocity 540 ± 140 nm/s (Korten and Diez, 2008).

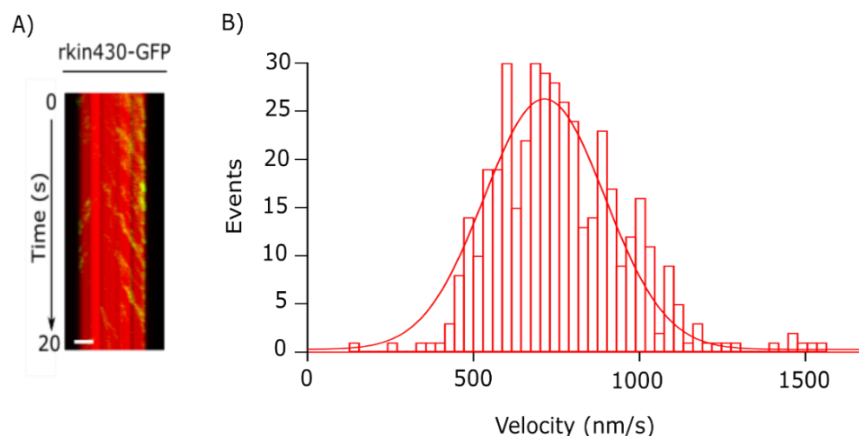


Figure 3.6. Kinesin-1 stepping assay. A) Representative kymograph showing the interaction of rKin430-GFP (green) with GMPCPP-stabilised, rhodamine labelled microtubules (red), scale bar 2 μ m. B) Histogram showing the distribution of events (moving rkin430-GFP molecules on microtubules) at various velocities calculated. Two sets of stepping assay experiments were carried out, and the average velocity was 714 ± 258 nm/s (mean \pm SD, $n= 427$). Bin size; 30 nm/s.

3.3.2 KIF12-434 does not translocate on microtubules

KIF12-434 was then studied in this TIRF stepping assay. KIF12-434 did not display the directed motion seen for Kinesin-1, but was observed to either transiently bind to microtubules or **attach to microtubules** over longer timescales (**Figure 3.7A**). Hence, to see if this interaction is a real interaction; meaning that the molecules are not just non-specifically bind to microtubules, the first aspect to look at is the protein concentration. The interaction of KIF12-434 with microtubules was found to be a concentration-dependent. At 0.3 nM KIF12-434 in the presence of ATP, GFP signal intensity on microtubules was 919 ± 517 (mean \pm SD), while it was 4212 ± 1603 at 1.6 nM KIF12-434, and the p-value was equal to 0.0001 (**Figure 3.7A and B**). The next aspect to look at is the nucleotide dependence of the interaction. Therefore I compared the behaviour of KIF12-434 in the presence of ATP with the activity in the presence of AMP-PNP; a non-hydrolysable analogue of ATP. In the presence of AMP-PNP at 0.3 nM KIF12-434, GFP signal intensity on microtubules was 3316 ± 2218 whereas it was 919 ± 517 with ATP, and p-value equals 0.0001. Same observation was when comparing GFP signal intensity on microtubules in the presence of AMP-PNP to that in the presence of ATP at the same KIF12-434 concentration (1.6 nM), **where it was 6435 ± 2949 compared to 4221 ± 1603** , respectively, and the p-value was equal to 0.0054 (**Figure 3.7 A and B**). **The fact that the interaction of KIF12-434 with microtubules changes with the nucleotide is what confirms that this is not just a non-specific interaction with microtubules, but it is a nucleotide-dependent**

interaction. When AMP-PNP occupies the nucleotide binding pocket of KIF12-434 it does not get hydrolysed and as a result does not cause conformational changes to motor domain of KIF12-434 when interacting with microtubules, and therefore KIF12-434 remains in a tight binding state to microtubules. This is in contrast to when the pocket is filled with ATP as the ATP hydrolysis causes conformational changes to the motor domain of KIF12-434 which what causes the transient binding of KIF12-434 to microtubules.

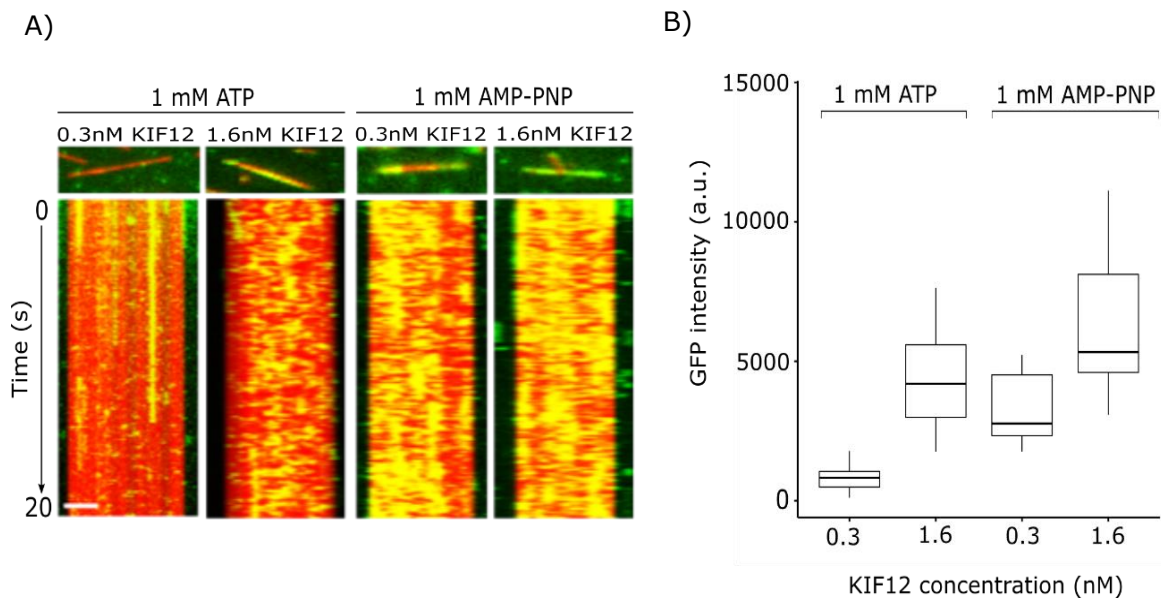


Figure 3.7. KIF12-434-GFP does not show a translocating motility along microtubules. A) Still images and kymographs show the behaviour of KIF12-434-GFP (yellow) on rhodamine- labelled GMPCP- stabilised microtubules (red), scale bar $2\mu\text{m}$. B) Average fluorescence intensity of microtubule-bound KIF12-434-GFP at two different concentrations in the presence of either 1mM Mg-ATP or 1mM AMP-PNP. Solid black lines represent the mean. $N=20$ microtubules for each condition.

Since the microtubule gliding assay shows that KIF12-434 is not a translocating kinesin and the stepping assay confirms this, it is unlikely

that KIF12 is translocating kinesin with a carrying cargo function within the primary cilia.

3.4 KIF12-434 does not depolymerise microtubules but may stabilise them

Data for KIF12-434 from gliding assays and TIRF assays show no evidence of translocation activity. If KIF12 is not a translocating kinesin, it may be that it acts to regulate microtubule dynamics. Many kinesins that regulate microtubule dynamics are depolymerases; such as the Kinesin-13 family. Some members of the Kinesin-13 family of microtubule depolymerases, for example KIF24 and KIF2A localize to the centrosome/basal bodies and remodel cilia via depolymerisation of microtubules (Miyamoto et al., 2015, Kobayashi et al., 2011).

Microtubule depolymerisation can be observed using an assay in which fluorescently labelled microtubule are adhered to the surface of a glass coverslip and imaged over time using widefield fluorescence microscopy (Gell et al., 2010). This assay was carried out using a concentration of 32nM for KIF12-434 (2.12). For MCAK for example, ~40nM is used as the maximum depolymerisation activity for it was seen at this concentration (Helenius et al., 2006). In **Figure 3.8** it can be seen how a microtubule depolymerising kinesin, such as, MCAK would behave in this assay.

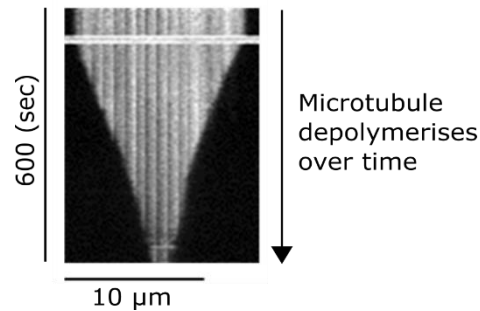


Figure 3.8. Microtubule depolymerisation by MCAK. Kymograph showing microtubule (white) shortening by MCAK (unlabelled) during depolymerization assay. The microtubule is shown at the top of the image and the same slice from a time series of images is shown underneath, showing the decrease in microtubule length over time. Image is from (Belsham, 2019).

KIF12-434 does not seem to depolymerise microtubules (**Figure 3.9 A**). In the absence of KIF12-434 the intrinsic rate of depolymerisation observed here is $0.04 \pm 0.02 \mu\text{m}/\text{min}$ (mean \pm SD). This is similar to that stated in the literature for GMPCPP-stabilised microtubules in the absence of added protein: $0.092 \pm 0.022 \text{ nm}/\text{s}$ for the plus end and $0.047 \pm 0.012 \text{ nm}/\text{s}$ for the minus end (Díaz-Valencia et al., 2011). The microtubule depolymerisation rate in the presence of KIF12-434 is $0.01 \pm 0.005 \mu\text{m}/\text{min}$ (**Figure 3.9 B**). This is a small but statistically significant decrease compared to the intrinsic depolymerisation rate ($p=0.0002$). These data suggest that KIF12-434 may stabilise microtubules, as the depolymerisation rate in its presence is slower than when there is no protein around.

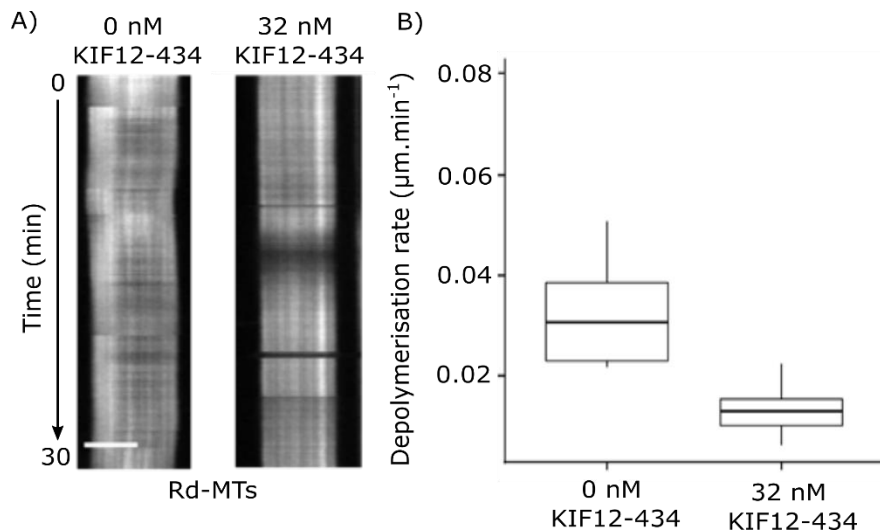


Figure 3.9. KIF12-434 slows down microtubule depolymerisation rate. A) Representative kymographs showing the impact of KIF12-434 on microtubule depolymerisation, Rd-MTs: rhodamine-labelled microtubules, scale bar $5\mu\text{m}$. B) Depolymerisation rate in the presence and absence of KIF12-434 measured using depolymerisation assay. For each case $n=10$.

3.5 KIF12-434 increases microtubules growth rate but cannot be detected on microtubule plus ends

Data from microtubule depolymerisation assays suggest that KIF12-434 reduces the intrinsic depolymerisation rate of GMPCPP-stabilised microtubules. This may indicate that KIF12-434 has a stabilising effect on microtubules. However, as the intrinsic depolymerisation rate of stabilised microtubules is already very low so the impact of additional stabilisation will be very small. Therefore, we proceeded to study the impact of KIF12-434 on microtubules in a microtubule dynamic assay. In this assay, **biotinylated** microtubule seeds stabilised using GMPCPP and grown using 5% Rhodamine labelled tubulin were fixed on a glass surface via anti-biotin antibodies. To initiate microtubule growth, microtubule extension mix of $20\mu\text{M}$ tubulin, 10% Rhodamine-labelled

supplemented with GTP in the imaging buffer was then added to the seeds, and imaging was carried out using TIRF microscopy (**Figure 3.10**) (**2.13**).

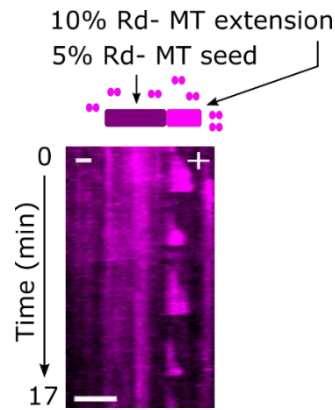


Figure 3.10. Microtubule dynamics assay setup. Kymograph showing GMPCPP-stabilised microtubule seed (5% Rhodamine labelled), dynamic extensions grown from the microtubule plus end (fast growing end) by adding 10% Rhodamine labelled $20\mu\text{M}$ tubulin in imaging buffer supplemented with 1mM GTP. Imaging was performed using super-resolution microscope equipped with TIRF. Scale bar $2\mu\text{m}$.

From this type of assay, various parameters that describe microtubule dynamics can be measured. These parameters are; the growth rate, the growth length, growth time, and catastrophe frequency. These parameters were calculated for dynamic microtubule growth in the absence and presence of KIF12-434 (**Figure 3.11**). In the presence of 300nM KIF12-434, the growth rate and growth length increased from 0.465 ± 0.016 to 0.652 ± 0.157 ($\mu\text{m}/\text{min}$) ($p < 0.0001$) and from 0.957 ± 0.048 to 1.254 ± 0.147 (μm) ($p < 0.0001$), respectively. This increase is small but significant. However, by comparison with other proteins that regulate microtubule dynamics, we might have expected to see a bigger effect.

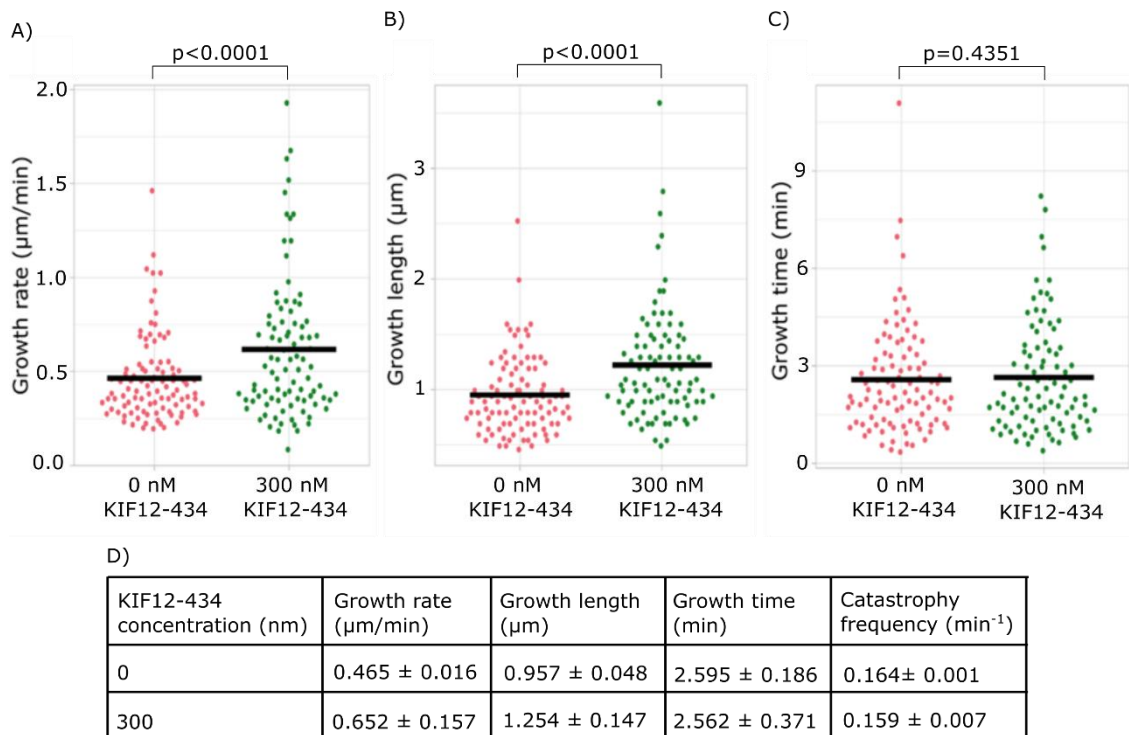


Figure 3.11. KIF12-434 affects microtubule dynamics. A) Growth rate, B) growth length, C) growth time, D) microtubule dynamics parameters (mean \pm SD). Data obtained using microtubule growth dynamics assay. $N = 98$ and 92 in the absence and presence of KIF12-434, respectively.

For instance, Kip2, a motor protein found in yeast cells and known for its ability to control microtubule growth besides transporting its cargo to the plus end of the microtubules, at 28°C and $12\mu\text{M}$ tubulin, 40 nM Kip2 increased the growth rate 3-fold from 0.32 ± 0.02 to 0.94 ± 0.05 ($\mu\text{m}/\text{min}$), and the growth length 8.8-fold from 1.0 ± 0.1 to 8.8 ± 0.6 (μm) (Hibbel et al., 2015). Another microtubule growth regulating protein is Kinesin-5, a kinesin that slides antiparallel microtubules during spindle assembly and controls the branching of growing axons, at 30°C and $10\mu\text{M}$ tubulin, 30 nM Kin5_18 increased the growth rate 2.3-fold from 8.1 ± 0.9 to $19.1 \pm 1.3\text{ nm}/\text{s}$ (Chen and Hancock, 2015). A non-kinesin example is XMAP215, a microtubule-associated protein belongs

to a conserved family of proteins that are essential for the growth of microtubules and mitotic spindle assembly. At a higher temperature; 35°C compared to 27°C and a lower tubulin concentration; 7µM compared to 20µM, but the protein concentration was close to the one we used for KIF12 (300 nM); 200nM XMAP215 increased the growth rate from 0.58 ± 0.02 to 6.16 ± 0.46 (µm/min) (Zanic et al., 2013), which is a 10.6 fold raise, compared to only 1.4-fold seen for KIF12, although we thought that the high concentration of tubulin we used would compensate the lower temperature we set up for our assay, and so as a result the increase in growth rate would be higher similar to that measured for XMAP215 (see **Table 1**; a summary table of the impact of KIF12-434 and the other mentioned proteins on microtubule growth dynamics). KIF12-434 had no impact on microtubule growth time as it was 2.595 ± 0.186 min and 2.562 ± 0.371 min in the absence and presence of KIF12-434, respectively, and the p-value was equal to 0.435 (**Figure 3.11C and D**). The catastrophe frequency was not effected by KIF12-434 either, as it was 0.164 ± 0.001 and 0.159 ± 0.007 in the absence and presence of KIF12-434, respectively.

Table 2. Summary table of the impact of different proteins on microtubule dynamics.

	Concentration (nM)	Grow rate (µm/min)	Growth length (µm)
KIF12-434	0 nM	0.465 ± 0.016	0.957 ± 0.048
	300 nM	0.652 ± 0.157	1.254 ± 0.147
Kip2	0 nM	0.32 ± 0.02	1.0 ± 0.1
	40 nM	0.94 ± 0.05	8.8 ± 0.6
Kin5_18	0 nM	8.1 ± 0.9	-
	30 nM	19.1 ± 1.3	-
XMAP215	0 nM	0.58 ± 0.02	-
	200 nM	6.16 ± 0.46	-

3.6 KIF12-434 can be sequestered from microtubules by unpolymerised tubulin

Not only did KIF12-434 not have a large impact on microtubule dynamics, it did not appear to interact with microtubules, either the dynamic extensions or stabilised seeds as no GFP signal was detected on both (**Figure 3.12**, upper panel). This observation disagrees with the previous observation that KIF12-434 was observed to interact with stabilised microtubules in the absence of unpolymerized tubulin (**Figure 3.7 A**). Therefore, this assay was repeated with microtubule seeds but without unpolymerised tubulin. Under these conditions, KIF12-434 did interact with microtubules (**Figure 3.12**, lower panel).

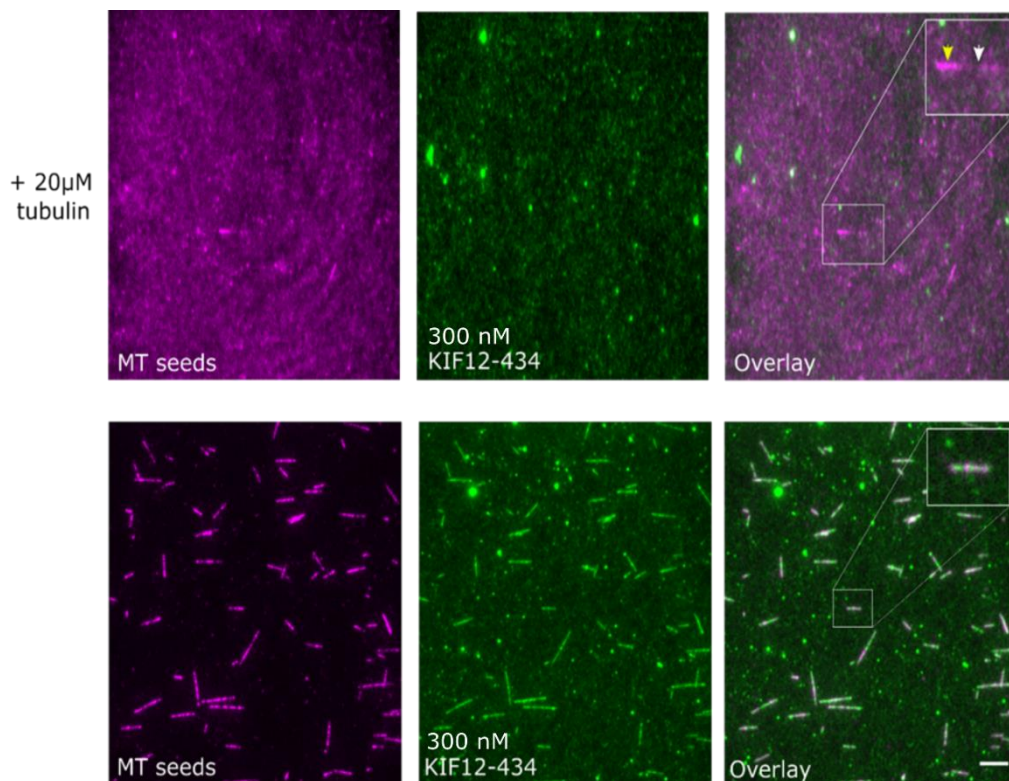
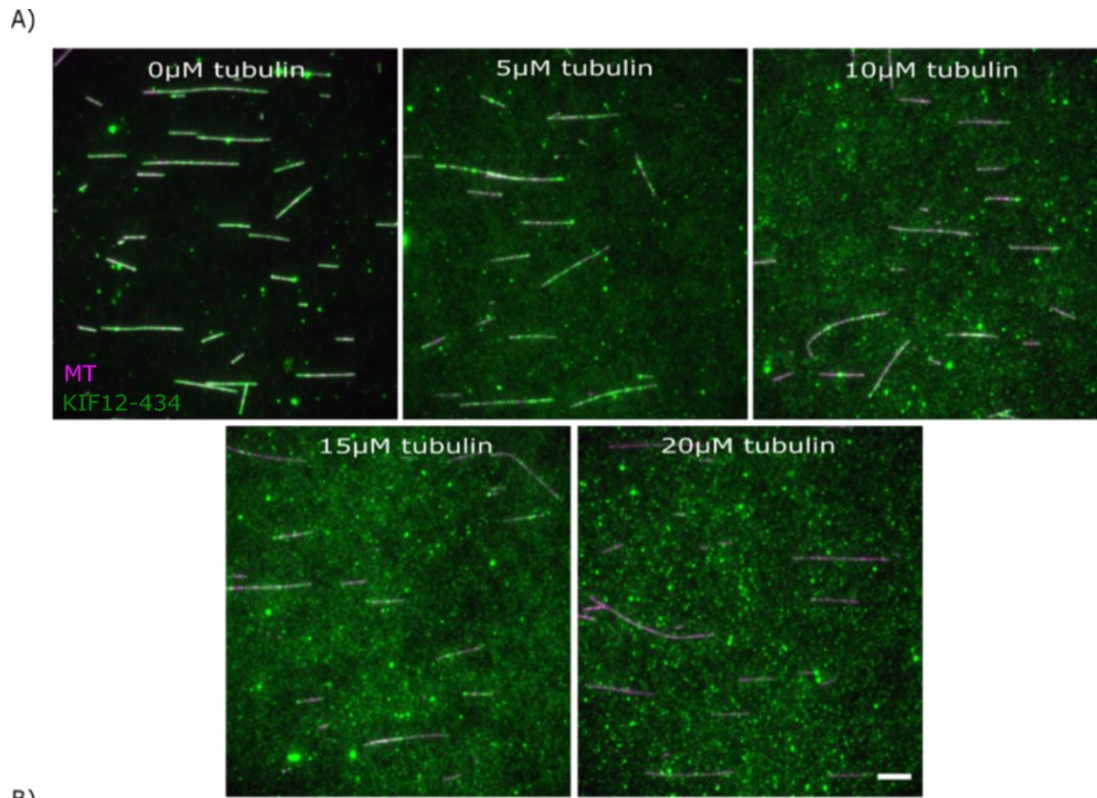


Figure 3.12. KIF12-434 interacts with microtubule seeds in the absence of unpolymerised tubulin. Upper panel showing GFP-labelled KIF12-434 (green) sequestered away from microtubule seeds and extensions (magenta) in the presence of unpolymerised tubulin. The right upper corner insert represents a magnification of microtubule seed (5% rhodamine- labelled (indicated by white arrow), and 10% rhodamine- labelled extension (indicated by yellow arrow). Lower panel showing KIF12-434 interacting with microtubule seeds in the absence of unpolymerised tubulin. The right lower corner insert is a magnification of KIF12-434 decorating a microtubule seed. Scale bar 5 μm .

Therefore, we hypothesised that the unpolymerised tubulin was sequestering KIF12-434 away from microtubules. To further study the impact of unpolymerized tubulin on the ability of KIF12-434 to interact with microtubules, increasing concentrations of unpolymerised tubulin were introduced to an assay containing stabilised microtubule seeds and KIF12-434. This was carried out in the absence of added GTP to avoid growth of microtubule extensions. As the concentration of unpolymerized tubulin was increased, intensity of the GFP signal on the microtubules decreases, and at a tubulin concentration between 15 μM and 20 μM KIF12 was no longer observed on microtubules (**Figure 3.13 A and B**). This suggests that unpolymerized tubulin begins to compete with microtubules for the binding of KIF12-434.



B)

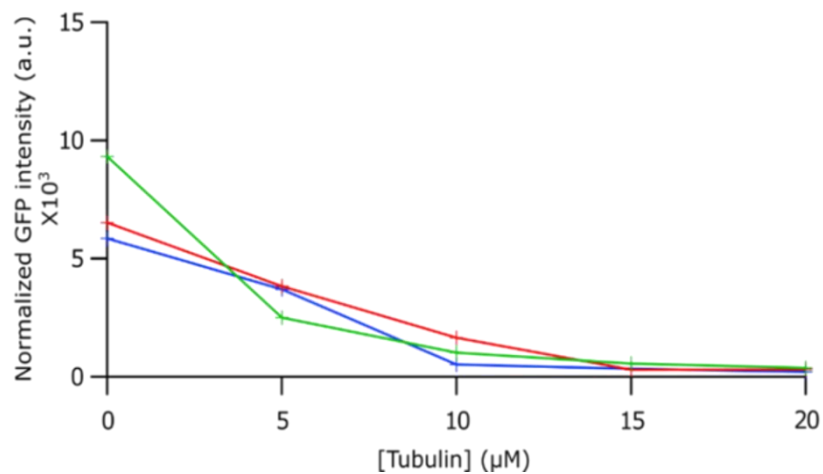


Figure 3.13. KIF12-434 is sequestered away by unpolymerised tubulin from microtubules. A) Still images show the loss of KIF12-434-GFP (300nM) interaction with microtubules as the concentration of free tubulin increases. Scale bar 5 μ m. B) Line scan based analysis of GFP intensity along microtubule at the indicated free tubulin concentrations. **Data were collected from three independent competition assay experiments.**

To try to quantify the interaction of KIF12 with tubulin and microtubules the data were then fit to a competitive binding model by David Sept, Department of Biomedical Engineering, Centre for Computational Medicine and Bioinformatics, University of Michigan, Michigan (**Figure 3.14**). The red line is a fit to a model that assumes each kinesin binds a single tubulin dimer, and the green line the fit to a model in which each kinesin binds two tubulin dimers. The two-dimer model give a much better fit to the data. The shape of this curve depends weakly on the affinity of KIF12-434 for the microtubule, since the affinity of KIF12-434 to tubulin can be adjusted to compensate. Thus the figure shows only one curve for microtubule affinity (K_1) = 500 nM. The table shown in the inset shows three potential microtubule affinity values (K_1 = 100 nM, 500 nM and 1 μ M) and the corresponding tubulin affinities (K_2).

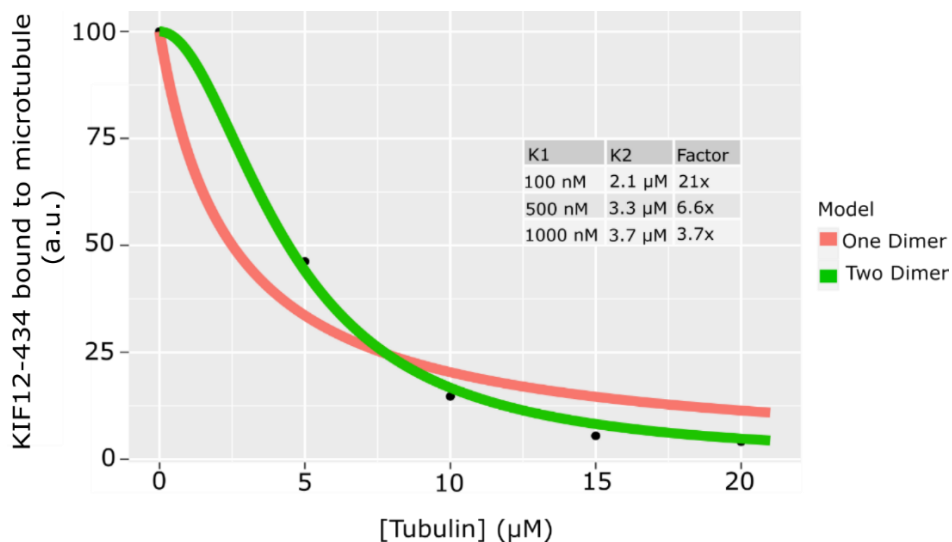


Figure 3.14. KIF12-434 binds two tubulin dimers rather than one dimer. Green curve represents one-tubulin dimer model and red curve represents two-tubulin dimer model. The inset shows three potential KIF12-434 microtubule affinity values (K_1) = 100nM, 500nM and 1 μ M) and the corresponding tubulin affinities (K_2), and the curves for K_1 = 500nM. Data from the competition assay were fit to competitive binding model. *a.u.*; arbitrary unit.

Then, to better distinguish between the one dimer and two-dimer models, data was collected for additional tubulin concentrations. Additional data was also collect at a lower concentration of KIF12. Instead of fitting for the affinities of KIF12 for the microtubules and for the tubulin dimer(s), these data were fitted for the ratio of these two quantities. There is a quantity that is defined as $a = K1/K2^2$ where K1 is the affinity for the microtubules and K2 is the affinity for the tubulin dimer (it is squared since it binds two dimers). The fitting gives a value of $a = 0.000248$. This means that if $K1 = 100 \text{ nM}$, the corresponding $K2 = 630 \text{ nM}$, or if $K1 = 500 \text{ nM}$, $K2 = 1420 \text{ nM}$ as shown in **Figure 3.15**.

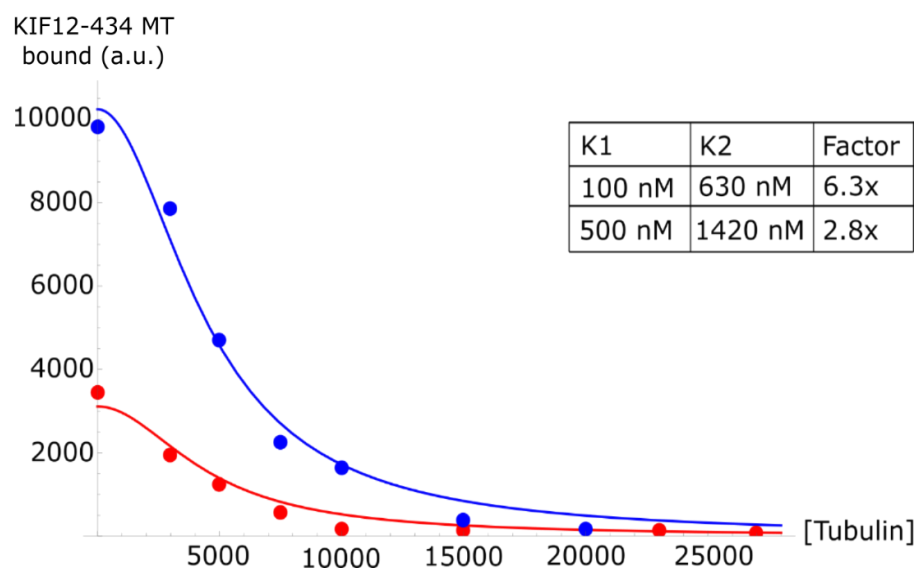


Figure 3.15. KIF12-434 binding to tubulin dimers model. Blue curve represents the data collected for 300nM KIF12-434, and red curve for 200nM KIF12-434. The inset shows two KIF12-434 microtubule affinity values ($K1$) = 100nM and 500nM and the corresponding tubulin affinities ($K2$). Data from competition assay data (with additional intermediate tubulin concentrations and lower KIF12 concentration) were fitted to the ratio of KIF12-434 microtubule affinity to its affinity to tubulin dimers. **a.u; arbitrary unit.**

The accuracy of the parameters determined from the fit to this model could be improved if the affinity of KIF12-434 for microtubule was determined. Therefore, to obtain a more accurate determination of the affinity of KIF12 for tubulin, an assay to measure the affinity of KIF12 for microtubules was performed. In brief, microtubules were grown and fixed on a glass coverslip through anti tubulin anti-body, GFP tagged-KIF12-434 in an imaging buffer was then added to the fixed microtubules at increasing concentrations, and imaging was carried out using TIRF microscopy. GFP signal intensity along microtubules was quantified and the data were fit to **Equation 3.1**: $AB = AB_{max} \left(\frac{[B]}{[B] + K_D} \right)$,

Where AB is the mean intensity of the GFP signal on microtubules which reports on the amount of KIF12-434-GFP bound to microtubules. AB_{max} is the maximum microtubule associated GFP signal at saturating concentrations of KIF12-434-GFP. K_D is the dissociation constant for KIF12-434-GFP from the microtubule. As shown in **Figure 3.16**, GFP fluorescence intensity was plotted against the concentration of KIF12-434-GFP. As the concentration of KIF12-434 increases, the GFP signal intensity on microtubule increases to a plateau defined by AB_{max} . Both K_D and AB_{max} can be acquired by fitting the data with a nonlinear regression function using **Equation 3.1**. The AB_{max} determined was 13.45 ± 8.53 , and K_D was $0.6\mu\text{M} \pm 0.5\mu\text{M}$. K_D represents the concentration of KIF12-434-GFP where the AB is half the maximum value (i.e. $0.5 AB_{max} = 6.7$). However, since the binding isotherm does not reach a plateau, the predicted K_D is twice the highest concentration

used (300nM). Therefore, there is large error associated with the quantification of K_D .

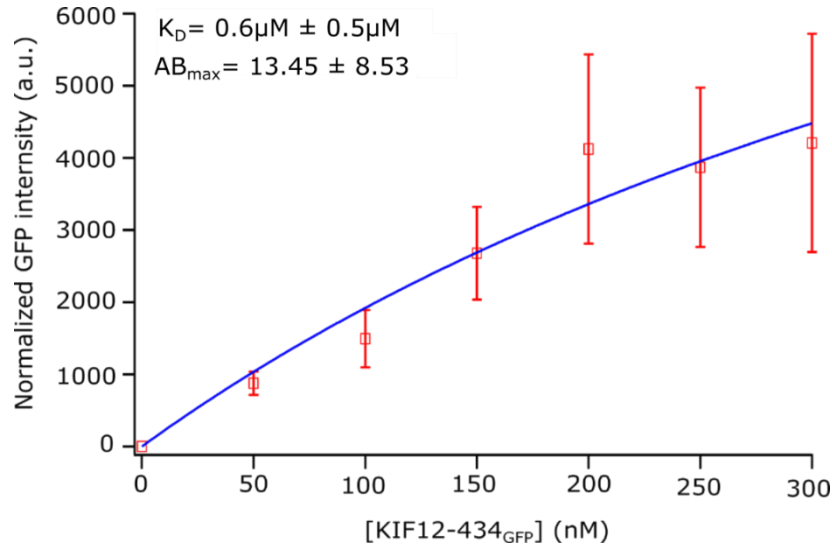


Figure 3.16. KIF12-434 affinity for microtubule. Biomolecular binding curve obtained from plotting GFP units (the amount of KIF12-434_{GFP}.microtubule versus [KIF12-434_{GFP}]. Shown are the K_D and AB_{max} (coefficient values \pm SD) used to generate the data points and curve. The data was obtained using microtubule affinity assay. $N=30-40$ microtubules per each protein concentration.

3.7 KIF12-434 is able to distinguish the ends of Taxol-stabilised

Some kinesins such as KIF7, which is a non-translocating kinesin, found in primary cilia of mammalian cells, recognise the growing microtubule tip by preferential binding to GTP-tubulin, which is found at growing microtubule plus ends, over the GDP-tubulin of the microtubule lattice (Jiang et al., 2019, Nakata et al., 2011). To test whether KIF12 could distinguish GTP- from GDP-tubulin, two populations of microtubules were grown: GMPCPP-stabilised and Taxol-stabilised. Microtubules grown in the presence of GMPCPP, a slowly hydrolysing analogue of GTP, have GMPCPP-tubulin throughout the length of the microtubule and

are analogous to the GTP cap, found at growing microtubule ends. A second population of microtubules were grown in the presence of GTP and stabilised after growth by addition of Taxol. In these microtubules GTP will mainly be hydrolysed to GDP within the microtubule lattice. These two microtubule populations were mixed and adhered to the surface of glass coverslips. GFP-labelled KIF12-434 was then added and imaged using TIRF microscopy (**Figure 3.17 A**).

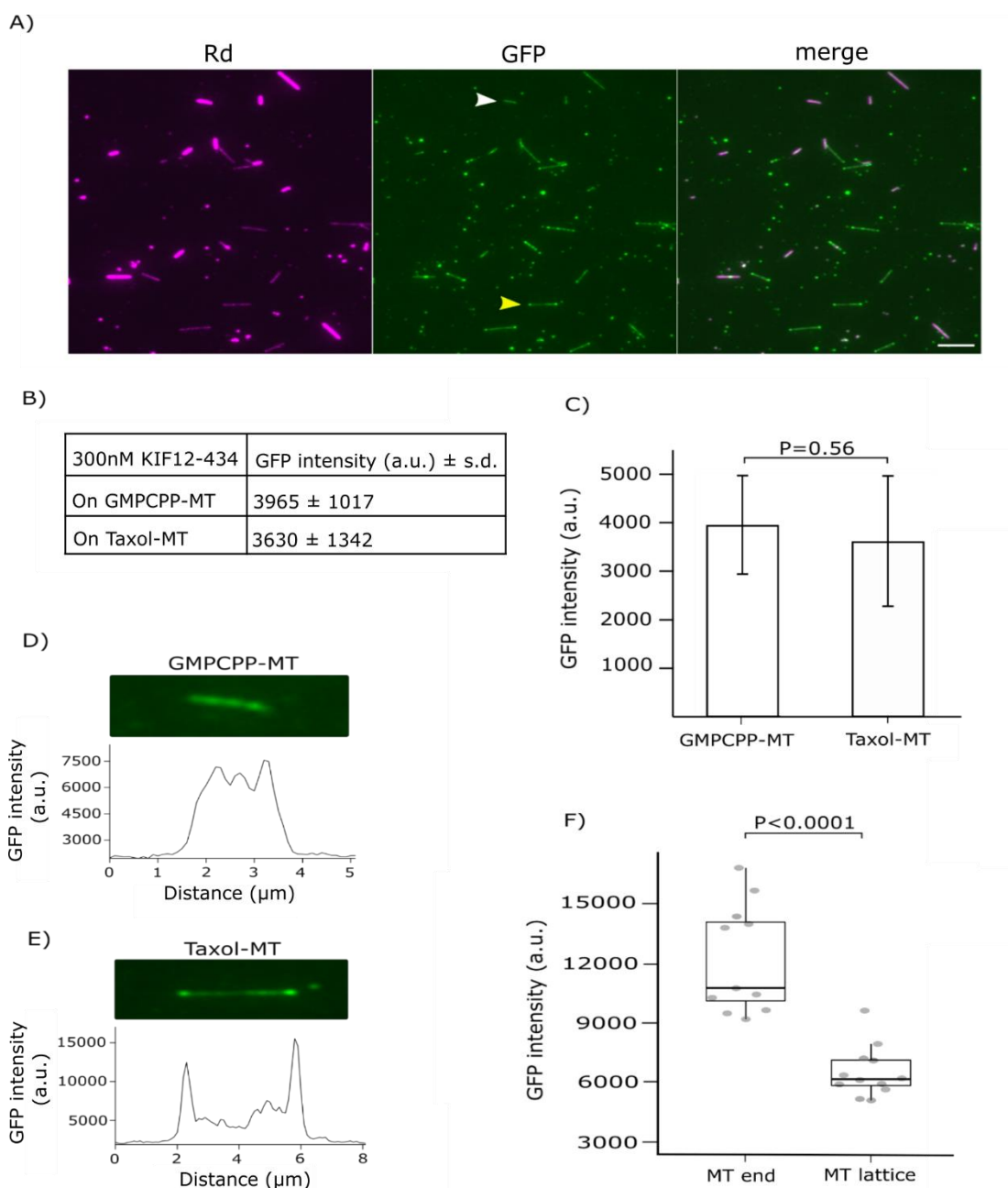


Figure 3.17. KIF12-434 cannot distinguish GMPCPP from Taxol stabilized microtubules. A) Representative images of a mixture of Taxol-stabilized and GMPCPP-stabilized microtubules, 5% and 25% rhodamine labelled, respectively, Rd: rhodamine channel, GFP: GFP channel, white and yellow arrows indicate representative GMPCPP- and Taxol- stabilised microtubules, merged: overlay of Rh and GFP channels, scale bar 5 μ m. B) and C) measurements of GFP signal intensities of KIF12-434 on microtubules (mean \pm SD). GFP quantification was carried out only along microtubule lattice (bright microtubule ends were excluded), n=9-28. D) and E) white and yellow arrow indicated microtubule are magnified, with GFP intensity profiles along microtubule underneath. F) GFP intensity quantification on end and lattice of Taxol-stabilised microtubules, n=12.

The intensity of the GFP signal along microtubules was quantified and compared. The intensity of the GFP signal on GMPCPP stabilised-microtubules (GTP equivalent) was 3965 ± 1017 (mean \pm SD) while on Taxol stabilised-microtubules (GDP equivalent) it was 3630 ± 1342 (**Figure 3.17 B and C**). These data suggest that KIF12-434 does not distinguish GTP- from GDP-tubulin within microtubules as there is no significant difference between the amount of KIF12-434-GFP bound to GTP equivalent microtubules and GDP microtubules (p-value = 0.56). Interestingly, for Taxol-stabilised microtubules, GFP intensity on the ends was significantly higher than on the lattice (**Figure 3.17 A and E**). This is in contrast to GMPCPP-stabilised microtubules for which the GFP signal was evenly distributed along the microtubules (**Figure 3.17 A and D**), The mean GFP intensity on microtubule end and lattice for Taxol stabilized microtubules were 10746 ± 2106 and 6101 ± 1020 , respectively (p < 0.0001) (**Figure 3.17 F**). These data suggest that a different conformation of tubulin is found at the ends of Taxol-stabilised

microtubules and that this conformation is preferentially recognised by KIF12-434.

3.8 KIF12 tail does not interact with microtubules

For some kinesins, the tail domain can interact with microtubules such as Kinesin-4, KIF21B which shows plus-end directed motility with greater processivity than Kinesin-4, KIF4 (van Riel et al., 2017). This improved processivity results from an additional microtubule binding region located in the tail. As KIF12-434 is a truncation, one possible explanation for its low affinity for microtubules is that its activity is not the full activity for KIF12. Thus, the tail may have an affinity for microtubules and would shift the equilibrium towards microtubules and allow KIF12 to bind to microtubules even at high concentrations of unpolymerised tubulin. Therefore, to see if KIF12 tail interacts with microtubules, we tried to express the tail independently from the rest of the protein. Two tail constructs were then made; one starting where KIF12-434 ends, which is KIF12 tail [434-651]. This construct includes the remaining part of the coiled coil domain besides the rest of the protein. The second construct consists of the sequence following the coiled coil domain, starting from amino acid 478 until the end of the protein, KIF12 tail [478-651] (**Figure 3.18**).

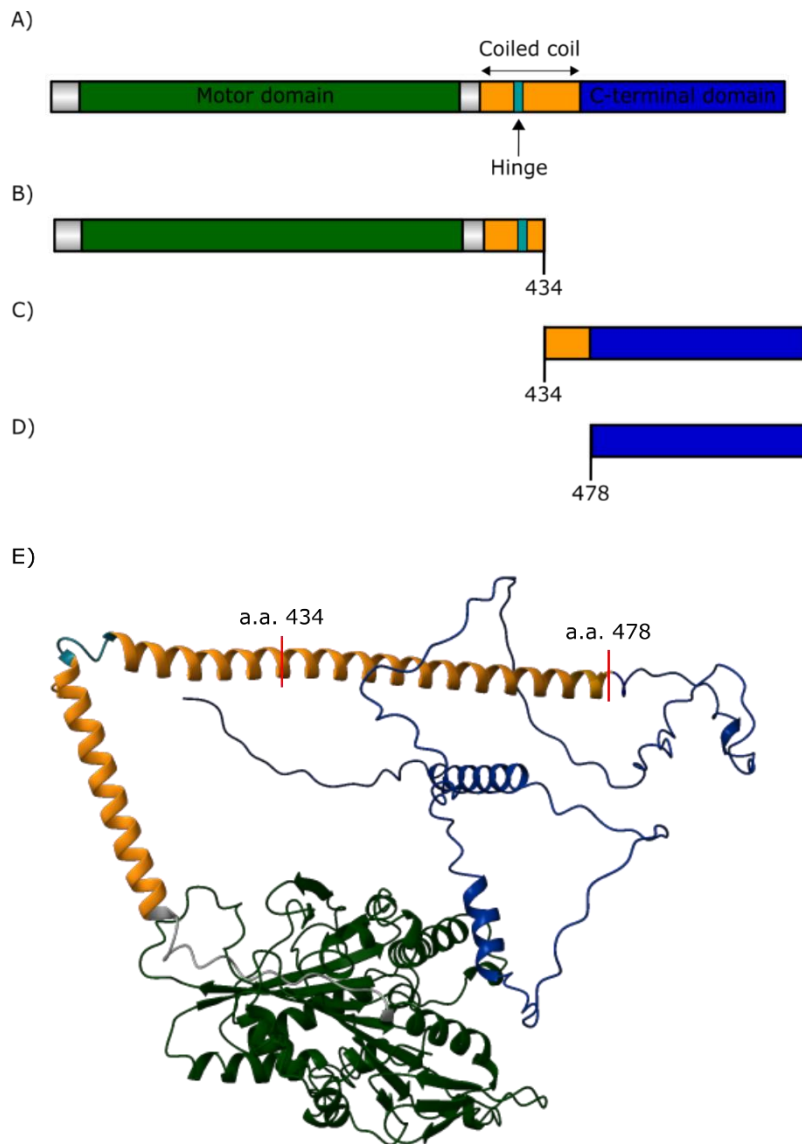


Figure 3.18. KIF12 tail constructs. A) Full length KIF12, B) KIF12-434, C) KIF12 tail [434-651], and D) KIF12 tail [478-651], E) AlphaFold's predicted structure for full length human KIF12, red lines indicate where the KIF12 tail [434-651] and KIF12 tail [478-651] start.

Both constructs had C-terminal GFP and 7xHis tags. Both constructs were transformed into XL10 gold *E.coli* cells; however, no colonies grew for KIF12 tail [478-651]. Hence, KIF12 tail [434-651] was then taken further for protein expression in Sf9 cells and purification using nickel-affinity chromatography (2.3.1). KIF12 tail [434-651] was soluble but

not pure (**Figure 3.19**, gel (left)), and since this construct had no other purification tag, cation exchange chromatography was then used as a second purification step as described for Kinesin-1 2.5). However, the protein did not bind to the column, then anion exchange chromatography was tried, but the protein did not bind to the column either (**Figure 3.19**, gel (right)).

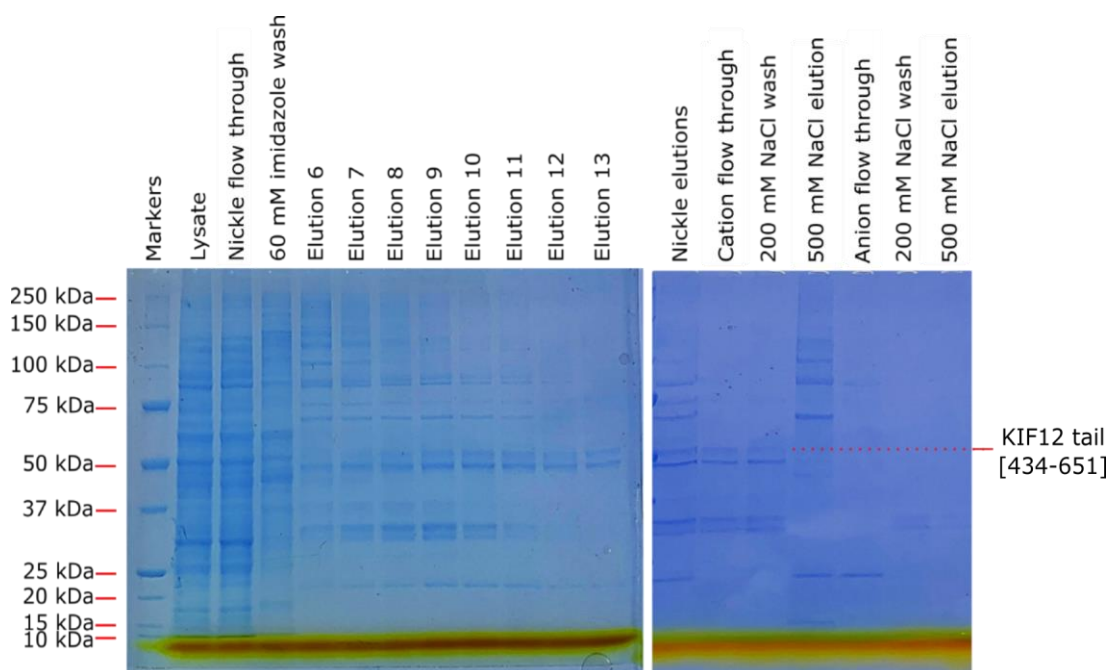


Figure 3.19. Purification of KIF12 tail [434-651]-GFP-7xhis. Instant Blue stained SDS-PAGE gels of progression of wild type KIF12 tail [434-651]-GFP-7xhis purification, lysate: cleared cell lysate, nickel flow through: flow through from cleared lysate applied to nickel affinity column, 60mM imidazole wash: wash with 60mM imidazole, elutions 6-13: 200mM imidazole elutions, nickel elutions: (6-13) 200mM imidazole elutions combined, cation flow through: flow through from anion exchange column, 200mM NaCl wash: wash with 200mM NaCl, 500mM NaCl elution: protein was eluted with 500mM NaCl, anion flow through: eluted protein from anion exchange column was applied to cation exchange column, 200mM NaCl wash: wash with 200mM NaCl, 500mM NaCl elution: protein was eluted with 500mM NaCl. The expected molecular weight of the protein is 53 kDa. Protein PI (isoelectric point) = 8.053.

Since it was not possible to get KIF12 tail [434-651] with only one purification tag (his tag) pure enough to carry out the subsequent assay, and the use of ion exchange chromatography was not successful, another trial to express the tail constructs but with two purification tags was carried out. For that, pFastBac 11 was utilised which introduces an N-terminal 6xhis tag and C-terminal GFP and StrepII tags. However, KIF12 tail [434-651] was not soluble, as the pellet was green florescent after cells were lysed and centrifuged, and no protein was detected in the supernatant. Another plasmid with two purification tags then has been used. This plasmid is pFB-Skin0+GFP, which has C-terminal GFP, also SPB (Streptavidin-Binding Peptide), and a 6xhis tags. Despite using a two-step purification methods, the KIF12 tail [434-651] was found to be soluble but not pure as there were different proteins present in the elute (**Figure 3.20**).

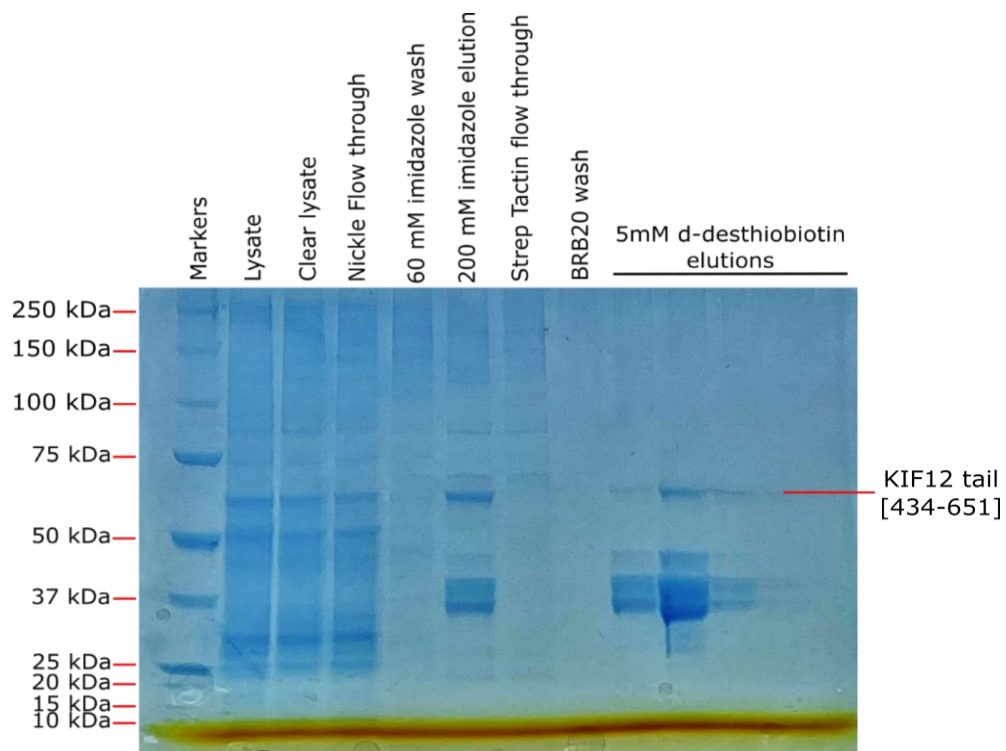


Figure 3.20. Purification of KIF12 tail [434-651]-GFP-SBP-6xHis. SDS-PAGE gel stained with Instant Blue of progression through purification of KIF12 tail [434-651]-GFP-SBP-6xHis. Lysate: cell lysate, cleared lysate: cell lysate supernatant after centrifugation, **nickel** flow through: flow through from cleared cell lysate applied to **nickel** affinity column, wash: wash with 60mM imidazole, elution: protein was eluted with 200mM imidazole, Strep Tactin flow through: the eluted protein from **nickel** affinity column applied to Strep-Tactin column, BRB20 wash: BRB20, 75mM KCl, 0.1% T20 wash, 5mM desthiobiotin elutions: protein was eluted with BRB20, 75mM KCl, 0.1% T20, supplemented with 5mM desthiobiotin. The expected molecular weight of the KIF12 tail is 58 kDa.

The KIF12 tail [478-651] was soluble but not pure as well (**Figure 3.21**).

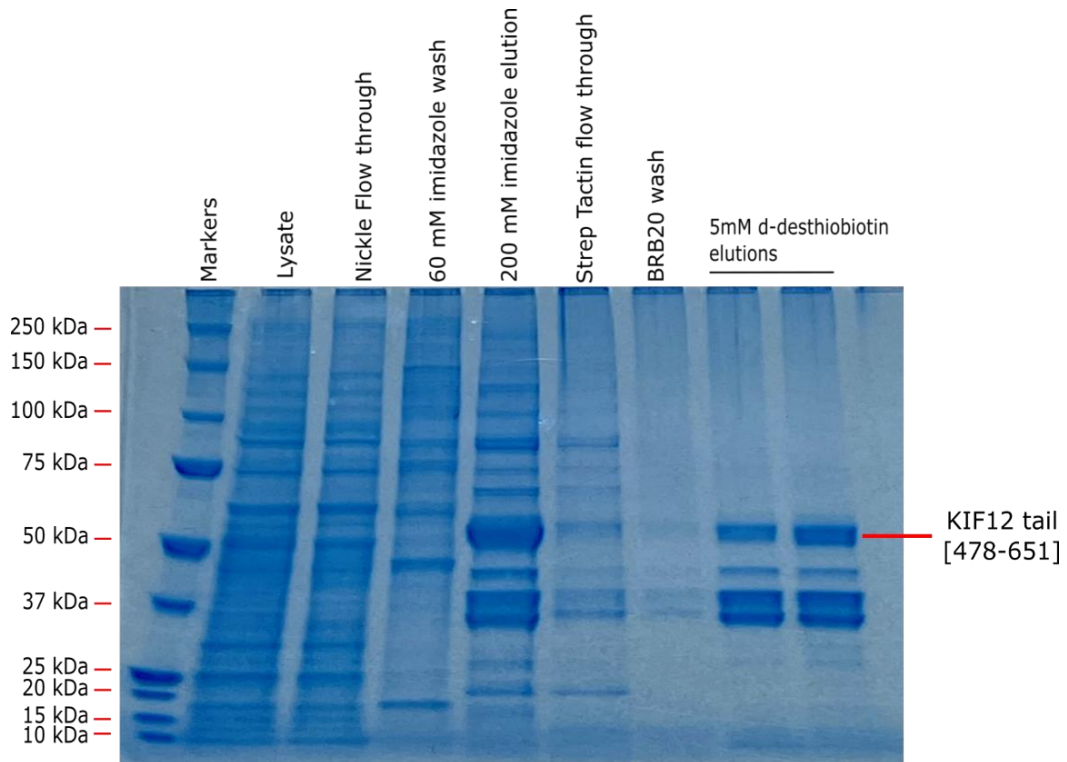


Figure 3.21. Purification of KIF12 tail [478-651]-GFP-SBP-6xHis. SDS-PAGE gel stained with Instant Blue of the steps of purification of wild type KIF12 tail [478-651]-GFP-SBP-6xHis. Lysate: cleared lysate, **nickel** flow through: flow through from **nickel** affinity column after applying cleared cell lysate, 60mM imidazole wash: wash with 60mM imidazole, 200mM imidazole elution: protein was eluted with 200mM imidazole, Strep Tactin flow through: eluted protein with 200mM imidazole was applied to Strep Tactin column, BRB20 wash: wash with BRB20, 75mM KCl, 0.1% T20, 5mM d-desthiobiotin elutions: protein was eluted with 5mM d-desthiobiotin. The expected molecular weight of the KIF12 tail is 52 kDa.

Despite being not pure, these proteins were trialled in a microtubule affinity assay to see whether the KIF12 tail interacts with microtubules, as they are the only GFP-tagged proteins and therefore can be distinguished from other proteins. The KIF12 tails were not observed to interact with microtubules, as there were no GFP signals detected on microtubules (**Figure 3.22**). Therefore, it is likely that the tail region of KIF12 does not interact with microtubules. Perhaps this agrees with AlphaFold's prediction that this domain is largely disordered (**Figure 3.18 E**). The activity seen for KIF12-434 in the dynamic microtubule growth assay is the full activity of the protein and not because it is a truncation. However, the presence of other proteins with the purified KIF12 tails may prevent the interaction with microtubules.

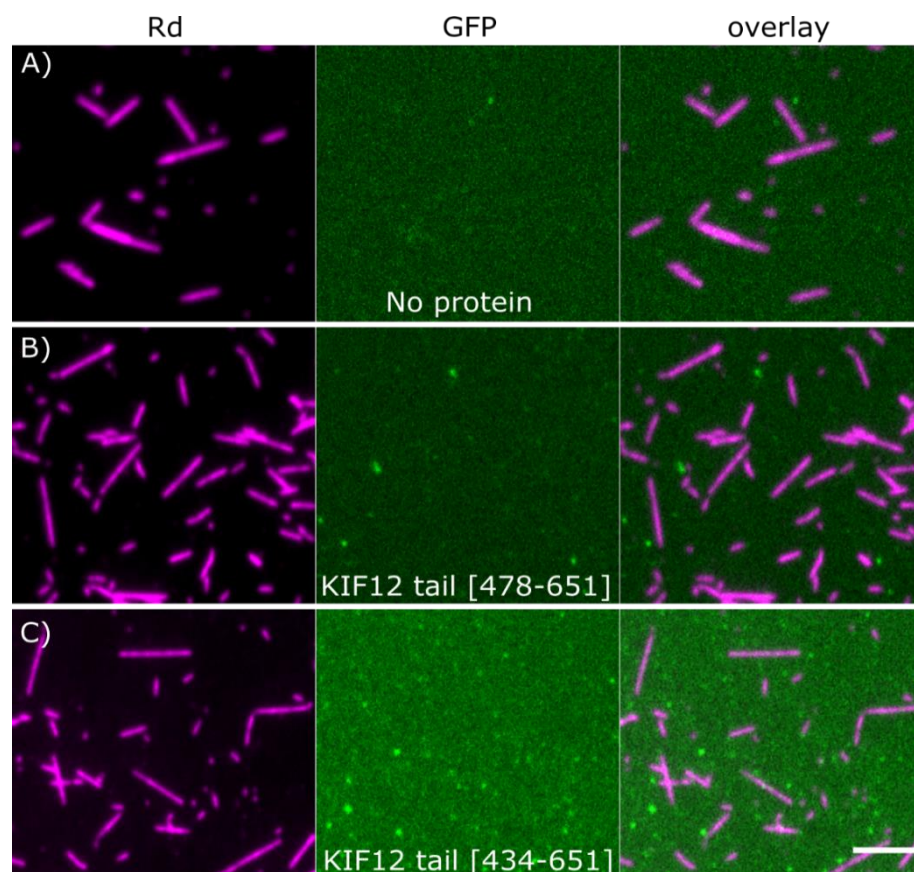


Figure 3.22. KIF12 tail does not interact with microtubules. A) No protein was added to the microtubules, B) 8nM KIF12 tail [478-651]-GFP was added to microtubules, C) 13nM KIF12 tail [434-651]-GFP was added to microtubules. Rd: rhodamine channel, GFP: GFP channel, overlay: overlay of rhodamine and GFP channels. GFP intensity was normalized to the intensity when there is no protein added. Scale bar 5 μ m. Data acquired using microtubule affinity assay.

3.9 KIF12-434 has a low microtubule-stimulated ATPase

To understand the relationship between the lack of processive motility observed for KIF12 and the ATP turnover cycle, the ATP turnover rate (ATPase) for KIF12 was measured under different conditions: in solution (basal ATPase, with unpolymerised tubulin, with microtubules).

Reactions were started by addition of KIF12 to ATP containing buffer. Reactions were then quenched at various time intervals with acid and then neutralized (**2.16.1**). The amount of ADP and ATP present in the samples was measured by separating the nucleotides by HPLC and quantitation by absorbance at 259nm (**Figure 3.23**).

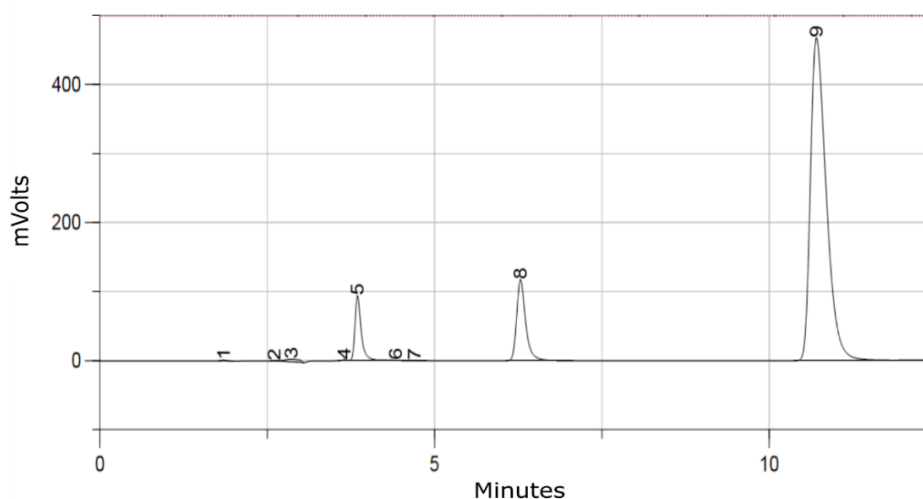


Figure 3.23. ADP and ATP were separated by HPLC and produced peaks with concentration dependent integrals. HPLC traces from a solution containing a mixture of ADP (peak 8) and ATP (peak 9).

The amount of ADP as a proportion of total nucleotide was calculated and plotted against time (**Figure 3.24 A**). The increase in ADP over time was calculated by fitting the linear region of these plots. The ATP turnover rate of KIF12-434 in solution was very slow, $0.007 \pm 0.003 \text{ s}^{-1}$. This rate is close to the basal ATPase of the processive translocating Kinesin-1 family (0.009 s^{-1}) (Hackney, 1988). However, in the presence of microtubules KIF12 ATPase was $0.164 \pm 0.024 \text{ s}^{-1}$, a microtubule-stimulated acceleration of ~ 23 -fold (**Figure 3.24 B**). Members of the Kinesin-1 family typically show ~ 5000 -fold increase in ATPase by interaction with microtubules (Yildiz et al., 2008, McVicker et al., 2011, Coy et al., 1999). The behaviour seen for KIF12-434 is similar to that of immotile Kinesin-4 KIF7, where a very small microtubule-dependent acceleration of ATP turnover was observed (0.02 s^{-1}) even at a high microtubule concentration ($25\mu\text{M}$), which reflected only a five-fold enhancement of KIF7's basal ATPase rate (Yue et al., 2018). Therefore, this agrees with the previous data that suggest KIF12 is not a translocating kinesin, and may give a suggestion that KIF12 does not possess a translocating motility due to a weak stimulation of its ATP turnover by microtubules. In the presence of unpolymerised tubulin KIF12-434 ATPase rate was not significantly increased, $0.013 \pm 0.005 \text{ s}^{-1}$ ($p=0.149$) (**Figure 3.24 B**). This could explain why KIF12 has high affinity for unpolymerised tubulin and can sequester KIF12 away from microtubules if KIF12 binds unpolymerised tubulin in a nucleotide state where it binds tightly, then unpolymerised tubulin is not encouraging

KIF12 to move out of that nucleotide state into a less tightly bound state because it is not accelerating the ATPase.

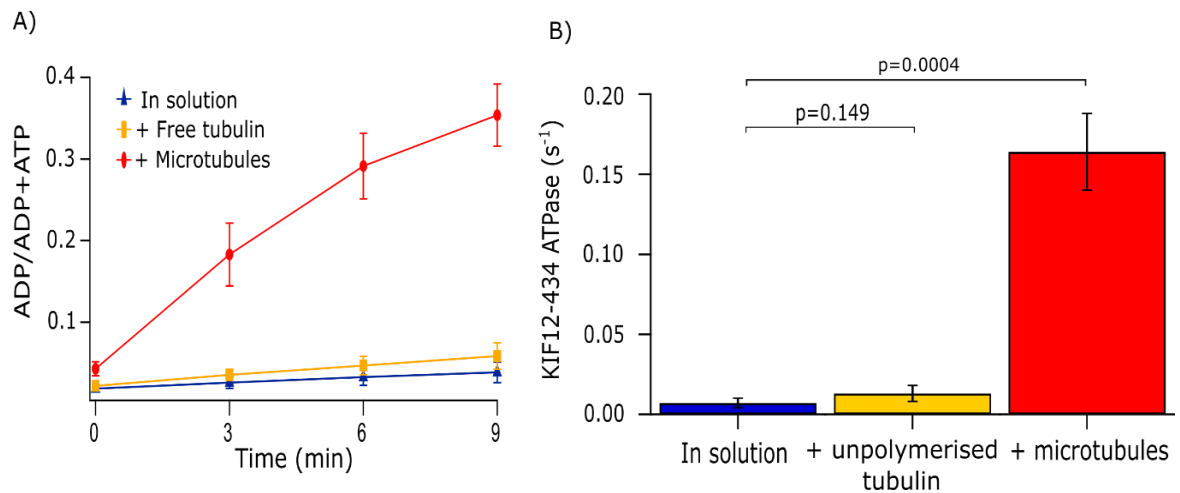


Figure 3.24. KIF12-434 has a low microtubule-stimulated ATP turnover. A) The change in the proportion of ADP of total nucleotides at three minute intervals was measured using HPLC. Points are mean \pm standard deviation, $n=3$ for each time point, and a line of best fit is shown. B) Average ATP turnover rate, from the gradient of the fit for each experiment \pm standard deviation is shown for each condition.

3.10 KIF12-434 microtubule-dependent ADP dissociation is likely to be the rate limiting step

For each ATP turnover cycle by a kinesin whether in solution, or in the presence of tubulin polymerised or unpolymerised, it is important to determine the rate limiting step, because the rate limiting step dictates the nucleotide state in which the kinesin would mainly exist under the particular conditions.

To see whether ADP dissociation is the rate limiting step stopped-flow was used to measure the rate of ADP dissociation from KIF12 (**2.17**). To

carry out this, KIF12-434 was preloaded with mantADP, which is ADP attached to a small fluorophore-mant (**Figure 3.25**).

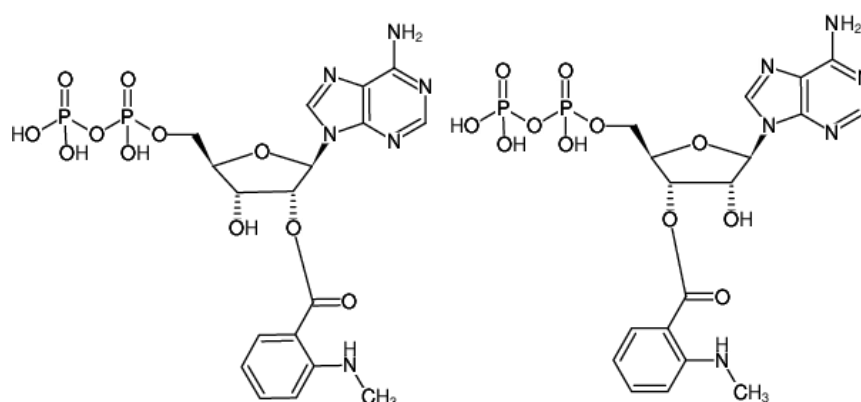


Figure 3.25. Structural formula of Mant-ADP. The nucleotide analogue mant-ADP is modified on the ribose moiety by attaching mant fluorophore. It combines fluorescence with close mimicry of the properties of natural nucleotide in respect of protein binding and interaction.

When mantADP is bound to KIF12-434 it displays a higher fluorescence intensity than when it is free in solution. Hence when KIF12-434.mantADP is mixed with an excess of ATP, the fluorescence intensity decreases as mantADP dissociates and unlabelled ATP binds to KIF12-434 (**Figure 3.27 A**). The measured rate constant of ADP dissociation from KIF12-434 in solution was $0.056 \pm 0.002 \text{ s}^{-1}$ (**Figure 3.27 B**), which is 8-fold faster than KIF12-434 ATPase in solution in solution ($0.007 \pm 0.003 \text{ s}^{-1}$). Therefore, ADP dissociation does not seem to be the rate limiting step in the ATP turnover cycle in solution. This is similar to the case of MCAK, a non-translocating kinesin which has a ADP dissociation rate constant of $0.148 \pm 0.015 \text{ s}^{-1}$ in solution, faster than its ATPase rate constant of $0.00095 \pm 0.00005 \text{ s}^{-1}$ (Friel and Howard,

2011). This may support the previous results obtained suggesting that KIF12 is a non- translocating kinesin.

These data indicate that another step in the ATP turnover cycle is rate-limiting for KIF12 in solution. This could be ATP binding, ATP cleavage, or phosphate dissociation (**Figure 3.26**). It is unlikely that binding of ATP would be slow, as ATP binding has not been found to be rate-limiting for any kinesin studied to date. Phosphate dissociation is very rare to be rate-limiting. Hence the rate limiting step may be most likely to be ATP cleavage. Further work is required to confirm the rate-limiting step for the KIF12 ATPase cycle in solution.

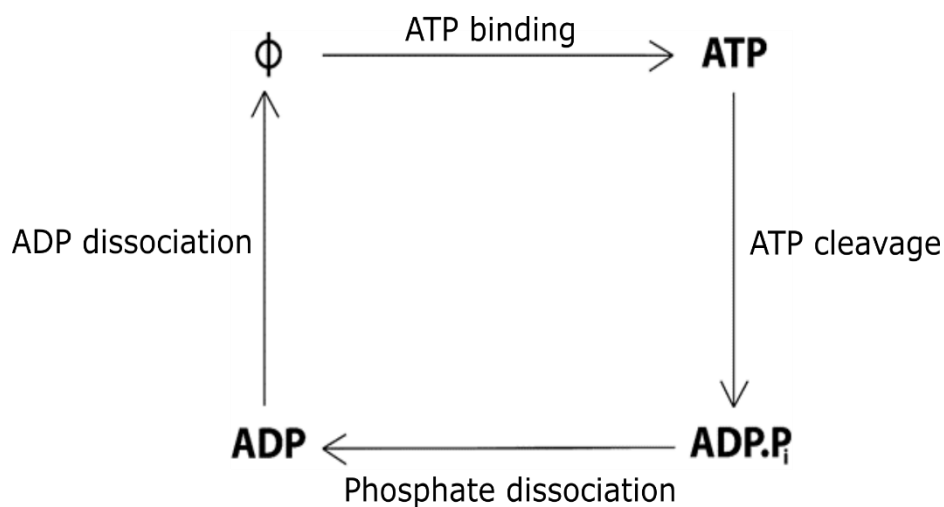


Figure 3.26. The ATP turnover cycle. ATP turnover consists of ATP binding to the nucleotide-free site (ϕ), ATP cleavage to ADP-P_i, dissociation of the free phosphate and release of ADP. Modified from (Friel and Howard, 2012).

In the presence of unpolymerised tubulin, the rate constant for ADP dissociation was 1.6- fold lower than in solution: $0.034 \pm 0.004 \text{ s}^{-1}$ and $0.056 \pm 0.002 \text{ s}^{-1}$, respectively. This reduction is statically significant as

the p value equals 0.001 (**Figure 3.27 A and B**). If, the rate-limiting step in the ATPase cycle in solution is ATP cleavage, KIF12 would be mainly in the ATP bound state when in solution. Therefore, when it interacts then with unpolymerised tubulin it is likely that it will bind tightly, and as unpolymerised tubulin does not accelerate the ATPase so KIF12 could remain tightly bound to unpolymerised tubulin in agreement with the data indicating that tubulin sequesters KIF12 away from microtubules. These data are also in agreement with the fits to the tubulin-microtubule competition assay data (**Figure 3.14**). The parameters determined from the model used to fit these data suggest that KIF12 has a higher affinity for unpolymerised tubulin than for microtubules.

In the presence of microtubules, the ADP dissociation from KIF12-434 is well described by a double-exponential function, as the ADP dissociation rate has two phases; fast and slow (**Figure 3.27 A and B**). The faster phase is ~ 3 -fold higher than basal ADP dissociation ($p=0.0143$).

However, this increase is small compared to that of Kinesin-1 family where ADP dissociation is accelerated 5000-fold on interaction with microtubules (Hackney, 1988), resulting in an increase in the ATPase rate from 0.01 s^{-1} to around 50 s^{-1} (Kuznetsov and Gelfand, 1986, Hackney and Stock, 2008). The faster phase is close to the microtubule-stimulated ATPase; 0.171 ± 0.048 compared to 0.164 ± 0.024 , respectively, and the p value equals 0.83 indicating that there is no statistical significance between the two. Therefore, the microtubule-

stimulated ADP dissociation is possibly what is limiting the rate of the full reaction.

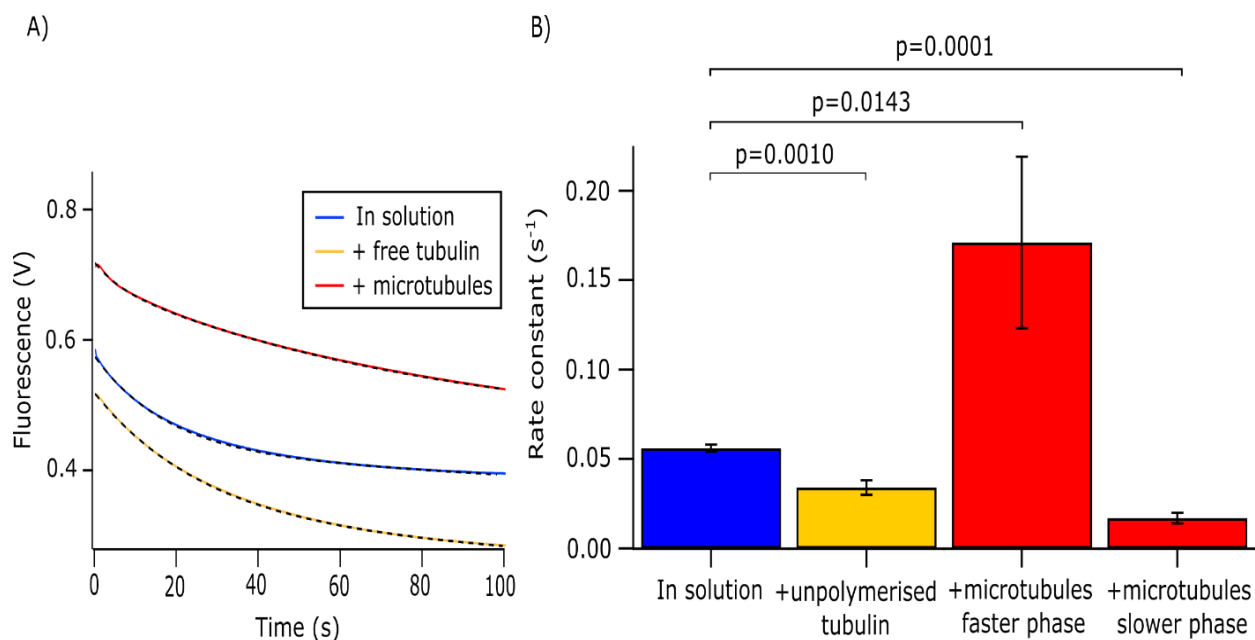


Figure 3.27. ADP dissociation from KIF12-434 is weakly stimulated by microtubules. KIF12-434 was pre-loaded with mantADP and then rapidly mixed with ATP. A) Fluorescence decreases upon the dissociation of mantADP from KIF12-434, the fluorescence signal (blue and yellow lines) and (red) were fit to single and double exponential functions, respectively, plus a line of constant negative slope to account for photobleaching of the mant group. Data fit is the black dashed line. $N=3$ for each condition.

Table 3. Summary table of KIF12-434 ATPase and mADP dissociation data. Constants and rate constant amplitudes (mean \pm s.d., $n=3$). * Indicates where there is a statistically significant difference from in solution.

	ATPase rate constant (s ⁻¹)	ADP dissociation	
		Rate constant (s ⁻¹)	Rate constant amplitudes
In solution	0.007 \pm 0.003	0.056 \pm 0.002	0.150 \pm 0.013
+ Unpolymerised tubulin	0.013 \pm 0.005	0.034 \pm 0.004 *	0.208 \pm 0.157
+ Microtubules	0.164 \pm 0.024 *	k_{fast} 0.171 \pm 0.048 * k_{slow} 0.017 \pm 0.003 *	A_{fast} 0.040 \pm 0.021 A_{slow} 0.148 \pm 0.027

To summarise, the findings of microtubule gliding assay and stepping assay confirm that KIF12-434 does not translocate along microtubule, therefore KIF12 cannot bring a cargo carrying function to the primary cilia. Results of microtubule depolymerisation assay and microtubule growth dynamic assay show that KIF12-434 possess no microtubule depolymerising activity; however, KIF12-434 has a small but significant stabilising effect on both GMPCPP and dynamic microtubules and likely acts in cilia as a microtubule regulating kinesin. Competition assay results show that KIF12-434 has a higher affinity for tubulin dimer than for tubulin monomer and for microtubules, and further investigation is required to explain this behaviour in the context of KIF12 function in the primary cilia. The results of microtubule binding assay carried out on a mixture of GMPCPP- and taxol- stabilised microtubules show that KIF12-434 does not recognise the growing microtubule tip by preferential binding to GTP-tubulin over GDP-tubulin in the lattice. However, KIF12-434 is able to distinguish the ends of Taxol- stabilised microtubules which suggests that a different conformation of tubulin is found at the ends of these microtubules and that this conformation is preferentially recognised by KIF12-434. Studying partially purified different constructs of KIF12 tail show that the tail region of KIF12 does not interact with microtubules. Therefore, the activity seen for KIF12-434 in the dynamic microtubule growth assay is the full activity of the protein and not because it is a truncation. ATP turnover by KIF12 is not accelerated by the presence of unpolymerized tubulin resulting in KIF12 remaining in a tightly bound ATP containing state when interacting with unpolymerized

tubulin. Microtubules accelerate the ATPase of KIF12 ~20-fold, suggesting that KIF12 is driven into a nucleotide state that binds less tightly to microtubules by interaction with microtubules.

Chapter 4 In vitro characterisation of the activity of

KIF12-434ΔPPGGG

Genetic studies carried out on mouse models of polycystic kidney disease (PKD) show that KIF12 is a modifier gene for PKD and has a major impact on the severity of the disease phenotype (Mrug et al., 2005, Mrug et al., 2015). These studies identified a variant of KIF12 in which five amino acid region (PPGGG) is missing from the motor domain (**Figure 4.1**).

A)

```
Homo 21 GPETPIQVVLRVRPMSAAELRRGQQSVLHCSGTRTLQVSPPPGGGPEVAFR 120
      |||
Mus   21 GPETPIQVVLRVRPMSAAELRRGQQSVLHCSGTRTLQVS-----PEVAFR 115
```

B)

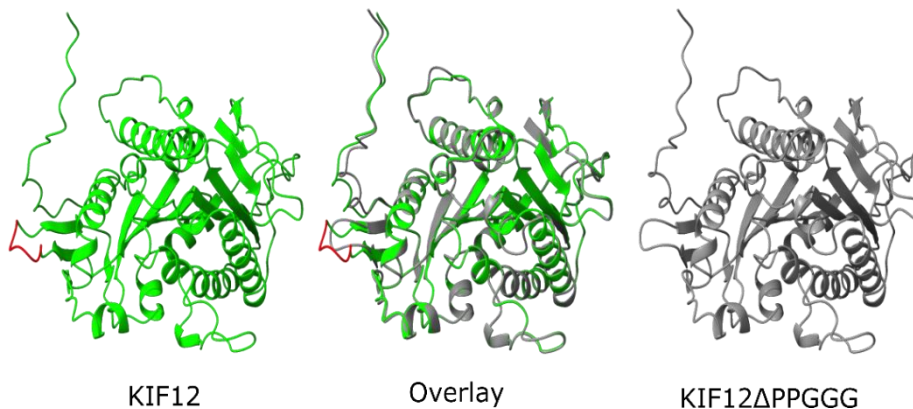


Figure 4.1. Sequence and structural alignment of wild type KIF12 and KIF12ΔPPGGG. A) Alignment of Homo sapiens (Human) KIF12 (residues 21 - 120) and Mus musculus (Mouse) KIF12ΔPPGGG (residues 21 - 115), PPGGG coloured in red. B) The structures of wild type KIF12 motor domain [1-363] based on human KIF12 primary sequence (Kato and Kato, 2005), and motor domain of Mouse KIF12ΔPPGGG (Mrug et al., 2015, Mrug et al., 2005) are shown separately and then the two structures were superimposed.

To determine whether the PPGGG region is a deletion or an insertion, Littledale (2017) first checked the position of the PPGGG sequence against known human splice boundaries to ensure that the differences in the human and mouse sequences were not due to a splicing error. The alignment showed that the 5 nucleotides of this INDEL (insertions and deletions) are three codons away from the splice boundary suggesting that its presence in the human sequence is unlikely to be due to a splicing error. Secondly, an alignment of an inbred (CRA) and an outbred (ICR) mouse line was carried out and it shows that PPGGG were present in the outbred line but not in the inbred line. Finally, an alignment of the reference standard Kif12 sequences for other mammals shows that they contain this PPGGG sequence. Thus, based on these results collectively it was suggested that PPGGG is present in wild type KIF12, with the absence in the mouse rsKif12 being due to a deletion in an inbred line.

This mutation is located in the predicted loop 2 (L2) of the motor domain; a structural element that is commonly involved in microtubule-binding interface. The length of L2 is considerably different between kinesin families, ranging from 2-3 residues in Kinesin-1 to 13-15 residues in Kinesin-13 family. For Kinesin with a long L2, this region becomes a more important element of the microtubule interface (Ogawa et al., 2004, Shipley et al., 2004, Kim et al., 2014). In KIF12, L2 is longer than that of Kinesin-1 (**Figure 4.2**), consisting of 9 residues. Therefore, as this mutation results in shortening Loop 2 we have

speculated that this mutation may impair the interaction of KIF12 with microtubules.

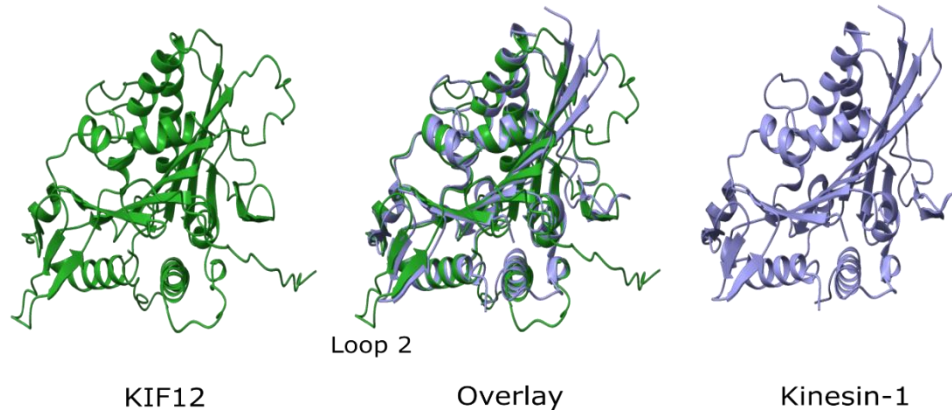


Figure 4.2. Structural alignment of KIF12 and Kinesin-1. Structural prediction of KIF12 motor domain [1-363] based on the primary sequence of human KIF12 (Katoh and Katoh, 2005) and structure of Kinesin-1 motor domain (P212121 crystal form, PDB ID: 5LT0) are shown separately and then the two structures were overlaid.

To study the impact of this mutation on the activity of KIF12, these 5 residues were deleted from the previously studied KIF12 truncation construct to make the construct KIF12-434 Δ PPGGG with C-terminal GFP and a 7 his tag (supplied by C. Friel) (**Figure 4.3**).

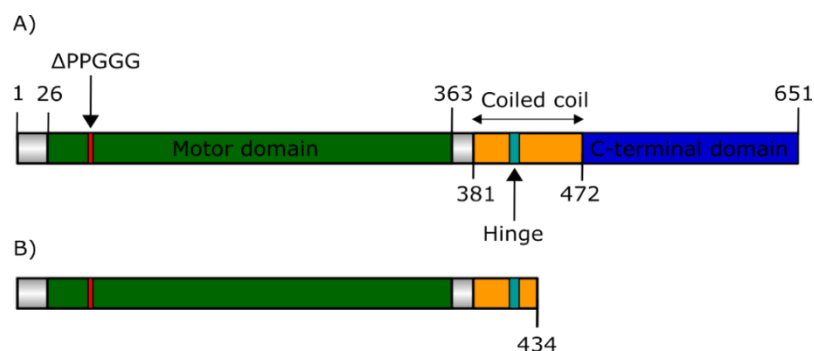


Figure 4.3. Domain structure of KIF12 Δ PPGGG. A) KIF12 has three domains; the N-terminal motor domain, coiled coil domain with internal hinge region, and C-terminal tail domain, numbered according to the sequence of human KIF12 (Katoh and Katoh, 2005), Δ PPGGG mutation coloured in red. B) Truncated form of the mutant KIF12 which has the first 434 amino acids of the full length protein.

4.1 KIF12-434ΔPPGGG is less soluble than the wild type

KIF12-434ΔPPGGG-GFP-7his was expressed in Sf9 cells as described in **section 2.2.4**, the cells were then lysed and centrifuged, and samples of the cell lysate, supernatant, and cell pellet were run on a gel (2.2.5). It was noted that the pellet from the cell lysate contains some GFP signal, indicating that this mutant version of KIF12-434 may be less soluble than the wild-type. Therefore, the protein band intensity was quantified relative to the lane intensity for each sample and normalized to the relative intensity of the protein band in the cell lysate. As seen in **Figure 4.4**, it seems that the mutation does not have an effect on the level of protein expression, as the relative band intensities of the wild type and the mutant in the cell lysate look similar; 0.0119 and 0.0127, respectively. However, the protein solubility appears to be decreased by the mutation as most of the mutant protein was found in the pellet, where the normalized ratio for the protein band relative intensity was 1.32 in the pellet compared to 0.90 in the supernatant, while it was 1.26 for the wild type in supernatant compared to 0.98 in the pellet. This suggests that the amount of mutant protein found in the pellet was 1.35-fold higher than the amount of wild-type protein found in the pellet. These data indicate that this 5-residue deletion reduces the solubility of KIF12.

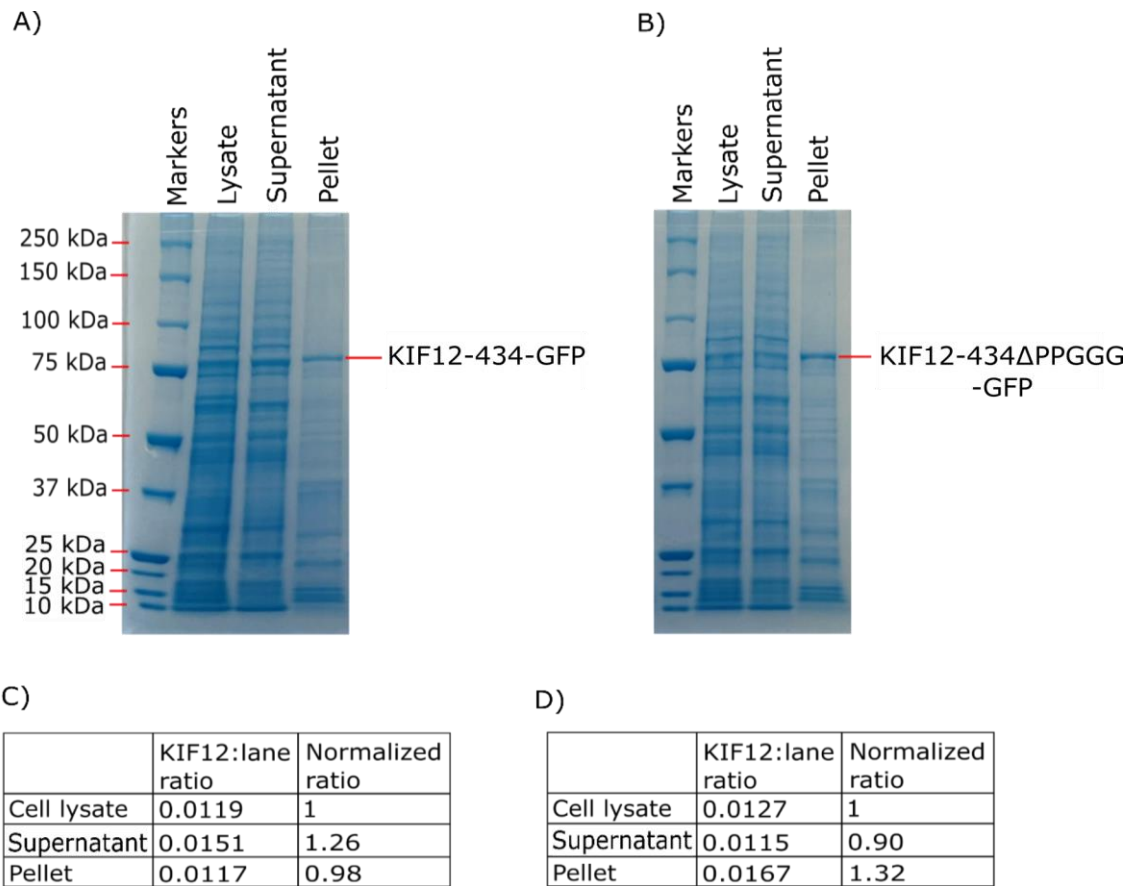


Figure 4.4. Wild type KIF12-434-GFP and KIF12-434 Δ PPGGG-GFP estimated level of expression and solubility. A) and B) Instant Blue stained SDS PAGE gels of wild type KIF12-434-GFP and KIF12 434 Δ PPGGG-GFP expressed in Sf9 cells, lysate: cell lysate, supernatant: centrifuged cell lysate, pellet: cell pellet. C) and D) tables of band intensity quantification for wild type KIF12-434-GFP and KIF12-434 Δ PPGGG-GFP, respectively, KIF12: lane ratio: ratio of KIF12 band intensity value to the whole lane intensity value, normalized ratio: cell lysate, supernatant and pellet intensity values were normalized to the band intensity value of the protein in the cell lysate (see Appendix 2 for full tables).

4.2 KIF12-434 Δ PPGGG purification using Nickel affinity chromatography

To see if the mutation affects the functional characteristics of KIF12, KIF12-434 Δ PPGGG-GFP with a 7 his tag was expressed in Sf9 cells and purified using nickel affinity chromatography (Figure 4.5).

As can be seen, the amount of the protein in the pellet is higher than in the elutions due to the reduction in protein solubility caused by the mutation, as previously shown in **Figure 4.4** where the amount of the protein in the pellet was 1.5-fold higher than in the supernatant. However, it was possible to obtain enough protein for the subsequent assays.

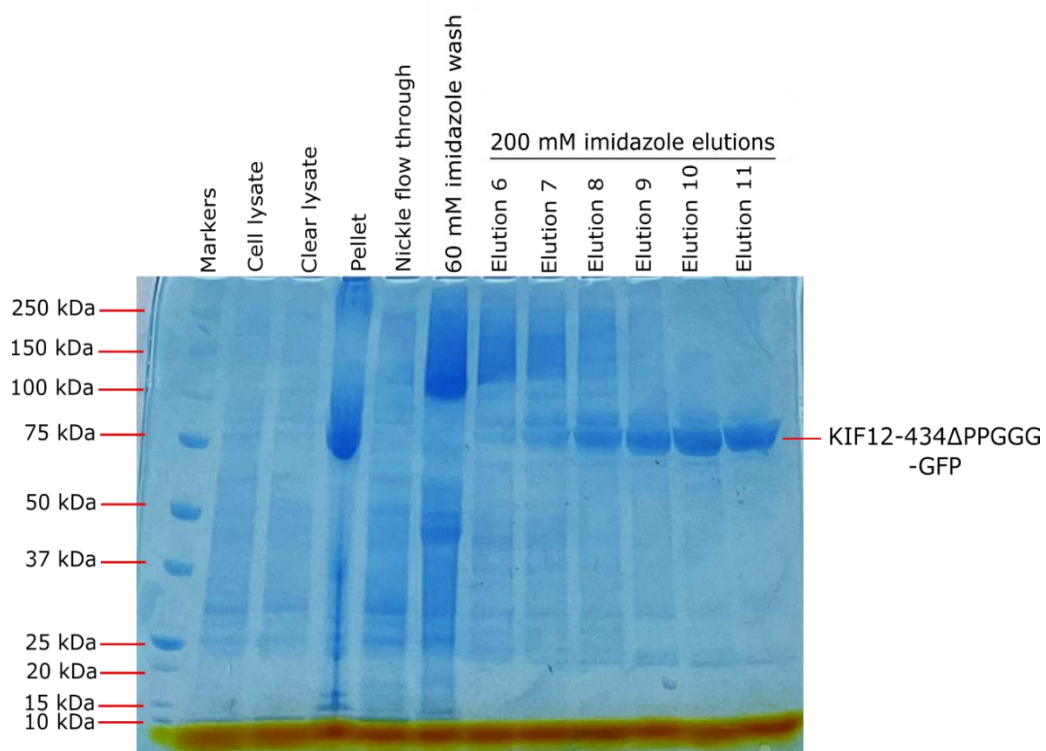


Figure 4.5. Purification of KIF12-434 Δ PPGGG-GFP-7His. Instant Blue stained SDS-PAGE gel of the steps of KIF12 -434 Δ PPGGG-GFP-7His purification, cell lysate: cell lysate before centrifugation, clear lysate: centrifuged cell lysate, pellet: cell pellet, **nickel** flow through: flow through from **nickel** affinity column after applying cleared cell lysate into the column, 60mM imidazole wash: wash with 60mM imidazole, 6-11 elutions: 200mM imidazole elutions. The expected molecular weight of the protein is 77 kDa.

4.3 KIF12-434ΔPPGGG seems to have a **higher** affinity for **microtubules** than the wild type

To explore whether the mutation has an impact on the affinity of KIF12 for microtubules, a microtubule affinity assay was executed as described in section (2.15), and the data were fit to **Equation 3.1**, as seen in **Figure 4.6**. Fitting these data suggests that the mutation has **increased the affinity** of KIF12-434 for microtubules from $0.6\mu\text{M} \pm 0.5\mu\text{M}$ to $0.06\mu\text{M} \pm 0.09\mu\text{M}$ for the wild type and the mutant, respectively. However, since the data are noisy, the parameters determined from the fit have large error associated with them. Therefore, although these data suggest that there may be an impact of affinity for microtubules, it is not possible to be certain. It may be possible to obtain a more accurate measure of affinity using a different assay, such as a pelleting assay in which microtubules are incubated with various concentrations of the protein then spun down. Then samples from the supernatant and the pellet at each protein concentration are run on a gel. The band intensities are then measured and plotted against corresponding protein concentrations and the data fit to an equation from which affinity for microtubules can be obtained. This type of assay has been successfully used previously for this type of measurement (Talapatra et al., 2015, Spittle et al., 2000).

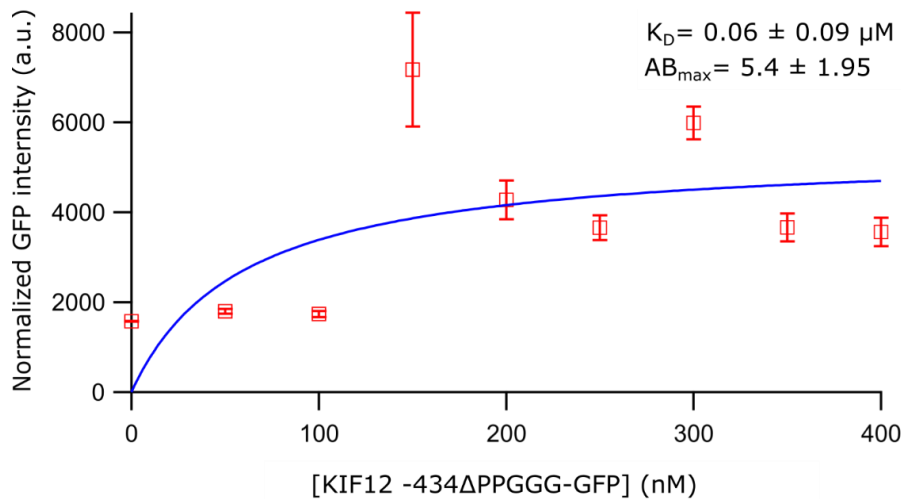


Figure 4.6. KIF12-434ΔPPGGG-GFP affinity for microtubule. Biomolecular binding curve obtained from plotting GFP signal intensity (the amount of KIF12 -434ΔPPGGG -GFP.microtubule versus [KIF12-434ΔPPGGG-GFP]. Shown are the K_D and AB_{max} (coefficient values \pm SD) used to generate the data points and curve. The data was obtained using microtubule affinity assay. $N=30-40$ microtubules for each protein concentration.

4.4 KIF12-434ΔPPGGG is able to distinguish the ends of Taxol-stabilised microtubules.

In-cell data shows that the full length KIF12ΔPPGGG does not discriminate the tip of the primary cilium from the main body of the cilium in the way that the full length wild type appears to (Varga lab, Institute of Molecular Genetics of the Czech Academy of Sciences, Prague, Czech Republic) (**Figure 4.7**). The *in vitro* data for the truncated wild type KIF12-434 shows that KIF12-434 is able to distinguish the end of Taxol stabilised microtubules which suggests that there is a tubulin conformational change at the ends of these microtubules and that change is preferentially recognised by the wild type (**Figure 3.17**).

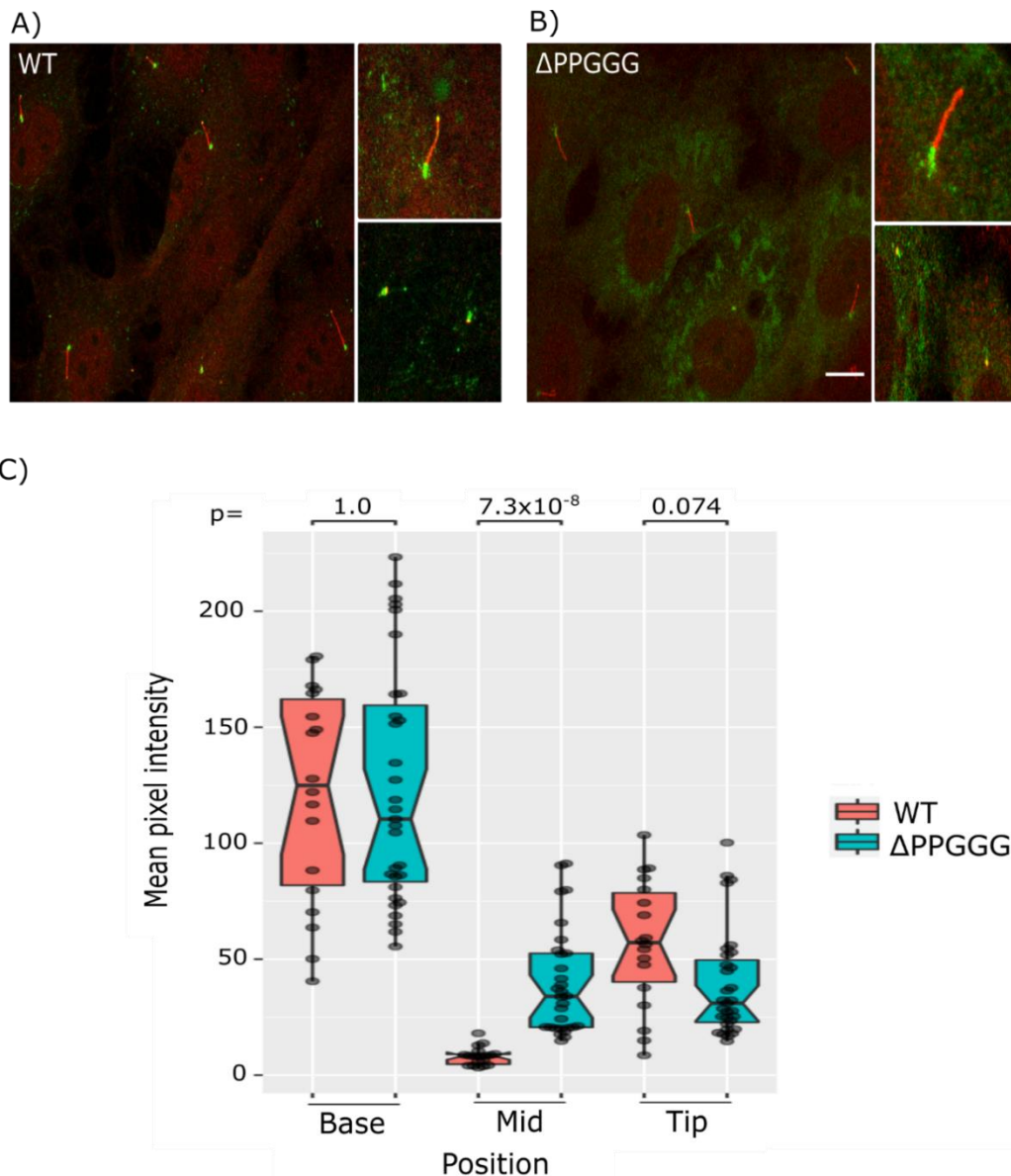
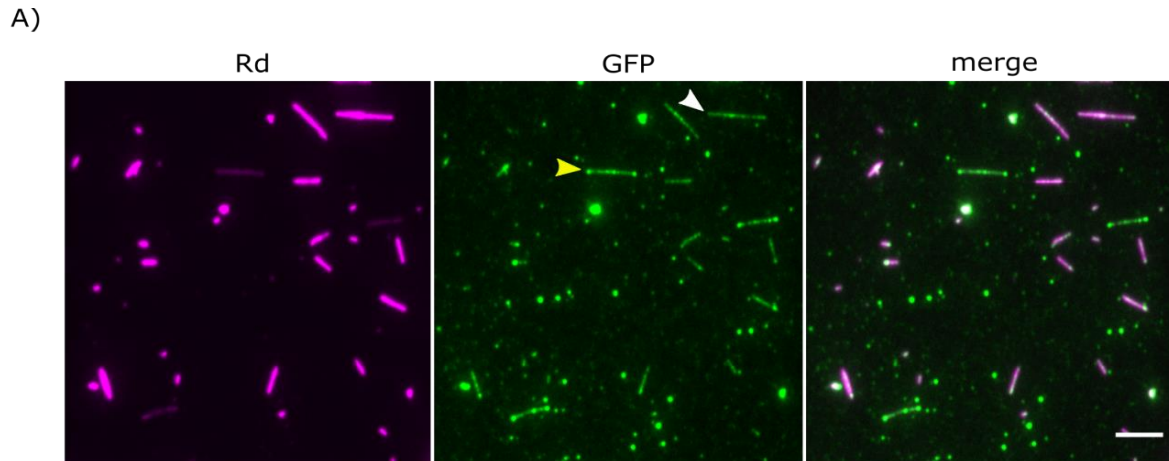


Figure 4.7. KIF12 Δ PPGGG cannot distinguish between the tip of primary cilium and the main body of the cilium. A) Left image: wild type KIF12 localises to the tip and base of the primary cilium, upper right image: a magnified primary cilium, lower right image: KIF12 co-localised with the centriole (to distinguish the localisation of KIF12 to the base of the cilium from the tip). B) Left image: full length KIF12 Δ PPGGG localises to base of the primary cilium, scale bar 10 μ m, upper right image: zoomed in primary cilium, lower right image: KIF12 Δ PPGGG localises to the centriole. KIF12 wild type and mutant were labelled with Neon green, primary cilia with anti-Arl13b, and centriole with red anti-Cep 164 marker, **cell line used: RPE1**. Data were collected by Varga lab (2021). C) GFP intensity quantification along primary cilium was carried by Bill Wickstead.

Therefore, it is possibly that when the wild-type reaches the tip of the primary cilium it gets retained due to its ability to recognise a tubulin conformational change there while the mutant does not. To test this hypothesis for the mutant, KIF12-434 Δ PPGGG-GFP has been tried in the assay in which the wild-type was observed to preferentially bind to the ends of Taxol stabilised microtubules, as seen in **Figure 4.8 A**. In this assay two populations of microtubules were grown: GMPCPP-stabilised and Taxol-stabilised. Microtubules grown in the presence of GMPCPP, a slowly hydrolysing analogue of GTP, have GMPCPP-tubulin throughout the length of the microtubule and are analogous to the GTP cap, found at growing microtubule ends at the ciliary tip. A second population of microtubules were grown in the presence of GTP and stabilised after growth by addition of Taxol. In these microtubules GTP will mainly be hydrolysed to GDP within the microtubule lattice. These two microtubule populations were mixed and adhered to the surface of glass coverslips. GFP-labelled KIF12-434 Δ PPGGG was then added and imaged using TIRF microscopy. GFP signal intensities along microtubules were then quantified and compared. As observed for the wild type, KIF12-434 Δ PPGGG has no preference for binding GTP- over GDP- tubulin *in vitro*. The average GFP intensity on GMPCPP stabilised microtubules was 2156 ± 746 and on Taxol stabilised was 2120 ± 754 ($p = 0.89$) (**Figure 4.8 B** and **C**). However, as also observed for wild-type the GFP intensity on the ends of Taxol stabilized microtubules was higher than on the lattice (**Figure 4.8 A** and **E**), unlike for GMPCPP stabilised microtubules where GFP signal was evenly distributed along the microtubule (**Figure**

4.8 A and D). The GFP intensities on microtubule end and lattice for Taxol stabilized microtubules were 9050 ± 1881 and 3996 ± 582 , respectively (**Figure 4.8 F**) ($p < 0.0001$).



B)

300nM KIF12- Δ PPGGG-434	GFP intensity (a.u.)
On GMPCPP-MT	2156 ± 746
On Taxol-MT	2120 ± 754

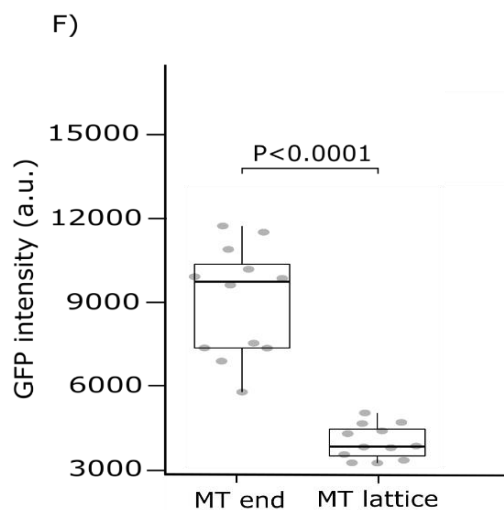
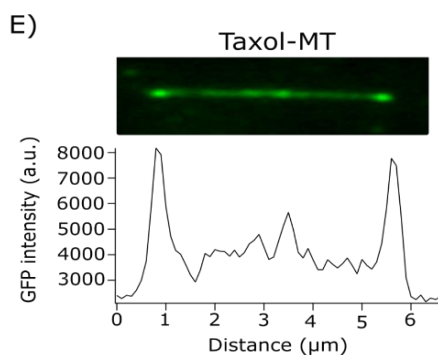
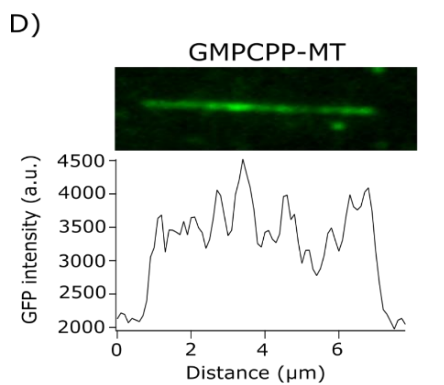
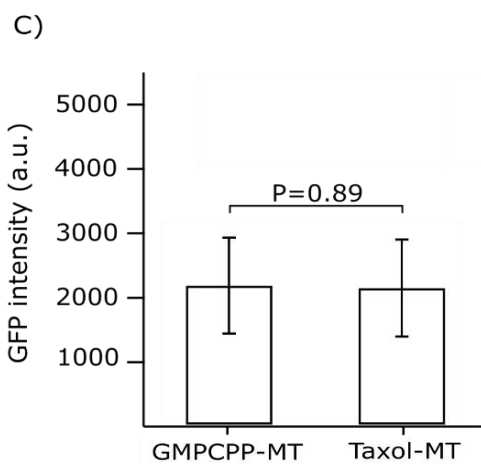


Figure 4.8. KIF12-434ΔPPGGG cannot distinguish GMPCPP from Taxol stabilized microtubules. A) Representative still images of a mixture of Taxol-stabilized and GMPCPP-stabilized microtubules, 5% and 25% rhodamine labelled, respectively, Rd: rhodamine channel, GFP: GFP channel, white and yellow arrows indicate representative GMPCPP- and Taxol-stabilised microtubules, merged: overlay of Rh and GFP channels, scale bar 5µm. B) and C) measurements of GFP signal intensities of KIF12-434ΔPPGGG on microtubules (mean ± SD). GFP quantification was carried out only along microtubule lattice (bright microtubule ends were excluded), n=9-28. D) and E) white and yellow arrow indicated microtubule are magnified, with GFP intensity profiles along microtubule underneath. F) GFP intensity quantification on ends and lattice of Taxol-stabilised microtubules, n=12.

This is in contrast to what would be expected for the mutant **as the mutation was thought to affect the ability of KIF12 to recognise and accumulate at the ends of microtubules**; however, this could be attributed to many reasons which are going to be discussed in the discussion chapter.

On the other hand, when comparing GFP signal intensities for the wild-type to that for the mutant on both types of microtubules (GMPCPP- and Taxol- stabilised microtubules), the intensity is consistently lower for the mutant than for wild-type. At 300nM protein concentration, GFP signal intensity of KIF12-434 on GMPCPP-stabilised microtubules is 3965 ± 1017 , whilst for the mutant is 2156 ± 746 ($p < 0.0001$), a 1.8 fold reduction. On the lattice of Taxol-**stabilised** microtubule the GFP intensity for wild-type is 3630 ± 1342 and for the mutant is 2120 ± 754 ($p = 0.0039$), a 1.7 fold reduction. On the ends of Taxol-stabilised microtubules GFP intensity was 10746 ± 2106 for wild-type and 9050 ± 1881 for the mutant ($p = 0.0493$), a 1.2 fold reduction (**Figure 4.9**).

These data may indicate that the affinity of the mutant for microtubules

is lower than for wild-type leading to less protein binding at a given concentration (**Figure 4.9**).

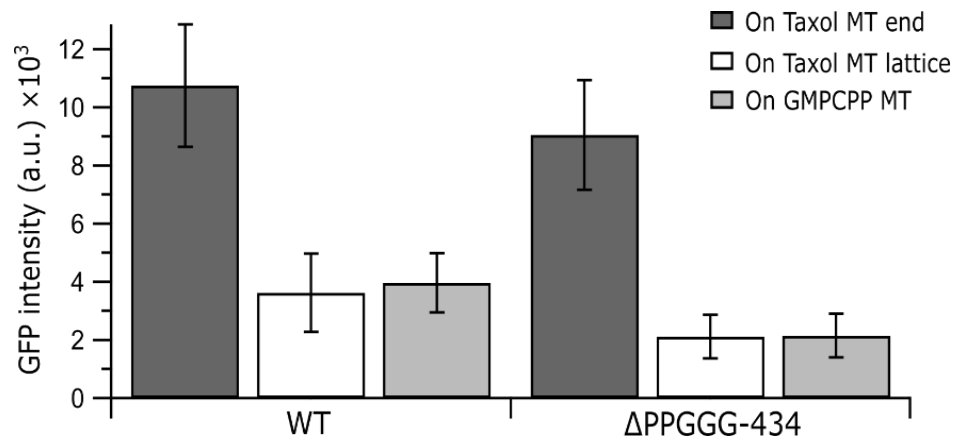


Figure 4.9. Affinity of wild type KIF12-434 and KIF12 Δ PPGGG-434 for GMPCPP- and Taxol- stabilised microtubules. N=9-28 microtubules.

Chapter 5 In vivo characterisation of the activity of

KIF12

Full length KIF12 was insoluble upon recombinant expression and so we worked with a truncated version (KIF12-434) to carry out *in vitro* assays that required purified protein. To study the activity of full length KIF12 and determine if the tail region missing from KIF12-434 contribute to this activity, we expressed full length KIF12 in mammalian cells in culture. This would also allow us to determine if KIF12 has a microtubule binding partner to enhance its processivity or function. To test these hypotheses for KIF12 behaviour in cell, and also to see KIF12 impact on microtubule dynamics, the full length KIF12 was overexpressed in HEK293a cells, the cells were imaged using fluorescence microscopy, and the behaviour of KIF12 was analysed. We also attempted to purify full length KIF12 from mammalian cells to obtain full length protein for *in vitro* assays, to compare with the truncated version of KIF12 previously studied.

5.1 Expression and purification of full length KIF12 using Nickel affinity chromatography

Expression of full-length KIF12 was previously attempted using an insect cell expression system (Littledale, 2017). However, the full length protein was insoluble when tagged at either the N- or C- terminus. Therefore, I attempted to express full-length KIF12 using a mammalian expression system. I selected Human Embryonic Kidney (HEK) 293 cell line for two reasons. Firstly, KIF12 was originally found in human kidney

cells, and expressing it in such cell line would enable it to be natively post-translationally modified for a proper protein folding and stability, which may help improve the solubility upon purification. Secondly, this cell line is one of the commonly used cell lines for transient gene expression, as it allows the fast and affordable lab-scale production of recombinant proteins (Nettleship et al., 2015). I used a mammalian protein expression construct pCMV as it was available in the lab. This vector is used for transient gene expression as it does not get integrated into the cellular genome, and has CMV promoter which allows for the production of high level recombinant protein in mammalian cells (Xia et al., 2006). A construct of N-terminus 6xHis and C-terminus GFP tagged full length KIF12 in pCMV was then made, transfected into HEK293a cells. The expression appeared successful as the cells showed fluorescence in the GFP channel, as approximately 70% of the total cells were transfected (**Figure 5.1**), and the identity of the expressed protein was confirmed by co-expressing the construct with mCherry tubulin in the same cell line as described in section **5.2**. The expressed protein was then purified using nickel affinity chromatography (as explained in section **2.3.1**).

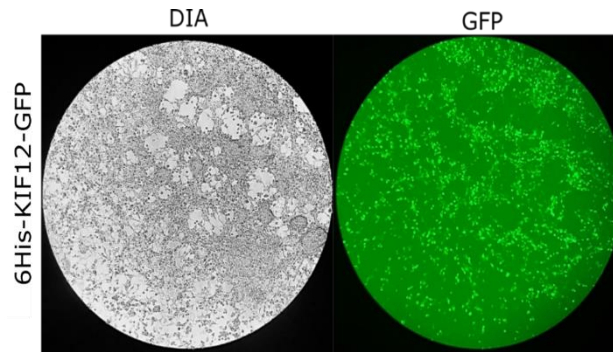


Figure 5.1. HEK293a cells were successfully transfected with 6his-full length KIF12-GFP. Cells transfected with 6his-full length KIF12-GFP showed fluorescence in GFP channel. Cells were imaged using diascopic (DIA) and epi-fluorescence microscopy equipped with GFP filter. Magnification: 10 \times .

However, the purification was not successful as most of the purified protein was found either in the pellet, or in the flow through which means that the protein did not bind to the column. This is possibly due to the his-tag being cleaved off. A band was present at \sim 75 kDa (indicated with a black arrow in **Figure 5.2 A**), which is the molecular weight of the full length without the GFP tag, suggesting that the GFP tag may also be cleaved (**Figure 5.2 A**). Such cleavage could be caused by proteolytic degradation, therefore, I tested both freshly made up protein inhibitors and additional protease inhibitors (**Figure 5.2 B**). However, even with fresh and additional protease inhibitors, purification of full-length KIF12 was unsuccessful, as the protein was either insoluble or degraded.

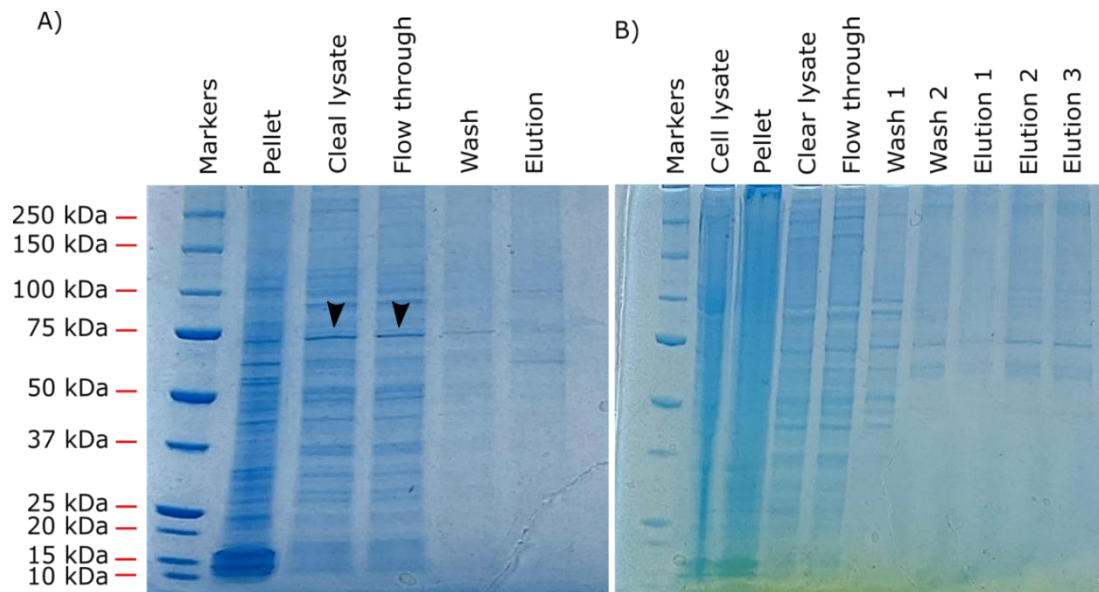


Figure 5.2. Purification of 6xHis-Full-length KIF12-GFP. SDS-PAGE gels stained with Instant Blue of progress of wild type 6xHis-FL-KIF12-GFP purification. The expected molecular weight of the KIF12 is 99 kDa. A) Pellet: pellet of lysed cell after centrifugation, clear lysate: cleared lysate after centrifugation, flow through: flow through from **nickel** affinity column after applying the cleared lysate, wash: wash with 60mM imidazole, elution: protein eluted with 200mM imidazole. B) Cell lysate: cell lysate before centrifugation, pellet: cell pellet after centrifugation, clear lysate: cleared lysate after centrifugation, flow through: flow throw from **nickel** affinity column after applying cleared cell lysate into the column, washes 1-2: washes with 60mM imidazole, elutions 1-3: elutions with 200mM imidazole (in this purification, freshly made up protein inhibitors and additional protease inhibitors were used).

5.2 Full length KIF12 localises to microtubules in cell

Since, KIF12 may have been expressed in the HEK293a cells but it did not prove possible to purify full length KIF12 from these cells, I looked at the localisation of the GFP signal in the transfected HEK293a cells to determine if the protein expressed was KIF12-GFP. To see if the GFP signal in KIF12-GFP transfected cells localised to microtubules, HEK293a cells were transfected either with GFP tagged full length KIF12 or only with GFP. The cells were then fixed and imaged (**2.2.8**). Only KIF12-

GFP appears to localise to microtubules. In cells which transfected with GFP only, the fluorescence signal appeared uniform across the cytoplasm. This indicates that cells transfected with a KIF12-GFP plasmid did express KIF12-GFP as the GFP signal appears localised to microtubules as would be expected for a kinesin (**Figure 5.3**).

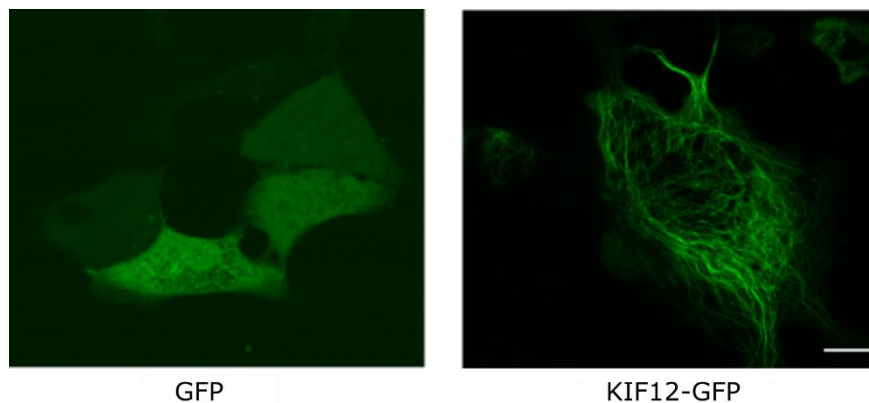


Figure 5.3. KIF12 localizes to microtubules. GFP labelled full-length KIF12 and GFP were expressed in HEK293a cell line. Scale bar 10 μ m.

To confirm the localization of KIF12 on microtubules, HEK293a cells were then co-transfected with constructs for full length KIF12-GFP and mCherry tubulin (**Figure 5.4 A-C**), as described in section **2.2.7**. A line scan based analysis of GFP-labelled full length KIF12 and mCherry-labelled microtubules fluorescence intensities across selected microtubules (indicated yellow lines and numbers in image C) was then carried out, and the intensities against distance were plotted (**Figure 5.4 D**). The intensity profile for GFP labelled-KIF12 overlays that of mCherry tubulin indicating that KIF12-GFP localised to microtubules.

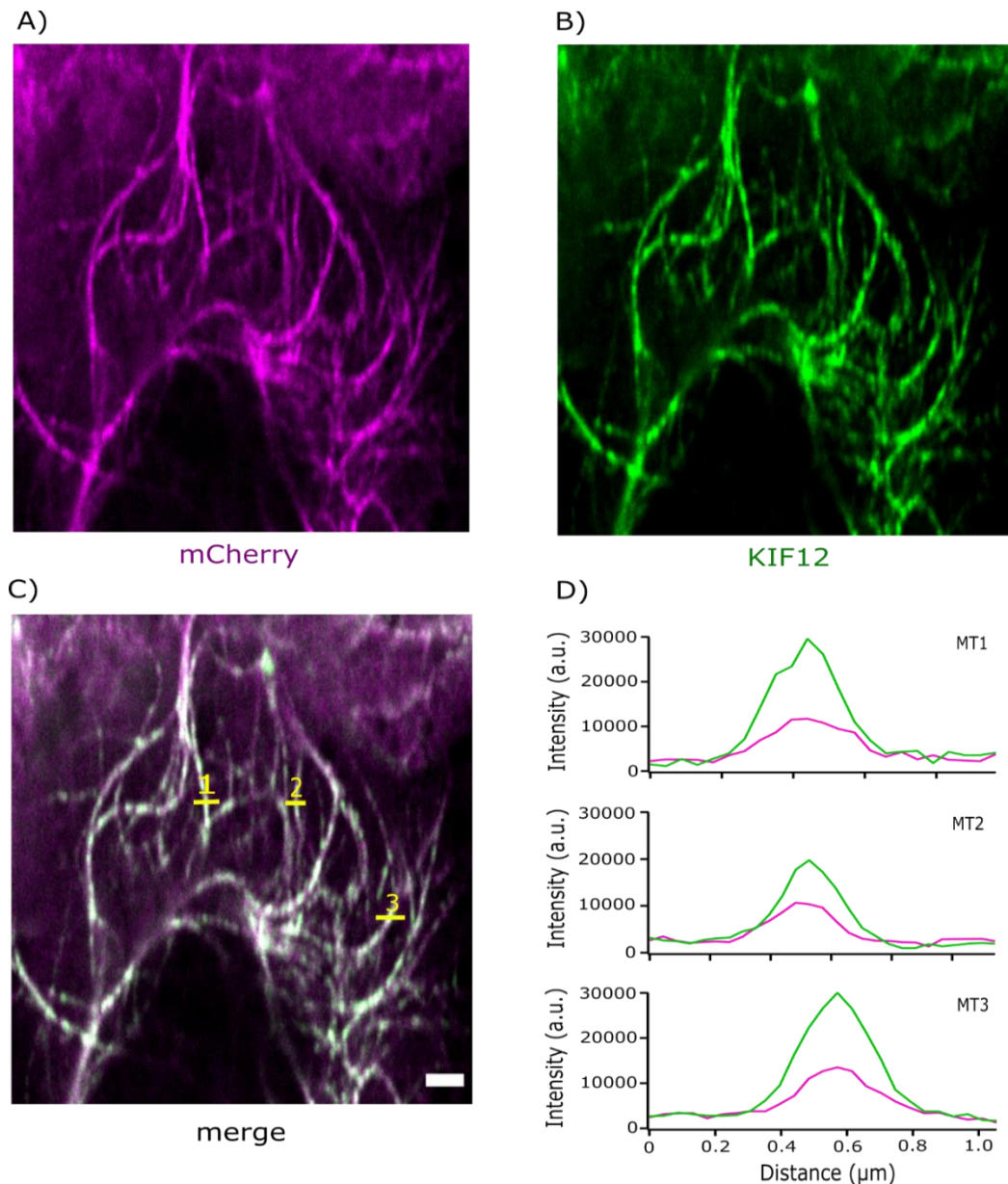


Figure 5.4. Full length KIF12-GFP localization on microtubules. GFP labelled full-length KIF12 and mCherry-tubulin were co-expressed in HEK293a cells and imaged using confocal microscopy. A) Rhodamine channel shows mCherry-tubulin, B) GFP channel shows GFP labelled full-length KIF12, C) overlay of Rhodamine and GFP channels. Scale bar 2 μ m. The numbered yellow lines indicate the microtubules selected for (D) line scan analysis of full length KIF12-GFP (green) and tubulin-mCherry (magenta) fluorescence intensity along the microtubule, .a.u., arbitrary units.

5.3 Full length KIF12 exhibits only diffusive motility in cell

In an attempt to see whether full-length KIF12 could translocate on microtubules, also to see its impact on microtubule dynamics, HEK293a

cells were co-transfected with constructs for full length KIF12-GFP and mCherry tubulin, live-cell imaging was carried out (**2.2.7**). To analyse the behaviour of full-length KIF12-GFP single molecules on microtubules kymographs were generated. Kymographs show that full-length KIF12-GFP shows only diffusive mode of motility (**Figure 5.5**).

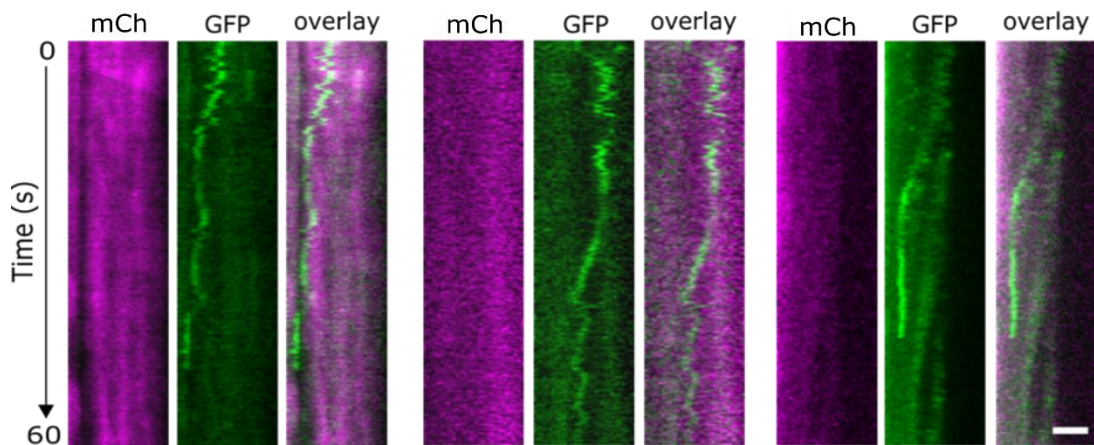


Figure 5.5. Full-length KIF12-GFP shows a diffusive movement in cell. GFP labelled full-length KIF12 and mCherry-tubulin were co-expressed in HEK293a cells, and imaged using TIRF microscopy, time interval: 220ms, **mCh: mCherry channel**, GFP: GFP channel, overlay: overlaid Rhodamine and GFP channels, scale bar 2 μ m.

Diffusive motion was previously observed for truncated KIF12 (KIF12-434-GFP) *in vitro* microtubule gliding assay (**Figure 3.5**) where it was moving microtubules in a diffusive manner. During live-cell imaging it proved difficult to focus on the protein in the GFP channel and on the microtubules in Rhodamine channel simultaneously, hence it is not possible to further analyse this type of motion in relation to microtubule.

5.4 The impact of the full length KIF12 on microtubule dynamics was not possible to determine

We also attempted to use live cell TIRF imaging to observe if KIF12 has an influence on microtubule dynamics. However, this was not possible as it requires cells to be flat and well adhered to the surface to be able to image the cell periphery where well separated dynamic microtubule ends can be found, and would facilitate the generation of kymographs from individual microtubules to observe dynamics. However, in my initial attempts at live-cell imaging using TIRF microscopy the cells were not sufficiently well adhered to permit observation of individual dynamic microtubule ends (**Figure 5.6**).

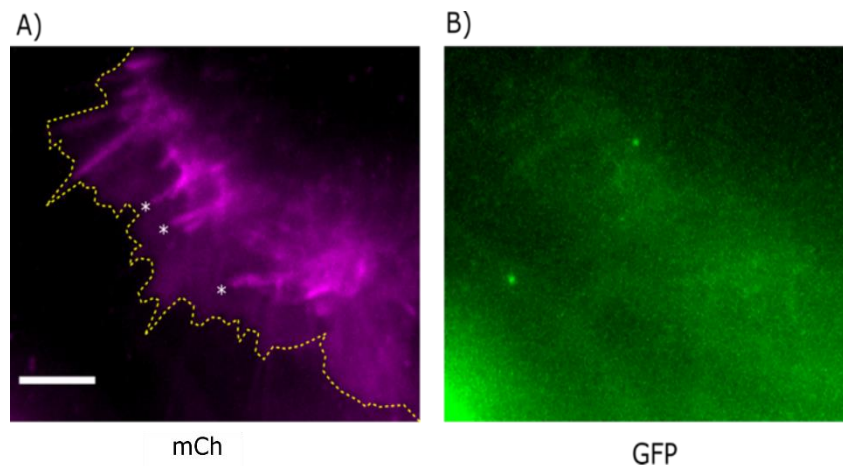


Figure 5.6. Impact of KIF12 on microtubule dynamics in cell could not be measured. A) A HEK293a cell co-transfected with full length KIF12-GFP and mCherry tubulin and imaged using TIRF microscopy, **mCh: mCherry channel**, dotted yellow line indicates cell periphery, and white asterisks indicate dynamic single microtubules. B) GFP: GFP channel where GFP-labelled KIF12 should have been focused on. Scale bar 5 μm .

To enhance cell-adhesion to the surface, the surface of the culture was coated with Polylysine, a reagent that improves electrostatic interaction

of the cell membrane negatively-charged ions with positively-charged surface ions of attachment factors on the culture surface (Mazia et al., 1975). However, that was not successful as instead of being firmly attaching to the surface cells were floating. Perhaps Poylysine concentration used was toxic to the cells, and trying different concentrations of Poylysine to find the right concentration or use another adhesion reagent would solve the problem. However, due to time limitation troubleshooting that was not possible.

Chapter 6 Discussion

Phylogenetic analysis of the kinesin superfamily illustrates that members of the Kinesin-16 family are found only in organisms that build cilia or flagella (Wickstead et al., 2010). The human Kinesin 16, KIF12, has been shown to localise to the primary cilia in **mouse IMCD3 (Inner Medullary Collecting Duct-3)** cells (**Figure 1.5**)(Mrug et al., 2015).

These data indicate that KIF12 functions with cilia either to facilitate intra-flagellar transport carrying cargo within the primary cilia, or to regulate microtubule dynamics.

6.1 KIF12 does not act as a translocating kinesin

The domain layout of KIF12 is akin to that of translocating kinesins, which may suggest a cargo-carrying function. Members of the Kinesin-2 family are known to carry cargo within cilia and this function is necessary for the building and maintenance of cilia (Scholey, 2013). Cargo carrying kinesins, such as members of the Kinesin-2, family translocate in a directed manner along microtubules. To determine if KIF12 acted as a translocating kinesin we observed its behaviour in a microtubule gliding assay. KIF12-434 did not support directed movement on microtubules. Instead, microtubules attached to KIF12-434 were either static or showed rapid back and forth motion over a distance of 1-2 microns (**Figure 3.5 A**). Similar behaviour was observed for the Kinesin-13, MCAK, which has been shown to interact with microtubules in a diffusive fashion (Helenius et al., 2006). These data indicates that KIF12-434 interacts with microtubules in a diffusive rather

than a translocating manner. To further characterise the activity of KIF12-434 on microtubules, I carried out a TIRF stepping assay. In this type of assay, KIF12-434 did not exhibit the directed motion typical of a translocating kinesin. Instead KIF12-434 bound transiently or became stuck on microtubules over longer timescales (**Figure 3.7 A**). The interaction of KIF12-434 with microtubules was found to be concentration dependent (**Figure 3.7 A and B**). In the presence of AMP-PNP, more KIF12-434 bound to microtubules than in the presence of ATP at the same concentration. This indicates that the interaction of KIF12-434 with microtubules is a specific nucleotide dependent interaction (**Figure 3.7 A and B**). These data indicate that KIF12-434 is not a translocating kinesin but displays a diffusive interaction with microtubules. Therefore, it is unlikely that KIF12 is a translocating kinesin with a carrying cargo function within the primary cilia.

6.2 KIF12-434 does not depolymerise microtubules but may have a stabilising effect on microtubules

If KIF12 is not a translocating kinesin, it may act as a regulator of microtubule dynamics. Kinesins that regulate microtubule dynamics can act as depolymerisers/destabilisers or polymerisers/stabilisers.

KIF2A and KIF24, members of the Kinesin-13 family of microtubule depolymerases, localize to the centrosome/basal body of cilia. KIF2A is involved in driving disassembly of cilia and KIF24 suppresses inappropriate cilia assembly (Miyamoto et al., 2015, Kobayashi et al., 2011). To determine if KIF12-434 could act as a microtubule

depolymeriser in cilia, I performed a microtubule depolymerisation assay. KIF12-434 did not depolymerise microtubules (**Figure 3.9 A**), but reduced the rate of depolymerisation below the intrinsic rate of depolymerisation of GMPCPP stabilised microtubules (**Figure 3.9 B**). This decrease in depolymerisation rate was small but statistically significant. These data suggest that KIF12-434 may act to stabilise microtubules.

6.3 KIF12-434 increases microtubules growth rate but cannot be detected on microtubule plus ends

To determine if KIF12 acts as a microtubule stabiliser we studied the impact of KIF12-434 in a dynamic microtubule assay. In the presence of 300 nM KIF12-434, at 20 μ M tubulin and at 27°C the growth rate and growth length increased by approximately 1.4-fold and 1.3-fold, respectively. This increase is a small but significant. However, by comparison with other proteins that regulate microtubule dynamics, we might have expected to see a bigger effect. For instance, at 12 μ M tubulin and at 28°C 40 nM Kip2 increased the growth rate and the growth length by around 3-fold and 8.8-fold, respectively (Hibbel et al., 2015). Another example is Kinesin-5, Kin5_18, at 10 μ M tubulin and at 30°C 30 nM Kin5_18 increased the growth rate by around 2.3-fold (Chen and Hancock, 2015). The non-kinesin microtubule growth promoting protein, XMAP215, is observed to increase the microtubule growth rate by 10.6 fold (Zanic et al., 2013). KIF12-434 has no significant impact on

microtubule growth time or the catastrophe frequency of dynamic microtubules (**Figure 3.11**).

6.4 KIF12-434 can be sequestered from microtubules by unpolymerised tubulin

In the dynamic microtubule assay, KIF12 was not observed to interact with microtubules as no GFP signal could be detected on either dynamic extensions or stabilised seeds (**Figure 3.12**, upper panel). This observation did not agree with the previous observation that KIF12-434 was observed to interact with stabilised microtubules in the absence of unpolymerized tubulin (**Figure 3.7 A**). Therefore, I repeated this assay with microtubule seeds but without unpolymerised tubulin. Under these conditions, KIF12-434 did interact with microtubules (**Figure 3.12**, lower panel). Therefore, we hypothesised that the unpolymerised tubulin was sequestering KIF12-434 away from microtubules. To further explore the effect of unpolymerized tubulin on the interaction of KIF12-434 with microtubules, increasing concentrations of unpolymerised tubulin were introduced to an assay containing stabilised microtubule seeds and a constant concentration of KIF12-434. This was carried out in the absence of added GTP to avoid growth of microtubule extensions. As the concentration of unpolymerized tubulin increases the intensity of the GFP signal on microtubules decreases, suggesting that unpolymerized tubulin competes with microtubules for the binding of KIF12-434. At concentrations between 15 μ M to 20 μ M unpolymerised tubulin KIF12-434 is no longer observed on microtubules (**Figure 3.13**).

Fitting these data to either a one tubulin or two tubulin binding model suggests that KIF12 most likely binds two tubulin heterodimers. The affinity of KIF12-434 for a single tubulin heterodimer is weak but binding to a dimer of tubulin heterodimers is stronger and also stronger than binding to microtubules (**Figure 3.15**). This apparent higher affinity for unpolymerised tubulin than for microtubules is unusual and hard to explain in the context of the activity of KIF12 in the primary cilia. The concentration of unpolymerised tubulin in cells is generally higher than in the microtubule dynamic assay. Therefore, if KIF12 has a higher affinity for unpolymerised tubulin than for microtubules, there is enough unpolymerized tubulin in cells to consistently sequester KIF12 away from microtubules. It is hard to imagine a function that KIF12 could be carrying out in cells when mainly bound to unpolymerized tubulin. However, the concentration of unpolymerised tubulin in the primary cilium may not be the same as in the cytoplasm. The localised concentration of tubulin has been shown to vary in different cellular compartments (Baumgart et al., 2019). It is possible that the concentration of unpolymerized tubulin is lower than the cytoplasm, thereby allowing KIF12 to interact with microtubules and impact the dynamics of axoneme assembly, disassembly or maintenance.

In one microtubule dynamic assay, I observed KIF12-434 having a greater impact on microtubule dynamics (**Figure A3.1**). KIF12-434 was able to initiate microtubule growth at 10 μ M tubulin; a concentration at which no microtubule growth was observed in the absence of KIF12-434. In the presence of 300 nM KIF12-434 microtubules did not grow

faster, but grew for longer times to a greater length. In this assay KIF12-434 did not accelerate the growth but stabilized dynamic microtubule extensions allowing them to persist for longer and obtain greater overall lengths. Further, the presence of KIF12-434 in this assay decreased the catastrophe frequency and reduced the rate of microtubule shrinkage upon catastrophe (**Figure A3.1**). However, whilst these data made a lot of sense in terms of the stabilising effect of KIF12 observed in a depolymerisation assay, they were not reproducible. Data of this type was observed only in a single dynamic microtubule assay. The more commonly obtain data are those presented in the results of this thesis. We did not manage to determine the reason behind our inability to reproduce the data shown in (**Figure A3.1**), however, it may be attributed to the stability of the protein. The full-length protein and a longer truncation (KIF12-472) were insoluble when expressed in Sf9 cells. It could be that KIF12-434 is close to the threshold of solubility and that subtle changes in experimental, purification or storage conditions may lead to a loss of activity.

6.5 KIF12-434 is able to distinguish the ends of Taxol-stabilised microtubules but not those of GMPCPP- stabilised microtubules.

Some kinesins such as KIF7, which is a non-translocating kinesin found in primary cilia of mammalian cells, recognise the growing microtubule tip by preferential binding to GTP-tubulin, which is found at growing microtubule plus ends (Jiang et al., 2019, Nakata et al., 2011). The data

presented in this thesis suggest that KIF12-434 does not distinguish GTP- from GDP-tubulin within microtubules. The amount of KIF12-434 bound to GMPCPP-microtubules (GTP equivalent) and Taxol-stabilised microtubules (GDP equivalent) microtubules was not significantly different. However, for Taxol-stabilised microtubules, GFP intensity on the ends was significantly higher than on the lattice (**Figure 3.17 A and E**). This is in contrast to GMPCPP-stabilised microtubules for which the GFP signal was evenly distributed along the microtubules (**Figure 3.17 A and D**). These data suggest that KIF12-434 can recognise a different conformation of tubulin found at the ends of Taxol-stabilised microtubules. It is not clear what about the ends of Taxol-stabilised microtubules is recognised by KIF12. The ability of KIF12 to differentiate the ends from the lattice of Taxol-stabilised microtubules may be due to a different nucleotide with a layer of GTP-tubulin possibly remaining at the microtubule ends. Alternatively, there may be a conformational difference at the ends of Taxol-stabilised microtubules irrespective of nucleotide state and this is what is recognised by KIF12-434. Taxol-stabilised microtubules are grown in a way more closely related to how microtubules grow in the cell and then stabilised by addition of Taxol. It may be that in cells KIF12 can recognise microtubule ends and most of its activity takes place at microtubule ends. The in-cell data obtained by Varga lab (Institute of Molecular Genetics of the Czech Academy of Sciences, Prague, Czech Republic) shows that the wild type KIF12 is concentrated at tip of primary cilia which has a concentration of microtubule plus ends (**Figure 4.7**).

6.6 KIF12 tail does not seem to interact with microtubules

Data from the reproducible microtubule dynamic assay and competition assay show that KIF12-434 has a higher affinity for unpolymerised tubulin than for microtubules. This was difficult to relate to possible functions of KIF12-434 in the primary cilia. Since this work was carried out with a truncated KIF12, it is possible that the missing tail region may contain microtubule binding sites that would increase the overall affinity for microtubules. The Kinesin-4, KIF21B, shows plus-end directed motility with greater processivity than another member of the Kinesin-4 family, KIF4 (van Riel et al., 2017). This increased processivity results from an additional microtubule binding region located in the tail. Therefore, to test this hypothesis for KIF12, I expressed the tail independently from the rest of the protein. Multiple attempts were made to express different length tail constructs with GFP tag and different purification tags. Some tail constructs were not soluble and those that were soluble could not be fully purified. Adding the partially purified tails constructs to microtubules suggest that they do not bind to microtubules. However, since there are other proteins present in these assays, it could be that these proteins prevent the tail from interacting with microtubules.

6.7 KIF12-434 has a low microtubule-stimulated ATPase

The ATP turnover rate of KIF12-434 in solution was very slow similar to that of Kinesin-1 (Hackney, 1988). However, the addition of microtubules stimulates the ATPase only by approximately 23-fold

(**Figure 3.24**). Members of Kinesin-1 family typically show ~5000-fold acceleration by microtubules (Yildiz et al., 2008, McVicker et al., 2011, Coy et al., 1999). Low acceleration of ATPase by microtubules is also observed for the immotile Kinesin-4, KIF7 (Yue et al., 2018). This agrees with the previous data that shows that KIF12-434 is not a translocating kinesin, and suggests that the lack of processive translocation observed for KIF12-434 might be due to the low stimulation of KIF12-434 ATPase by microtubules. In the presence of unpolymerised tubulin KIF12-434 ATPase rate was not significantly increased (**Figure 3.24**). This could explain why KIF12-434 shows a higher affinity for unpolymerised tubulin which can sequester KIF12-434 away from microtubules. If KIF12-434 binds unpolymerised tubulin in a nucleotide state where the binding is tight, then unpolymerised tubulin bound to KIF12-434 does encourage KIF12-434 to transfer to a less tight state because tubulin does not accelerate the ATPase.

6.8 KIF12-434 Δ PPGGG is less soluble than the wild type

KIF12 has been identified as a candidate polycystic kidney disease (PKD) modifier gene, which has a major effect on the severity of the renal phenotype associated with this disease (Mrug et al., 2005). A five-amino acid deletion (Δ PPGGG) in the KIF12 protein results in a less severe phenotype than the full-length variant of KIF12 (Mrug et al., 2015). The PPGGG region was confirmed to be a deletion rather than an insertion by Littledale (2017). This mutation is located in the predicted loop 2 (L2) of the motor domain; a secondary structural element that is

commonly involved in the microtubule-binding interface. The length of L2 is substantially different between kinesin families, ranging from 2-3 residues in Kinesin-1 to 13-15 residues in Kinesin-13 family. For Kinesin with a long L2, this region becomes a more important element of the microtubule interface (Ogawa et al., 2004, Shipley et al., 2004, Kim et al., 2014). In KIF12, L2 is longer than that of Kinesin-1 (**Figure 4.2**), consisting of 9 residues. Therefore, this mutation may impact the interaction of KIF12 with microtubules. Upon purifying this mutant it was observed that the pellet from the cell lysate contains GFP signal, indicating that this mutant version of KIF12-434 may be less soluble than the wild-type. The mutation did not alter the level of protein expression, but protein solubility appears to be decreased by the mutation.

6.9 KIF12-434 Δ PPGGG seems to have a higher affinity for microtubule than the wild type

Fitting the data from microtubule affinity assay suggests that **the mutation increased the affinity of KIF12-434 for microtubules by approximately 10-fold**. However, the data are noisy (**Figure 4.6**) and the parameters determined from the fit have large error. Therefore, although these data suggest that there may be an impact of affinity for microtubules, it is not possible to be certain. It may be possible to obtain a more accurate measure of affinity using a different assay, such as a pelleting assay. This type of assay has been successfully used

previously for this type of measurement (Spittle et al., 2000, Talapatra et al., 2015).

6.10 KIF12-434 Δ PPGGG can distinguish the ends of Taxol-stabilised microtubules but not those of GMPCPP-stabilised microtubules

In-cell data shows that the full length mutant does not discriminate the tip of the cilium from the main body of the cilium, in the way that the full length wild type seems to (Varga lab, Institute of Molecular Genetics of the Czech Academy of Sciences, Prague, Czech Republic) (**Figure 4.7**). Microtubules in primary cilia are all oriented with their plus-ends abutting the membrane at the tips of cilia (Dentler, 1980). Therefore, it is possible that when the wild type reaches the plus end of microtubules at tip of the primary cilia it gets retained due to its ability to recognise a conformational change in the GTP cap (**Figure 3.17**) while the mutant does not. As observed for the wild type, KIF12-434 Δ PPGGG has no preference for binding GTP- over GDP- tubulin *in vitro* (**Figure 4.8**). However, as what has been observed for the wild type the ends of Taxol-stabilised microtubules were brighter than the lattice (**Figure 4.8**). This suggests that the mutant is also able to recognise the conformational change at the GTP cap as the wild type. These *in-vitro* data appear to give no indication as to the reason for the differing behaviour of the wild-type and mutant KIF12 in the cilia of cultured cells. The contradiction in these two pieces of data may be due to the *in-cell* experiment was carried out with the full length while *in vitro* with

a truncation, or due the *in vitro* experiment was carried with individual microtubules compared to the axonemal microtubule structure in cilia.

On the other hand, when comparing GFP signal intensities for the wild type to that for the mutant on GMPCPP- and Taxol- stabilised microtubules, the intensity is consistently lower for the mutant than for wild-type. These data may indicate that the affinity of the mutant for microtubules is lower than for wild-type leading to less protein binding at a given concentration and agreeing with the microtubule affinity assay data.

6.11 Full length KIF12 characterisation

6.11.1 *In vitro* characterisation

Full length KIF12 was insoluble upon expression in Sf9 cells and so we worked with a truncated version (KIF12-434) to carry out *in vitro* assays that required purified protein. To study the activity of full length KIF12 and determine if the tail domain missing from KIF12-434 helps this activity, we expressed full length KIF12 in mammalian cells and attempted to purify it for *in vitro* assays to compare with the truncated version of KIF12 previously studied. A construct of N-terminus 6xHis and C-terminus GFP tagged full length KIF12 in pCMV was then made, and transfected into HEK293 cells. The expression was successful as the cells showed fluorescence in the GFP channel, as approximately 70% of the total cells were transfected (**Figure 5.1**). However, full length KIF12 proved difficult to purify from these cells as the protein was either

insoluble where it is mostly found in the pellet or was truncated (**Figure 5.2**).

6.11.2 *In vivo* characterisation

Since it was not possible to purify full length KIF12 from mammalian cells, I tried to characterise its activity *in vivo*. This would also allow us to determine if KIF12 has a binding partner to enhance its interaction with microtubules and perhaps even allow translocation activity not observed *in vitro*. A truncated *Xenopus* Kinesin-4, XKLP1, lacking the C-terminal domain shows a weak possessive microtubule plus end directed motility. However, full length XKLP1 in the presence of an interacting protein PRC1 is observed to translocate long distances along microtubules (Bringmann et al., 2004). KIF12-GFP was observed to localise to microtubules in HEK293 cells. However, there was no evidence of any translocating activity, KIF12-GFP single molecules kymographs suggested that KIF12-GFP moved in a diffusive manner on microtubules (**Figure 5.5**). This movement seen for KIF12-GFP *in cell* is like KIF12-434 movement *in vitro* where it also shows a diffusive motion.

6.12 Further areas for exploration

The most consistently reproducible effect observed of KIF12 on microtubule dynamics was a very small stabilising impact. However in a one-time assay KIF12 was observed to exert more dramatic stabilising effect on microtubules. This effect however was not reproducible in our microtubule dynamic assays. This may be due to issues with retaining

the activity of the protein upon purification. Longer versions of KIF12 are insoluble and the longest truncated version found to be soluble does not exist stably as a dimer. Therefore, it would be worth trying to produce a soluble more stable protein. For instance, making a construct of the motor domains dimerised by a leucine zipper. Leucine zipper domains are made up of a heptad repeat of leucines along an α -helix (leucine zipper) that can dimerize through formation of a coiled-coil structure involving paired contacts between hydrophobic leucine zipper domains (2017). Using different protein tags could also enhance stability of the protein by making the fusion protein more resistant to protease degradation in the host cell, thereby increasing stability. Such common tags include; glutathione S-transferase (GST-tag) as it can act as a chaperone to facilitate protein folding, and frequently the fusion protein can be expressed as a soluble protein rather than in inclusion bodies. In addition, the GST fusion protein can be affinity purified with relative ease (Harper and Speicher, 2011). Another tag that could be used is Maltose binding protein (MBP-tag), a solubility enhancing tag (di Guan et al., 1988) that can also be used for effective affinity purification, since it binds specifically to maltose or amylose. Another example is the small ubiquitin-like modifier (SUMO) tag, a member of a ubiquitin-like protein superfamily that is covalently attached to target proteins as a post-translational modification to alter the localization and stability of the protein (Wang et al., 2008).

As the affinity of KIF12 for microtubules could not be accurately measured by quantifying GFP signal for GFP-labelled KIF12 on

microtubules, another assay that may more accurately determine the affinity for microtubules is a pelleting assay. This type of assay is a more commonly used method of determining the affinity of microtubule interacting proteins (Spittle et al., 2000, Talapatra et al., 2015). A pelleting assay is likely to enable determination of affinity for microtubules with greater accuracy and permit confirmation or otherwise of the suggestion that the 5 amino acid deletion from Loop 2 found in a mutant version of KIF12 reduces the affinity of KIF12 for microtubules.

Observation of the localisation of wild-type KIF12 along primary cilium in IMCD3 cells shows a strong signal for wild type KIF12 at the base and the tip of the cilium. The data presented in this thesis indicates that KIF12 is not a translocating kinesin and so does not reach the tip of the cilia by directed motion. KIF12 may itself be carried to the tip of the cilium by interacting with another protein with microtubule translocating activity to take it to the ciliary tip. However, this needs further investigation of potential binding partners of KIF12. The localisation of a mutant version of KIF12 within the primary cilium differs from the wild type. KIF12 Δ PPGGG is more uniformly distributed along the length of the cilium and does not accumulate at the base and tip. The possibly reduced affinity for microtubules may play a role in this differing distribution of KIF12 Δ PPGGG, but it is difficult from the data currently available to explain these in cell findings. The future for this project requires finding the connection between the *in vitro* behaviour of KIF12

and its function in cells and then linking this to the various disease states in which dysfunction of Kinesin-16s is suggested to play a role.

Bibliography

2017. Chapter 10 - Gene Expression*. *In: POLLARD, T. D., EARNSHAW, W. C., LIPPINCOTT-SCHWARTZ, J. & JOHNSON, G. T. (eds.) Cell Biology (Third Edition)*. Elsevier.
- ALBERTS, B., JOHNSON, A., LEWIS, J., MORGAN, D., RAFF, M., ROBERTS, K. & WALTER, P. 2014. *Molecular Biology of the Cell*, New York, Garland Science.
- ALLAN, V. 1995. Protein phosphatase 1 regulates the cytoplasmic dynein-driven formation of endoplasmic reticulum networks in vitro. *Journal of Cell Biology*, 128, 879-891.
- ALUSHIN, GREGORY M., LANDER, GABRIEL C., KELLOGG, ELIZABETH H., ZHANG, R., BAKER, D. & NOGALES, E. 2014. High-Resolution Microtubule Structures Reveal the Structural Transitions in $\alpha\beta$ -Tubulin upon GTP Hydrolysis. *Cell*, 157, 1117-1129.
- AMOS, L. A. & LÖWE, J. 1999. How Taxol stabilises microtubule structure. *Chem Biol*, 6, R65-9.
- ASENJO, ANA B., CHATTERJEE, C., TAN, D., DEPAOLI, V., RICE, WILLIAM J., DIAZ-AVALOS, R., SILVESTRY, M. & SOSA, H. 2013. Structural Model for Tubulin Recognition and Deformation by Kinesin-13 Microtubule Depolymerases. *Cell Reports*, 3, 759-768.
- BASNET, N., NEDOZRALOVA, H., CREVENNA, A. H., BODAKUNTLA, S., SCHLICHTHAERLE, T., TASCHNER, M., CARDONE, G., JANKE, C., JUNGSMANN, R., MAGIERA, M. M., BIERTÜMPFEL, C. & MIZUNO, N.

2018. Direct induction of microtubule branching by microtubule nucleation factor SSNA1. *Nature Cell Biology*, 20, 1172-1180.
- BAUMGART, J., KIRCHNER, M., REDEMANN, S., BOND, A., WOODRUFF, J., VERBAVATZ, J. M., JÜLICHER, F., MÜLLER-REICHERT, T., HYMAN, A. A. & BRUGUÉS, J. 2019. Soluble tubulin is significantly enriched at mitotic centrosomes. *J Cell Biol*, 218, 3977-3985.
- BELLANNÉ-CHANTELOT, C., CHAUVEAU, D., GAUTIER, J. F., DUBOIS-LAFORGUE, D., CLAUIN, S., BEAUFILS, S., WILHELM, J. M., BOITARD, C., NOËL, L. H., VELHO, G. & TIMSIT, J. 2004. Clinical spectrum associated with hepatocyte nuclear factor-1beta mutations. *Ann Intern Med*, 140, 510-7.
- BELMONT, L. D. & MITCHISON, T. J. 1996. Identification of a Protein That Interacts with Tubulin Dimers and Increases the Catastrophe Rate of Microtubules. *Cell*, 84, 623-631.
- BELSHAM, H. 2019. *Dissecting the molecular mechanism of microtubule depolymerising kinesins*. PhD, University of Nottingham.
- BENSEL, B. M., WOODY, M. S., PYRPASSOPOULOS, S., GOLDMAN, Y. E., GILBERT, S. P. & OSTAP, E. M. 2020. The mechanochemistry of the kinesin-2 KIF3AC heterodimer is related to strain-dependent kinetic properties of KIF3A and KIF3C. *Proceedings of the National Academy of Sciences*, 117, 15632-15641.
- BIELING, P., TELLEY, I. A. & SURREY, T. 2010. A Minimal Midzone Protein Module Controls Formation and Length of Antiparallel Microtubule Overlaps. *Cell*, 142, 420-432.

- BLACQUE, O. E., REARDON, M. J., LI, C., MCCARTHY, J., MAHJOUR, M. R., ANSLEY, S. J., BADANO, J. L., MAH, A. K., BEALES, P. L. & DAVIDSON, W. S. 2004. Loss of *C. elegans* BBS-7 and BBS-8 protein function results in cilia defects and compromised intraflagellar transport. *Genes & development*, 18, 1630-1642.
- BRINGMANN, H., SKINIOTIS, G., SPILKER, A., KANDELS-LEWIS, S., VERNOS, I. & SURREY, T. 2004. A kinesin-like motor inhibits microtubule dynamic instability. *Science*, 303, 1519-22.
- BRITTO, M., GOULET, A., RIZVI, S., VON LOEFFELHOLZ, O., MOORES, C. A. & CROSS, R. A. 2016. *Schizosaccharomyces pombe* kinesin-5 switches direction using a steric blocking mechanism. *Proceedings of the National Academy of Sciences of the United States of America*, 113, E7483-E7489.
- BROWNHILL, K. Function and regulation of kinesin-1, -2 and -3. 2010.
- BURKHARDT, J. K., ECHEVERRI, C. J., NILSSON, T. & VALLEE, R. B. 1997. Overexpression of the Dynamitin (p50) Subunit of the Dynactin Complex Disrupts Dynein-dependent Maintenance of Membrane Organelle Distribution. *Journal of Cell Biology*, 139, 469-484.
- BURNS, KYLE M., WAGENBACH, M., WORDEMAN, L. & SCHRIEMER, DAVID C. 2014. Nucleotide Exchange in Dimeric MCAK Induces Longitudinal and Lateral Stress at Microtubule Ends to Support Depolymerization. *Structure*, 22, 1173-1183.
- CASE, R. B., PIERCE, D. W., HOM-BOOHER, N., HART, C. L. & VALE, R. D. 1997. The Directional Preference of Kinesin Motors Is Specified

- by an Element outside of the Motor Catalytic Domain. *Cell*, 90, 959-966.
- CASSIMERIS, L. & MORABITO, J. 2004. TOGp, the human homolog of XMAP215/Dis1, is required for centrosome integrity, spindle pole organization, and bipolar spindle assembly. *Molecular biology of the cell*, 15, 1580-1590.
- CASSIMERIS, L. U., WALKER, R. A., PRYER, N. K. & SALMON, E. D. 1987. Dynamic instability of microtubules. *BioEssays*, 7, 149-154.
- CAUDRON, F., ANDRIEUX, A., JOB, D. & BOSCHERON, C. C. 2008. A new role for kinesin-directed transport of Bik1p (CLIP-170) in *Saccharomyces cerevisiae*. *Journal of Cell Science*, 121, 1506-1513.
- CHANG-JIE, J. & SONOBE, S. 1993. Identification and preliminary characterization of a 65 kDa higher-plant microtubule-associated protein. *Journal of Cell Science*, 105, 891-901.
- CHEN, Y. & HANCOCK, W. O. 2015. Kinesin-5 is a microtubule polymerase. *Nature Communications*, 6, 8160.
- CHRÉTIEN, D., FULLER, S. D. & KARSENTI, E. 1995. Structure of growing microtubule ends: two-dimensional sheets close into tubes at variable rates. *The Journal of Cell Biology*, 129, 1311.
- CHRÉTIEN, D. & WADE, R. H. 1991. New data on the microtubule surface lattice. *Biol Cell*, 71, 161-74.
- CHU, H. M. A., YUN, M., ANDERSON, D. E., SAGE, H., PARK, H.-W. & ENDOW, S. A. 2005. Kar3 interaction with Cik1 alters motor structure and function. *The EMBO journal*, 24, 3214-3223.

- COLE, D. G., DIENER, D. R., HIMELBLAU, A. L., BEECH, P. L., FUSTER, J. C. & ROSENBAUM, J. L. 1998. Chlamydomonas kinesin-II-dependent intraflagellar transport (IFT): IFT particles contain proteins required for ciliary assembly in *Caenorhabditis elegans* sensory neurons. *The Journal of cell biology*, 141, 993-1008.
- COTTINGHAM, F. R. & HOYT, M. A. 1997. Mitotic Spindle Positioning in *Saccharomyces cerevisiae* Is Accomplished by Antagonistically Acting Microtubule Motor Proteins. *Journal of Cell Biology*, 138, 1041-1053.
- CRAIGE, B., TSAO, C.-C., DIENER, D. R., HOU, Y., LECHTRECK, K.-F., ROSENBAUM, J. L. & WITMAN, G. B. 2010. CEP290 tethers flagellar transition zone microtubules to the membrane and regulates flagellar protein content. *Journal of Cell Biology*, 190, 927-940.
- DE MARCO, V., BURKHARD, P., LE BOT, N., VERNOS, I. & HOENGER, A. 2001. Analysis of heterodimer formation by Xklp3A/B, a newly cloned kinesin-II from *Xenopus laevis*. *The EMBO journal*, 20, 3370-3379.
- DEANE, J. A., COLE, D. G., SEELEY, E. S., DIENER, D. R. & ROSENBAUM, J. L. 2001. Localization of intraflagellar transport protein IFT52 identifies basal body transitional fibers as the docking site for IFT particles. *Current Biology*, 11, 1586-1590.
- DEANE, J. A. & RICARDO, S. D. 2012. Emerging roles for renal primary cilia in epithelial repair. *Int Rev Cell Mol Biol*, 293, 169-93.

- DELGEHYR, N., RANGONE, H., FU, J., MAO, G., TOM, B., RIPARBELLI, MARIA G., CALLAINI, G. & GLOVER, DAVID M. 2012. Klp10A, a Microtubule-Depolymerizing Kinesin-13, Cooperates with CP110 to Control Drosophila Centriole Length. *Current Biology*, 22, 502-509.
- DESAI, A. & MITCHISON, T. J. 1998. Preparation and characterization of caged fluorescein tubulin. *Methods Enzymol*, 298, 125-32.
- DI GUAN, C., LI, P., RIGGS, P. D. & INOUE, H. 1988. Vectors that facilitate the expression and purification of foreign peptides in Escherichia coli by fusion to maltose-binding protein. *Gene*, 67, 21-30.
- DÍAZ-VALENCIA, JUAN D., MORELLI, MARGARET M., BAILEY, M., ZHANG, D., SHARP, DAVID J. & ROSS, JENNIFER L. 2011. Drosophila Katanin-60 Depolymerizes and Severs at Microtubule Defects. *Biophysical Journal*, 100, 2440-2449.
- DRECHSEL, D. N., HYMAN, A. A., COBB, M. H. & KIRSCHNER, M. W. 1992. Modulation of the dynamic instability of tubulin assembly by the microtubule-associated protein tau. *Molecular Biology of the Cell*, 3, 1141-1154.
- DÜSELDER, A., FRIDMAN, V., THIEDE, C., WIESBAUM, A., GOLDSTEIN, A., KLOPFENSTEIN, D. R., ZAITSEVA, O., JANSON, M. E., GHEBER, L. & SCHMIDT, C. F. 2015. Deletion of the Tail Domain of the Kinesin-5 Cin8 Affects Its Directionality. *The Journal of biological chemistry*, 290, 16841-16850.

- EDAMATSU, M. 2014. Bidirectional motility of the fission yeast kinesin-5, Cut7. *Biochemical and Biophysical Research Communications*, 446, 231-234.
- EMS-MCCLUNG, S. C. & WALCZAK, C. E. 2010. Kinesin-13s in mitosis: Key players in the spatial and temporal organization of spindle microtubules. *Seminars in cell & developmental biology*, 21, 276-282.
- ENDOW, S. A. & WALIGORA, K. W. 1998. Determinants of kinesin motor polarity. *Science*, 281, 1200-2.
- FAGERBERG, L., HALLSTROM, B. M., OKSVOLD, P., KAMPF, C., DJUREINOVIC, D., ODEBERG, J., HABUKA, M., TAHMASEBPOOR, S., DANIELSSON, A., EDLUND, K., ASPLUND, A., SJOSTEDT, E., LUNDBERG, E., SZIGYARTO, C. A., SKOGS, M., TAKANEN, J. O., BERLING, H., TEGEL, H., MULDER, J., NILSSON, P., SCHWENK, J. M., LINDSKOG, C., DANIELSSON, F., MARDINOGLU, A., SIVERTSSON, A., VON FEILITZEN, K., FORSBERG, M., ZWAHLEN, M., OLSSON, I., NAVANI, S., HUSS, M., NIELSEN, J., PONTEN, F. & UHLEN, M. 2014. Analysis of the human tissue-specific expression by genome-wide integration of transcriptomics and antibody-based proteomics. *Mol Cell Proteomics*, 13, 397-406.
- FLETCHER, D. A. & MULLINS, R. D. 2010. Cell mechanics and the cytoskeleton. *Nature*, 463, 485-492.
- FOLLIT, J. A., TUFT, R. A., FOGARTY, K. E. & PAZOUR, G. J. 2006. The intraflagellar transport protein IFT20 is associated with the Golgi

complex and is required for cilia assembly. *Molecular biology of the cell*, 17, 3781-3792.

- FRIEL, C. T. & HOWARD, J. 2011. The kinesin-13 MCAK has an unconventional ATPase cycle adapted for microtubule depolymerization. *Embo j*, 30, 3928-39.
- FRIEL, C. T. & HOWARD, J. 2012. Coupling of kinesin ATP turnover to translocation and microtubule regulation: one engine, many machines. *J Muscle Res Cell Motil*, 33, 377-83.
- GARDNER, M. K., ZANIC, M., GELL, C., BORMUTH, V. & HOWARD, J. 2011. Depolymerizing kinesins Kip3 and MCAK shape cellular microtubule architecture by differential control of catastrophe. *Cell*, 147, 1092-103.
- GARDNER, M. K., ZANIC, M. & HOWARD, J. 2013. Microtubule catastrophe and rescue. *Curr Opin Cell Biol*, 25, 14-22.
- GAUDIN, R., DE ALENCAR, B. C., JOUVE, M., BÈRRE, S., LE BOUDER, E., SCHINDLER, M., VARTHAMAN, A., GOBERT, F. X. & BENARROCH, P. 2012. Critical role for the kinesin KIF3A in the HIV life cycle in primary human macrophages. *J Cell Biol*, 199, 467-79.
- GELL, C., BORMUTH, V., BROUHARD, G. J., COHEN, D. N., DIEZ, S., FRIEL, C. T., HELENIUS, J., NITZSCHE, B., PETZOLD, H., RIBBE, J., SCHÄFFER, E., STEAR, J. H., TRUSHKO, A., VARGA, V., WIDLUND, P. O., ZANIC, M. & HOWARD, J. 2010. Chapter 13 - Microtubule Dynamics Reconstituted In Vitro and Imaged by Single-Molecule Fluorescence Microscopy. *In: WILSON, L. & CORREIA, J. J. (eds.) Methods in Cell Biology*. Academic Press.

- GOLDSTEIN, L. S. 1993. With apologies to scheherazade: tails of 1001 kinesin motors. *Annu Rev Genet*, 27, 319-51.
- GONG, Y., MA, Z., PATEL, V., FISCHER, E., HIESBERGER, T., PONTOGLIO, M. & IGARASHI, P. 2009. HNF-1beta regulates transcription of the PKD modifier gene Kif12. *J Am Soc Nephrol*, 20, 41-7.
- GOSHIMA, G. & VALE, R. D. 2003. The roles of microtubule-based motor proteins in mitosis : comprehensive RNAi analysis in the Drosophila S2 cell line. *Journal of Cell Biology*, 162, 1003-1016.
- GUAY-WOODFORD, L. M., WRIGHT, C. J., WALZ, G. & CHURCHILL, G. A. 2000. Quantitative trait loci modulate renal cystic disease severity in the mouse bpk model. *J Am Soc Nephrol*, 11, 1253-1260.
- HACKNEY, D. D. 1994. Evidence for alternating head catalysis by kinesin during microtubule-stimulated ATP hydrolysis. *Proc Natl Acad Sci U S A*, 91, 6865-9.
- HAIMO, L. T. & ROSENBAUM, J. L. 1981. Cilia, flagella, and microtubules. *Journal of Cell Biology*, 91, 125s-130s.
- HAMMOND, J. W., BLASIUS, T. L., SOPPINA, V., CAI, D. & VERHEY, K. J. 2010. Autoinhibition of the kinesin-2 motor KIF17 via dual intramolecular mechanisms. *The Journal of cell biology*, 189, 1013-1025.
- HAO, L. & SCHOLEY, J. M. 2009. Intraflagellar transport at a glance. *Journal of cell science*, 122, 889-892.
- HARADA, A., TAKEI, Y., KANAI, Y., TANAKA, Y., NONAKA, S. & HIROKAWA, N. 1998. Golgi Vesiculation and Lysosome Dispersion

- in Cells Lacking Cytoplasmic Dynein. *Journal of Cell Biology*, 141, 51-59.
- HARPER, S. & SPEICHER, D. W. 2011. Purification of proteins fused to glutathione S-transferase. *Methods in molecular biology (Clifton, N.J.)*, 681, 259-280.
- HE, M., SUBRAMANIAN, R., BANGS, F., OMELCHENKO, T., LIEM JR, K. F., KAPOOR, T. M. & ANDERSON, K. V. 2014. The kinesin-4 protein Kif7 regulates mammalian Hedgehog signalling by organizing the cilium tip compartment. *Nature Cell Biology*, 16, 663.
- HELENIUS, J., BROUHARD, G., KALAIIDZIDIS, Y., DIEZ, S. & HOWARD, J. 2006. The depolymerizing kinesin MCAK uses lattice diffusion to rapidly target microtubule ends. *Nature*, 441, 115-119.
- HIBBEL, A., BOGDANOVA, A., MAHAMDEH, M., JANNASCH, A., STORCH, M., SCHÄFFER, E., LIAKOPOULOS, D. & HOWARD, J. 2015. Kinesin Kip2 enhances microtubule growth in vitro through length-dependent feedback on polymerization and catastrophe. *eLife*, 4, e10542.
- HIROKAWA, N., NODA, Y., TANAKA, Y. & NIWA, S. 2009. Kinesin superfamily motor proteins and intracellular transport. *Nature Reviews Molecular Cell Biology*, 10, 682-696.
- HORIKAWA, Y., IWASAKI, N., HARA, M., FURUTA, H., HINOKIO, Y., COCKBURN, B. N., LINDNER, T., YAMAGATA, K., OGATA, M., TOMONAGA, O., KUROKI, H., KASAHARA, T., IWAMOTO, Y. &

- BELL, G. I. 1997. Mutation in hepatocyte nuclear factor-1 beta gene (TCF2) associated with MODY. *Nat Genet*, 17, 384-5.
- HOU, X., MRUG, M., YODER, B. K., LEFKOWITZ, E. J., KREMMIDIOTIS, G., D'EUSTACHIO, P., BEIER, D. R. & GUAY-WOODFORD, L. M. 2002. Cystin, a novel cilia-associated protein, is disrupted in the cpk mouse model of polycystic kidney disease. *J Clin Invest*, 109, 533-40.
- HU, Z., LIANG, Y., MENG, D., WANG, L. & PAN, J. 2015. Chapter Five - Microtubule-Depolymerizing Kinesins in the Regulation of Assembly, Disassembly, and Length of Cilia and Flagella. *In: JEON, K. W. (ed.) International Review of Cell and Molecular Biology*. Academic Press.
- HYMAN, A. A., CHRÉTIEN, D., ARNAL, I. & WADE, R. H. 1995. Structural changes accompanying GTP hydrolysis in microtubules: information from a slowly hydrolyzable analogue guanylyl-(alpha,beta)-methylene-diphosphonate. *J Cell Biol*, 128, 117-25.
- HYMAN, A. A., SALSER, S., DRECHSEL, D. N., UNWIN, N. & MITCHISON, T. J. 1992. Role of GTP hydrolysis in microtubule dynamics: information from a slowly hydrolyzable analogue, GMPCPP. *Mol Biol Cell*, 3, 1155-67.
- INOUE, H., NOJIMA, H. & OKAYAMA, H. 1990. High efficiency transformation of Escherichia coli with plasmids. *Gene*, 96, 23-8.
- IOMINI, C., LI, L., ESPARZA, J. M. & DUTCHER, S. K. 2009. Retrograde intraflagellar transport mutants identify complex A proteins with

- multiple genetic interactions in *Chlamydomonas reinhardtii*.
Genetics, 183, 885-896.
- ISHIKAWA, H. & MARSHALL, W. F. 2011. Ciliogenesis: building the cell's antenna. *Nature Reviews Molecular Cell Biology*, 12, 222-234.
- JENKINS, P. M., HURD, T. W., ZHANG, L., MCEWEN, D. P., BROWN, R. L., MARGOLIS, B., VERHEY, K. J. & MARTENS, J. R. 2006. Ciliary targeting of olfactory CNG channels requires the CNGB1b subunit and the kinesin-2 motor protein, KIF17. *Curr Biol*, 16, 1211-6.
- JIANG, S., MANI, N., WILSON-KUBALEK, E. M., KU, P.-I., MILLIGAN, R. A. & SUBRAMANIAN, R. 2019. Interplay between the Kinesin and Tubulin Mechanochemical Cycles Underlies Microtubule Tip Tracking by the Non-motile Ciliary Kinesin Kif7. *Developmental Cell*, 49, 711-730.e8.
- KANAI, Y., DOHMAE, N. & HIROKAWA, N. 2004. Kinesin transports RNA: isolation and characterization of an RNA-transporting granule. *Neuron*, 43, 513-525.
- KATOH, M. & KATOH, M. 2005. Characterization of KIF12 gene in silico. *Oncology Reports*, 13, 367-370.
- KIM, H., FONSECA, C. & STUMPF, J. 2014. A unique kinesin-8 surface loop provides specificity for chromosome alignment. *Mol Biol Cell*, 25, 3319-29.
- KOBAYASHI, T. & DYNLACHT, B. D. 2011. Regulating the transition from centriole to basal body. *Journal of Cell Biology*, 193, 435-444.

- KOBAYASHI, T., TSANG, W. Y., LI, J., LANE, W. & DYNLACHT, B. D. 2011. Centriolar kinesin Kif24 interacts with CP110 to remodel microtubules and regulate ciliogenesis. *Cell*, 145, 914-25.
- KORTEN, T. & DIEZ, S. 2008. Setting up roadblocks for kinesin-1: mechanism for the selective speed control of cargo carrying microtubules. *Lab on a Chip*, 8, 1441-1447.
- KOZMINSKI, K. G., BEECH, P. L. & ROSENBAUM, J. L. 1995. The Chlamydomonas kinesin-like protein FLA10 is involved in motility associated with the flagellar membrane. *The Journal of cell biology*, 131, 1517-1527.
- KOZMINSKI, K. G., JOHNSON, K. A., FORSCHER, P. & ROSENBAUM, J. L. 1993. A motility in the eukaryotic flagellum unrelated to flagellar beating. *Proceedings of the National Academy of Sciences*, 90, 5519-5523.
- KULL, F. J., SABLIN, E. P., LAU, R., FLETTERICK, R. J. & VALE, R. CRYSTAL STRUCTURE OF THE KINESIN MOTOR DOMAIN REVEALS A STRUCTURAL SIMILARITY TO MYOSIN. ACTA CRYSTALLOGRAPHICA A-FOUNDATION AND ADVANCES, 1996. INT UNION CRYSTALLOGRAPHY 2 ABBEY SQ, CHESTER, CH1 2HU, ENGLAND, C211-C211.
- KURASAWA, Y., EARNSHAW, W. C., MOCHIZUKI, Y., DOHMAE, N. & TODOKORO, K. 2004. Essential roles of KIF4 and its binding partner PRC1 in organized central spindle midzone formation. *The EMBO Journal*, 23, 3237-3248.

- LAWRENCE, C. J., DAWE, R. K., CHRISTIE, K. R., CLEVELAND, D. W.,
DAWSON, S. C., ENDOW, S. A., GOLDSTEIN, L. S. B., GOODSON,
H. V., HIROKAWA, N., HOWARD, J., MALMBERG, R. L.,
MCINTOSH, J. R., MIKI, H., MITCHISON, T. J., OKADA, Y., REDDY,
A. S. N., SAXTON, W. M., SCHLIWA, M., SCHOLEY, J. M., VALE, R.
D., WALCZAK, C. E. & WORDEMAN, L. 2004. A standardized
kinesin nomenclature. *The Journal of Cell Biology*, 167, 19.
- LEAF, A. & VON ZASTROW, M. 2015. Dopamine receptors reveal an
essential role of IFT-B, KIF17, and Rab23 in delivering specific
receptors to primary cilia. *Elife*, 4.
- LECHTRECK, K. F. 2015. IFT-Cargo Interactions and Protein Transport in
Cilia. *Trends in biochemical sciences*, 40, 765-778.
- LEDUC, C., RUHNOW, F., HOWARD, J. & DIEZ, S. 2007. Detection of
fractional steps in cargo movement by the collective operation of
kinesin-1 motors. *Proceedings of the National Academy of
Sciences*, 104, 10847.
- LEE, Y. M., KIM, E., PARK, M., MOON, E., AHN, S. M., KIM, W., HWANG,
K. B., KIM, Y. K., CHOI, W. & KIM, W. 2010. Cell cycle-regulated
expression and subcellular localization of a kinesin-8 member
human KIF18B. *Gene*, 466, 16-25.
- LIPPINCOTT-SCHWARTZ, J., COLE, N. B., MAROTTA, A., CONRAD, P. A.
& BLOOM, G. S. 1995. Kinesin is the motor for microtubule-
mediated Golgi-to-ER membrane traffic. *Journal of Cell Biology*,
128, 293-306.

- LITTLEDALE, C. 2017. *Investigation of cilia associated kinesin families*.
MPhil, The university of Nottingham.
- LÖWE, J., LI, H., DOWNING, K. H. & NOGALES, E. 2001. Refined structure of alpha beta-tubulin at 3.5 Å resolution. *J Mol Biol*, 313, 1045-57.
- MA, Y.-Z. & TAYLOR, E. W. 1997. Interacting Head Mechanism of Microtubule-Kinesin ATPase*. *Journal of Biological Chemistry*, 272, 724-730.
- MADDIREVULA, S., ALHEBBI, H., ALQAHTANI, A., ALGOUFI, T., ALSAIF, H. S., IBRAHIM, N., ABDULWAHAB, F., BARR, M., ALZAIDAN, H., ALMEHAIDEB, A., ALSASI, O., ALHASHEM, A., HUSSAINI, H. A., WALI, S. & ALKURAYA, F. S. 2019. Identification of novel loci for pediatric cholestatic liver disease defined by KIF12, PPM1F, USP53, LSR, and WDR83OS pathogenic variants. *Genet Med*, 21, 1164-1172.
- MANEY, T., HUNTER, A. W., WAGENBACH, M. & WORDEMAN, L. 1998. Mitotic centromere-associated kinesin is important for anaphase chromosome segregation. *The Journal of cell biology*, 142, 787-801.
- MARGOLIN, G., GREGORETTI, I. V., CICKOVSKI, T. M., LI, C., SHI, W., ALBER, M. S. & GOODSON, H. V. 2011. The mechanisms of microtubule catastrophe and rescue: implications from analysis of a dimer-scale computational model. *Molecular Biology of the Cell*, 23, 642-656.

- MARSHALL, W. F. & ROSENBAUM, J. L. 2001. Intraflagellar transport balances continuous turnover of outer doublet microtubules : implications for flagellar length control. *Journal of Cell Biology*, 155, 405-414.
- MARSZALEK, J. R. & GOLDSTEIN, L. S. B. 2000. Understanding the functions of kinesin-II. *Biochimica et Biophysica Acta (BBA) - Molecular Cell Research*, 1496, 142-150.
- MAYR, M. I., STORCH, M., HOWARD, J. & MAYER, T. U. 2011. A Non-Motor Microtubule Binding Site Is Essential for the High Processivity and Mitotic Function of Kinesin-8 Kif18A. *PLOS ONE*, 6, e27471.
- MAZIA, D., SCHATTEN, G. & SALE, W. 1975. Adhesion of cells to surfaces coated with polylysine. Applications to electron microscopy. *Journal of Cell Biology*, 66, 198-200.
- MESSITT, T. J., GAGNON, J. A., KREILING, J. A., PRATT, C. A., YOON, Y. J. & MOWRY, K. L. 2008. Multiple kinesin motors coordinate cytoplasmic RNA transport on a subpopulation of microtubules in *Xenopus* oocytes. *Developmental cell*, 15, 426-436.
- MIKI, H., SETOU, M., KANESHIRO, K. & HIROKAWA, N. 2001. All kinesin superfamily protein, KIF, genes in mouse and human. *Proceedings of the National Academy of Sciences*, 98, 7004-7011.
- MITCHISON, T. & KIRSCHNER, M. 1984. Dynamic instability of microtubule growth. *Nature*, 312, 237-242.
- MIYAMOTO, T., HOSOBABA, K., OCHIAI, H., ROYBA, E., IZUMI, H., SAKUMA, T., YAMAMOTO, T., DYNLACHT, B. D. & MATSUURA, S.

2015. The Microtubule-Depolymerizing Activity of a Mitotic Kinesin Protein KIF2A Drives Primary Cilia Disassembly Coupled with Cell Proliferation. *Cell Rep*, 10, 664-673.
- MRUG, M., LI, R., CUI, X., SCHOEB, T. R., CHURCHILL, G. A. & GUAY-WOODFORD, L. M. 2005. Kinesin family member 12 is a candidate polycystic kidney disease modifier in the cpk mouse. *J Am Soc Nephrol*, 16, 905-16.
- MRUG, M., ZHOU, J., YANG, C., ARONOW, B. J., CUI, X., SCHOEB, T. R., SIEGAL, G. P., YODER, B. K. & GUAY-WOODFORD, L. M. 2015. Genetic and Informatic Analyses Implicate Kif12 as a Candidate Gene within the Mpkd2 Locus That Modulates Renal Cystic Disease Severity in the Cys1cpk Mouse. *PLOS ONE*, 10, e0135678.
- NAKAGAWA, T., TANAKA, Y., MATSUOKA, E., KONDO, S., OKADA, Y., NODA, Y., KANAI, Y. & HIROKAWA, N. 1997. Identification and classification of 16 new kinesin superfamily (KIF) proteins in mouse genome. *Proc Natl Acad Sci U S A*, 94, 9654-9.
- NAKATA, T., NIWA, S., OKADA, Y., PEREZ, F. & HIROKAWA, N. 2011. Preferential binding of a kinesin-1 motor to GTP-tubulin-rich microtubules underlies polarized vesicle transport. *Journal of Cell Biology*, 194, 245-255.
- NAKAYAMA, K. & KATOH, Y. 2018. Ciliary protein trafficking mediated by IFT and BBSome complexes with the aid of kinesin-2 and dynein-2 motors. *J Biochem*, 163, 155-164.
- NETTLESHIP, J. E., WATSON, P. J., RAHMAN-HUQ, N., FAIRALL, L., POSNER, M. G., UPADHYAY, A., REDDIVARI, Y., CHAMBERLAIN, J.

- M., KOLSTOE, S. E., BAGBY, S., SCHWABE, J. W. & OWENS, R. J. 2015. Transient expression in HEK 293 cells: an alternative to *E. coli* for the production of secreted and intracellular mammalian proteins. *Methods Mol Biol*, 1258, 209-22.
- NICASTRO, D., FU, X., HEUSER, T., TSO, A., PORTER, M. E. & LINCK, R. W. 2011. Cryo-electron tomography reveals conserved features of doublet microtubules in flagella. *Proceedings of the National Academy of Sciences*, 108, E845-E853.
- NOGALES, E., WOLF, S. G. & DOWNING, K. H. 1998. Structure of the alpha beta tubulin dimer by electron crystallography. *Nature*, 391, 199-203.
- NOUR-ELDIN, H. H., GEU-FLORES, F. & HALKIER, B. A. 2010. USER cloning and USER fusion: the ideal cloning techniques for small and big laboratories. *Methods Mol Biol*, 643, 185-200.
- O'BEIRNE, S. L., SALIT, J., RODRIGUEZ-FLORES, J. L., STAUDT, M. R., ABI KHALIL, C., FAKHRO, K. A., ROBAY, A., RAMSTETTER, M. D., MALEK, J. A., ZIRIE, M., JAYYOUSI, A., BADI, R., AL-NABET AL-MARRI, A., BENER, A., MAHMOUD, M., CHIUCHIOLO, M. J., AL-SHAKAKI, A., CHIDIAC, O., STADLER, D., MEZEY, J. G. & CRYSTAL, R. G. 2018. Exome sequencing-based identification of novel type 2 diabetes risk allele loci in the Qatari population. *PLOS ONE*, 13, e0199837.
- OGAWA, T., NITTA, R., OKADA, Y. & HIROKAWA, N. 2004. A Common Mechanism for Microtubule Destabilizers—M Type Kinesins

Stabilize Curling of the Protofilament Using the Class-Specific Neck and Loops. *Cell*, 116, 591-602.

OU, G., E BLACQUE, O., SNOW, J. J., LEROUX, M. R. & SCHOLEY, J. M. 2005. Functional coordination of intraflagellar transport motors. *Nature*, 436, 583-587.

OUNJAI, P., KIM, KEUNHWAN D., LIU, H., DONG, M., TAUSCHER, ANDREW N., WITKOWSKA, H. E. & DOWNING, KENNETH H. 2013. Architectural Insights into a Ciliary Partition. *Current Biology*, 23, 339-344.

PATEL, J. T., BELSHAM, H. R., RATHBONE, A. J. & FRIEL, C. T. 2014. Use of stopped-flow fluorescence and labeled nucleotides to analyze the ATP turnover cycle of kinesins. *J Vis Exp*, e52142.

PAZOUR, G. J., DICKERT, B. L., VUCICA, Y., SEELEY, E. S., ROSENBAUM, J. L., WITMAN, G. B. & COLE, D. G. 2000. Chlamydomonas IFT 88 and its mouse homologue, polycystic kidney disease gene Tg 737, are required for assembly of cilia and flagella. *The Journal of cell biology*, 151, 709-718.

PEDERSEN, L. B. & ROSENBAUM, J. L. 2008. Chapter two intraflagellar transport (IFT): role in ciliary assembly, resorption and signalling. *Current topics in developmental biology*, 85, 23-61.

PIGINO, G., GEIMER, S., LANZAVECCHIA, S., PACCAGNINI, E., CANTELE, F., DIENER, D. R., ROSENBAUM, J. L. & LUPETTI, P. 2009. Electron-tomographic analysis of intraflagellar transport particle trains in situ. *Journal of Cell Biology*, 187, 135-148.

- PIGINO, G. & ISHIKAWA, T. 2012. Axonemal radial spokes: 3D structure, function and assembly. *Bioarchitecture*, 2, 50-58.
- PILLING, A. D., HORIUCHI, D., LIVELY, C. M. & SAXTON, W. M. 2006. Kinesin-1 and Dynein Are the Primary Motors for Fast Transport of Mitochondria in Drosophila Motor Axons. *Molecular Biology of the Cell*, 17, 2057-2068.
- PIPERNO, G. & MEAD, K. 1997. Transport of a novel complex in the cytoplasmic matrix of Chlamydomonas flagella. *Proceedings of the National Academy of Sciences*, 94, 4457-4462.
- PLOTNIKOVA, O. V., PUGACHEVA, E. N. & GOLEMIS, E. A. 2009. Primary cilia and the cell cycle. *Methods Cell Biol*, 94, 137-60.
- QIN, H., WANG, Z., DIENER, D. & ROSENBAUM, J. 2007. Intraflagellar transport protein 27 is a small G protein involved in cell-cycle control. *Current Biology*, 17, 193-202.
- REITER, J. F., BLACQUE, O. E. & LEROUX, M. R. 2012. The base of the cilium: roles for transition fibres and the transition zone in ciliary formation, maintenance and compartmentalization. *EMBO reports*, 13, 608-618.
- ROOSTALU, J., HENTRICH, C., BIELING, P., TELLEY, I. A., SCHIEBEL, E. & SURREY, T. 2011. Directional Switching of the Kinesin Cin8 Through Motor Coupling. *Science*, 332, 94-99.
- ROSENBAUM, J. L. & WITMAN, G. B. 2002. Intraflagellar transport. *Nature Reviews Molecular Cell Biology*, 3, 813-825.

- SABLIN, E. P., CASE, R. B., DAI, S. C., HART, C. L., RUBY, A., VALE, R. D. & FLETTERICK, R. J. 1998. Direction determination in the minus-end-directed kinesin motor ncd. *Nature*, 395, 813-816.
- SABLIN, E. P., JON KULL, F., COOKE, R., VALE, R. D. & FLETTERICK, R. J. 1996. Crystal structure of the motor domain of the kinesin-related motor ncd. *Nature*, 380, 555-559.
- SACK, S., MÜLLER, J., MARX, A., THORMÄHLEN, M., MANDELKOW, E.-M., BRADY, S. T. & MANDELKOW, E. 1997. X-ray Structure of Motor and Neck Domains from Rat Brain Kinesin. *Biochemistry*, 36, 16155-16165.
- SCHIMERT, K. I., BUDAITIS, B. G., REINEMANN, D. N., LANG, M. J. & VERHEY, K. J. 2019. Intracellular cargo transport by single-headed kinesin motors. *Proceedings of the National Academy of Sciences*, 116, 6152-6161.
- SCHINDELIN, J., ARGANDA-CARRERAS, I., FRISE, E., KAYNIG, V., LONGAIR, M., PIETZSCH, T., PREIBISCH, S., RUEDEN, C., SAALFELD, S., SCHMID, B., TINEVEZ, J. Y., WHITE, D. J., HARTENSTEIN, V., ELICEIRI, K., TOMANCAK, P. & CARDONA, A. 2012. Fiji: an open-source platform for biological-image analysis. *Nat Methods*, 9, 676-82.
- SCHMIDT, K. N., KUHNS, S., NEUNER, A., HUB, B., ZENTGRAF, H. & PEREIRA, G. 2012. Cep164 mediates vesicular docking to the mother centriole during early steps of ciliogenesis. *J Cell Biol*, 199, 1083-101.

- SCHOLEY, J. M. 2008. Intraflagellar transport motors in cilia: moving along the cell's antenna. *The Journal of cell biology*, 180, 23-29.
- SCHOLEY, J. M. 2013. Kinesin-2: A Family of Heterotrimeric and Homodimeric Motors with Diverse Intracellular Transport Functions. *Annual Review of Cell and Developmental Biology*, 29, 443-469.
- SHARP, D. J., BROWN, H. M., KWON, M., ROGERS, G. C., HOLLAND, G. & SCHOLEY, J. M. 2000. Functional Coordination of Three Mitotic Motors in *Drosophila* Embryos. *Molecular Biology of the Cell*, 11, 241-253.
- SHARP, D. J., MCDONALD, K. L., BROWN, H. M., MATTHIES, H. J., WALCZAK, C., VALE, R. D., MITCHISON, T. J. & SCHOLEY, J. M. 1999. The Bipolar Kinesin, KLP61F, Cross-links Microtubules within Interpolar Microtubule Bundles of *Drosophila* Embryonic Mitotic Spindles. *Journal of Cell Biology*, 144, 125-138.
- SHIPLEY, K., HEKMAT-NEJAD, M., TURNER, J., MOORES, C., ANDERSON, R., MILLIGAN, R., SAKOWICZ, R. & FLETTERICK, R. 2004. Structure of a kinesin microtubule depolymerization machine. *Embo j*, 23, 1422-32.
- SKOUFIAS, D. A., COLE, D. G., WEDAMAN, K. P. & SCHOLEY, J. M. 1994. The carboxyl-terminal domain of kinesin heavy chain is important for membrane binding. *J Biol Chem*, 269, 1477-85.
- SNOW, J. J., OU, G., GUNNARSON, A. L., WALKER, M. R., ZHOU, H. M., BRUST-MASCHER, I. & SCHOLEY, J. M. 2004. Two anterograde

- intraflagellar transport motors cooperate to build sensory cilia on *C. elegans* neurons. *Nat Cell Biol*, 6, 1109-13.
- SONG, L. & DENTLER, W. L. 2001. Flagellar protein dynamics in *Chlamydomonas*. *Journal of Biological Chemistry*, 276, 29754-29763.
- SONG, Y. H. & MANDELKOW, E. 1993. Recombinant kinesin motor domain binds to beta-tubulin and decorates microtubules with a B surface lattice. *Proc Natl Acad Sci U S A*, 90, 1671-5.
- SPIITTE, C., CHARRASSE, S., LARROQUE, C. & CASSIMERIS, L. 2000. The Interaction of TOGp with Microtubules and Tubulin *. *Journal of Biological Chemistry*, 275, 20748-20753.
- STEPHENS, R. E. 1997. Synthesis and turnover of embryonic sea urchin ciliary proteins during selective inhibition of tubulin synthesis and assembly. *Molecular biology of the cell*, 8, 2187-2198.
- TALAPATRA, S. K., HARKER, B. & WELBURN, J. P. I. 2015. The C-terminal region of the motor protein MCAK controls its structure and activity through a conformational switch. *eLife*, 4, e06421.
- TANOS, B. E., YANG, H. J., SONI, R., WANG, W. J., MACALUSO, F. P., ASARA, J. M. & TSOU, M. F. 2013. Centriole distal appendages promote membrane docking, leading to cilia initiation. *Genes Dev*, 27, 163-8.
- TAO, L., MOGILNER, A., CIVELEKOGLU-SCHOLEY, G., WOLLMAN, R., EVANS, J., STAHLBERG, H. & SCHOLEY, J. M. 2006. A homotetrameric kinesin-5, KLP61F, bundles microtubules and antagonizes Ncd in motility assays. *Curr Biol*, 16, 2293-302.

- TRAN, P. V., HAYCRAFT, C. J., BESSCHETNOVA, T. Y., TURBE-DOAN, A., STOTTMANN, R. W., HERRON, B. J., CHESEBRO, A. L., QIU, H., SCHERZ, P. J. & SHAH, J. V. 2008. THM1 negatively modulates mouse sonic hedgehog signal transduction and affects retrograde intraflagellar transport in cilia. *Nature genetics*, 40, 403-410.
- TSAO, C.-C. & GOROVSKY, M. A. 2008. Tetrahymena IFT122A is not essential for cilia assembly but plays a role in returning IFT proteins from the ciliary tip to the cell body. *Journal of cell science*, 121, 428-436.
- ÜNLÜSOY AKSU, A., DAS, S. K., NELSON-WILLIAMS, C., JAIN, D., ÖZBAY HOŞNUT, F., EVIRGEN ŞAHİN, G., LIFTON, R. P. & VILARINHO, S. 2019. Recessive Mutations in KIF12 Cause High Gamma-Glutamyltransferase Cholestasis. *Hepatol Commun*, 3, 471-477.
- VALE, R. D. & GOLDSTEIN, L. S. B. 1990. One motor, many tails: An expanding repertoire of force-generating enzymes. *Cell*, 60, 883-885.
- VAN RIEL, W. E., RAI, A., BIANCHI, S., KATRUKHA, E. A., LIU, Q., HECK, A. J., HOOGENRAAD, C. C., STEINMETZ, M. O., KAPITEIN, L. C. & AKHMANOVA, A. 2017. Kinesin-4 KIF21B is a potent microtubule pausing factor. *Elife*, 6.
- WALCZAK, C. E., GAN, E. C., DESAI, A., MITCHISON, T. J. & KLINE-SMITH, S. L. 2002. The microtubule-destabilizing kinesin XKCM1 is required for chromosome positioning during spindle assembly. *Curr Biol*, 12, 1885-9.

- WANG, H.-W. & NOGALES, E. 2005. Nucleotide-dependent bending flexibility of tubulin regulates microtubule assembly. *Nature*, 435, 911-915.
- WANG, Y., LADUNGA, I., MILLER, A. R., HORKEN, K. M., PLUCINAK, T., WEEKS, D. P. & BAILEY, C. P. 2008. The small ubiquitin-like modifier (SUMO) and SUMO-conjugating system of *Chlamydomonas reinhardtii*. *Genetics*, 179, 177-192.
- WICKSTEAD, B. & GULL, K. 2006. A "holistic" kinesin phylogeny reveals new kinesin families and predicts protein functions. *Mol Biol Cell*, 17, 1734-43.
- WICKSTEAD, B., GULL, K. & RICHARDS, T. A. 2010. Patterns of kinesin evolution reveal a complex ancestral eukaryote with a multifunctional cytoskeleton. *BMC Evol Biol*, 10, 110.
- XIA, W., BRINGMANN, P., MCCLARY, J., JONES, P. P., MANZANA, W., ZHU, Y., WANG, S., LIU, Y., HARVEY, S., MADLANSACAY, M. R., MCLEAN, K., ROSSER, M. P., MACROBBIE, J., OLSEN, C. L. & COBB, R. R. 2006. High levels of protein expression using different mammalian CMV promoters in several cell lines. *Protein Expression and Purification*, 45, 115-124.
- YANG, P., DIENER, D. R., YANG, C., KOHNO, T., PAZOUR, G. J., DIENES, J. M., AGRIN, N. S., KING, S. M., SALE, W. S., KAMIYA, R., ROSENBAUM, J. L. & WITMAN, G. B. 2006. Radial spoke proteins of *Chlamydomonas* flagella. *Journal of cell science*, 119, 1165-1174.

- YANG, W., TANAKA, Y., BUNDO, M. & HIROKAWA, N. 2014. Antioxidant Signaling Involving the Microtubule Motor KIF12 Is an Intracellular Target of Nutrition Excess in Beta Cells. *Developmental Cell*, 31, 202-214.
- YODER, B. K., HOU, X. & GUAY-WOODFORD, L. M. 2002. The polycystic kidney disease proteins, polycystin-1, polycystin-2, polaris, and cystin, are co-localized in renal cilia. *J Am Soc Nephrol*, 13, 2508-16.
- YU, W., SOLOWSKA, J. M., QIANG, L., KARABAY, A., BAIRD, D. & BAAS, P. W. 2005. Regulation of microtubule severing by katanin subunits during neuronal development. *The Journal of neuroscience : the official journal of the Society for Neuroscience*, 25, 5573-5583.
- ZANIC, M. 2016. Measuring the Effects of Microtubule-Associated Proteins on Microtubule Dynamics In Vitro. *Methods Mol Biol*, 1413, 47-61.
- ZANIC, M., WIDLUND, P. O., HYMAN, A. A. & HOWARD, J. 2013. Synergy between XMAP215 and EB1 increases microtubule growth rates to physiological levels. *Nature Cell Biology*, 15, 688-693.
- ZIMYANIN, V. L., BELAYA, K., PECREAU, J., GILCHRIST, M. J., CLARK, A., DAVIS, I. & ST JOHNSTON, D. 2008. In Vivo Imaging of *oskar* mRNA Transport Reveals the Mechanism of Posterior Localization. *Cell*, 134, 843-853.

Appendix 2

A2.1 USER cloning - PCR primers

KIF12 Tail [434-651]

F. Primer

GGG GAG CU AATGAGAGGCTCAGGAAAGAAAAG (24bp), T_m ($14 \times 2 + 10 \times 4$) = 68

R. Primer

GGG GAA CU ATGGGGAGGGAGGACTTGGC (20bp), T_m ($7 \times 2 + 13 \times 4$) = 66

KIF12 tail [478-651]

F. Primer

GGG GAG CU CAGGGTCCTGGCCTGACCCC (20bp), T_m ($= 5 \times 2 + 15 \times 4$) = 70

R. Primer

Same as the KIF12 Tail [434-561] r. primer

Full length KIF12

F. Primer

GGG GAG CU ATGGAAGAACGCGGGTCACCTG (22bp), T_m ($9 \times 2 + 13 \times 4$) = 70

R. Primer

Same as the KIF12 Tail [434-561] r. primer

KIF12-472 (motor domain+ Full length coiled coil)

F. Primer

Same as the full length KIF12 f. primer

R. Primer

GGG GAA CU GGCAGAGAGGAGACGCCTCTCTA (23bp), T_m ($9 \times 2 + 14 \times 4$)
=74

KIF12 Tail [434-651]

F. Primer (with Sal1 restriction site)

GTCGAC AATGAGAGGCTCAGGAAAGAAAAG (24bp), T_m ($14 \times 2 + 10 \times 4$)
=68

R. Primer (with Xba1 restriction site)

TCTAGA ATGGGGAGGGAGGACTTGGC (20bp), T_m ($7 \times 2 + 13 \times 4$) =66

KIF12 Tail [478-651]

F. Primer (with Sal1 restriction site)

GTCGAC CAGGGTCCTGGCCTGACCCC (20bp) T_m ($=5 \times 2 + 15 \times 4$) =70

R. Primer

Same as the Tail [434-651] r. primer

Appendix 3

A3.1 Oligomeric state assessment of purified wild type KIF12-434

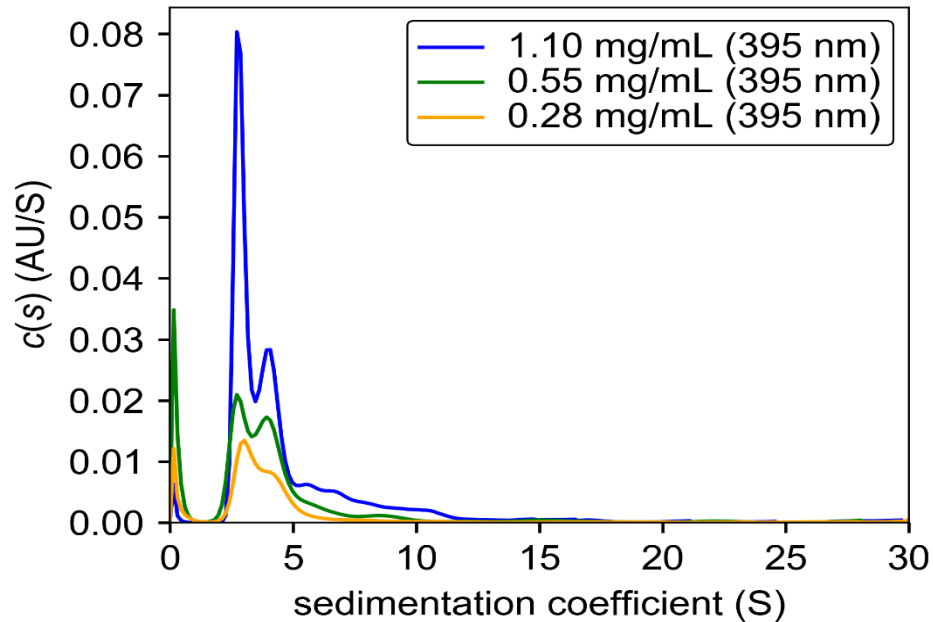


Figure A3.1. Around one-third of purified KIF12-434 is dimeric. Oligomeric state of KIF12-434 was assessed using Analytical ultracentrifugation. The assay was run at the indicated protein concentrations and wavelength of 395nm. The plots show the sedimentation coefficient distributions for the KIF12-434 purified sample. The assay carried out by Gemma Harris, Research Complex at Harwell, Rutherford Appleton Laboratory, Harwell.

Appendix 4

A4.1 Difference in solubility between the wild type KIF12-434 and KIF12-434 Δ PPGGG expressed in Sf9 cells.

Table 4. Band quantification on SDS-PAGE of wild type KIF12-434

Wild type KIF12-434				
	lane signal	KIF12 signal	KIF12:lane ratio	normalized ratio
Cell lysate	50365655	601486	0.0119	1.00
Clear lysate	45374335	683822	0.0151	1.26
Pellet	40927049	477459	0.0117	0.98

Table 5. Band quantification on SDS-PAGE of KIF12-434 Δ PPGGG

KIF12-434 Δ PPGGG				
	lane signal	KIF12 signal	KIF12:lane ratio	normalized ratio
Cell lysate	46317273	587635	0.0127	1.00
Clear lysate	42046819	481881	0.0115	0.90
Pellet	36536860	611966	0.0167	1.32

Appendix 5

A5.1 KIF12-434 effect on microtubule dynamics.

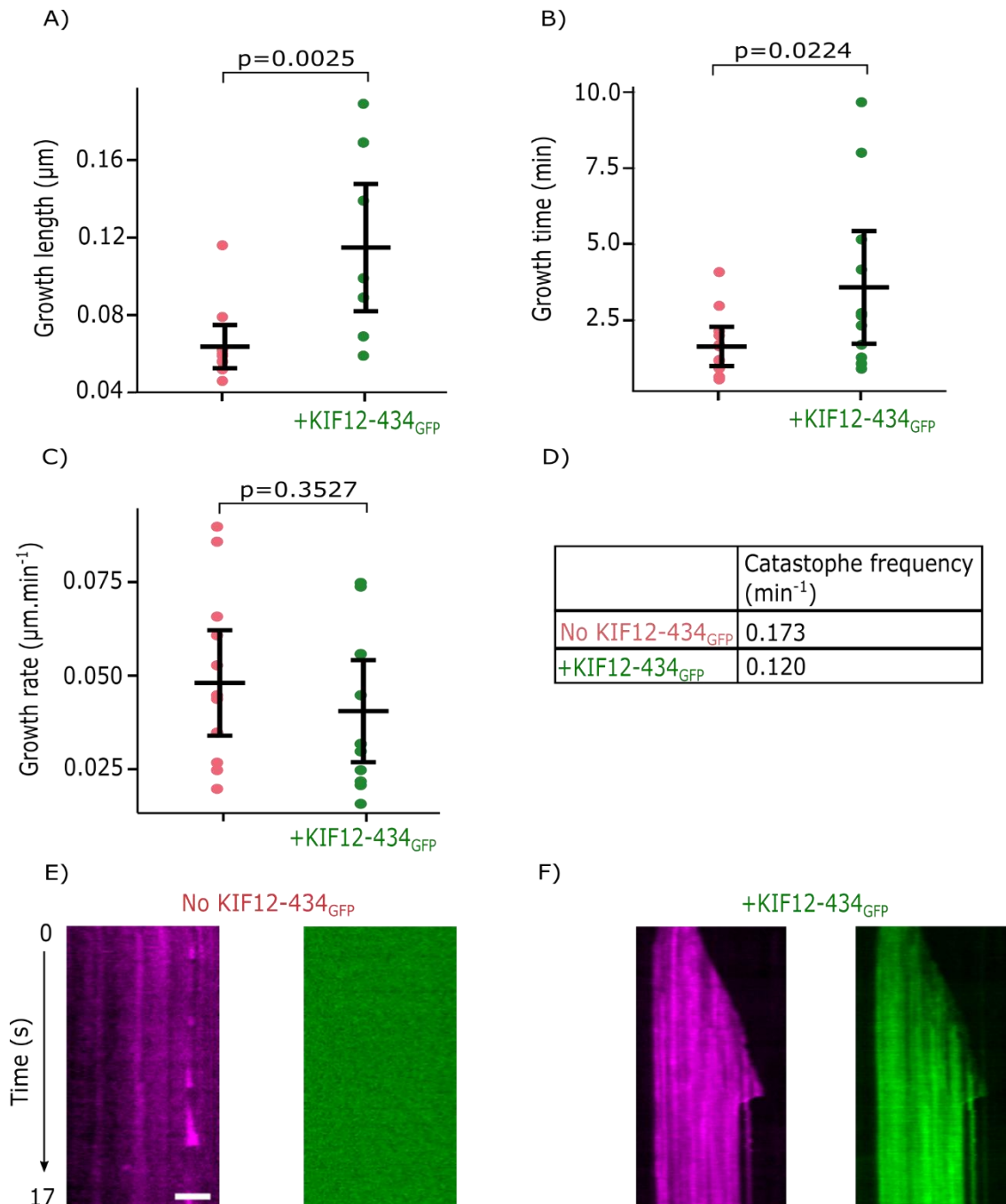


Figure A5.1. KIF12-434 affects microtubule dynamics. A and B) Growth length and growth time increased by GFP- labelled KIF12-434, but not C) growth rate and D) catastrophe frequency. E and F) kymographs of dynamic microtubules in the presence of unpolymerised tubulin, and absence and presence of KIF12-434, n=13 and 12, respectively. Scale bar 2 μ m. Data obtained using microtubule dynamic assay.